ABSTRACT

WILKINS, STEWART JOHN. Functionalization of III-V Materials for Modulated Surface Opto-Electronic Properties. (Under the direction of Dr. Albena Ivanisevic).

With recent interest in organic light-emitting diodes (LEDs) and solar cells, surface functionalization of semiconductors has gained substantial importance through modifications to surface optical and electrical properties. Surface functionalization utilizes dangling bonds on the surface to bind desired species to the substrate material. These adsorbates benefit the final device by imparting additional properties such as chemical stability, optical luminescence, additional binding sites, and modified work functions that are lacking from traditional semiconductor processing techniques. Of the semiconductors commercially available such as silicon (Si), gallium arsenide (GaAs), and indium arsenide (InAs), gallium nitride (GaN) stands out as an excellent candidate for biological and chemical sensing applications due to improved chemical resistance, biocompatibility, thermal stability, and higher breakdown voltages versus other semiconducting materials. Despite the natural chemical resistance, GaN is vulnerable to pH extreme solutions of molten potassium hydroxide, sodium hydroxide, phosphoric acid, sulfuric acid, and oxalic acid, which expose additional surface area via etching to form more binding sites. This dissertation focuses on utilizing phosphoric acid in conjunction with thiol and phosphonic acid adsorbates to modify the surface chemistry, topography, and optical/electrical properties of planar polar and nonpolar GaN as well as high aspect ratio GaN nanorods through simultaneous etching and functionalization with adsorbates. The formation of oxides and subsequent environmental stability of III-V materials (GaN and GaP) via hydrogen peroxide capping provides insight into binding events and interfacial reactions not reported to date. This work will investigate

the roles topography and surface chemistry via hydrogen peroxide plays with functionalization. Surface characterization techniques such as X-ray photoelectron spectroscopy (XPS), water goniometry, and atomic force microscopy (AFM) paired with kelvin probe force microscopy (KPFM) were utilized to examine the surface chemistry, hydrophobicity, topography, and surface potential respectively. Additional techniques such as inductively coupled plasma-mass spectrometry (ICP-MS) and photoluminesce (PL) identified leaching within various aqueous environments and the photoluminescent response from topography and surface groups.

Functionalization of III-V Materials for Modulated Surface Opto-Electronic Properties

by
Stewart John Wilkins

A dissertation submitted to the Graduate Faculty of
North Carolina State University
in partial fulfillment of the
requirements for the degree of
Doctor of Philosophy

Material Science and Engineering

Raleigh, North Carolina

2015

APPROVED BY:

_____	_____
Alper Bozkurt	Tania Paskova
_____	_____
Joseph Tracy	Albena Ivanisevic Committee Chair

BIOGRAPHY

Stewart Wilkins was born in Grand Rapids, Michigan from where he eventually landed in Georgia. Stewart attended the Georgia Institute of Technology within the Department of Materials Science and Engineering. He began his career in research under the direction of Dr. C. P. Wong, where Stewart investigated the effects of carbon nanotube catalysts on silicone stability. After graduating in the spring of 2011 with a B.S. in Materials Science and Engineering, Stewart was accepted to North Carolina State University. There he investigated surface modifications of III-V materials under the guidance of Dr. Albena Ivanisevic.

ACKNOWLEDGMENTS

The people who have enabled my success are many. Dr. Albena Ivanisevic: for her constant support, generosity, and direction. Without her, you would not be reading this right now. Dr. Tania Paskova, Dr. Joseph Tracy, and Dr. Alper Bozkurt: for their time and commitment as my committee members and collaborators. The NSF: for providing funding for the work below. Kim Hutchison: for her assistance with ICP-MS. Dr. Mark Walters: for his tireless support at SMiF. Roger Russell, Toby Tung, and Joe Matthews: for their expertise inside and outside of the lab. Edna Deas: for keeping the department running and answering my multitude of questions. Dr. Lauren Bain, Dr. Matthew Makowski, Corey Foster, Nora Berg, Nathaniel Rohrbaugh, Brady Pearce, Chris Ledford, Christer Akouala, Sam Rogers, Lauren Chisholm, John Medford, and Weston Straka: a special thanks to my lab and office mates, past and present, for their help and support in addition to putting up with my shenanigans on a daily basis. In addition to all the other people I've meet along the way (you know who you are): thanks for the great times and the better stories. Without them, my time here would have certainly been a lot duller. My parents: for the gentle reminder of: "…so, when are you graduating?"

TABLE OF CONTENTS

LIST OF TABLES

LIST OF FIGURES

ABBREVIATIONS

AFM	Atomic Force Microscopy
eV	Electron Volt
GaAs	Gallium Arsenide
Ga_2O_3	Gallium oxide
Ga_2O, GaO	Gallium sub-oxides
GaN	Gallium nitride
GaP	Gallium phosphide
HCl	Hydrochloric acid
HF	Hydrofluoric acid
H_3PO_4	Phosphoric acid
InAs	Indium arsenide
ICP-MS	Inductively Coupled Plasma Mass Spectrometry
InN	Indium nitride
KPFM	Kelvin Probe Force Microscopy
LED	Light-Emitting Diode
MUDPA	11-MercaptoUnDecylPhosphonic Acid
ODPA	1,8-OctaneDiPhosphonic Acid
PFOPA	1H,1H,2H,2H-PerFluorooctane Phosphonic Acid
PL	PhotoLuminescence
XPS	X-ray Photoelectron Spectroscopy

XRD	X-Ray Diffraction

1. Introduction

1.1 Overview

Surface treatments of semiconductors have been explored for many material sets as a way to modify host properties such as optical and electrical properties for unique applications. Organic molecules are frequently used to passivate surfaces due to structural flexibility and self-assembling properties that are associated with a wide variety of binding groups. This has been seen in many applications such as biosensors,[1-3] chemical sensors,[4-6] drug delivery systems,[7-9] solar cells,[10-12] and light emitting diodes (LEDs).[13-15] For biosensors, the use of polypeptide, antibody, or deoxyribonucleic acid (DNA) attachment provides an interaction site by which proteins, antigens, or base pairs of specific compositions result in an alteration in the bulk electrical characteristics of the host material. This has been seen where antibody coated high electron mobility transistors (HEMTs) provided the detection of breast cancer markers [16] as well as immobilized DNA on gallium phosphide (GaP) for cDNA collection.[17] Chemical sensors tend to operate much the same way, where the high sensitivity of the device is determined by the affinity of the bound adsorbates to species of interest. Drug delivery systems, often in the form of nano-particles due to the high aspect ratio of surface area to volume, utilize tailored environmental conditions (light, temperature, pH) [9] to control the release of drugs within a biological environment. Solar cells benefit from surface functionalization by allowing for work functions across material interfaces to be matched. The matching of such electrical properties

allow for improved charge injection and overall device efficiency.[18] For organic solar cell systems, disproportionate electrical junctions between materials can be lessened if not mitigated with careful selection of surface adsorbates. In the case of LEDs, surface passivation has shown to improve luminosity in some material systems,[14] which can provide better charge injection as well as surface combination not seen with bare surfaces..

The host substrate determines many device properties such as binding affinities, optical and electrical characteristics as well as the overall stability of the final device. This is measured through adsorbate coverage, luminescence and resistance, as well as leaching within various environments. Many of the bio and chemical sensors mentioned currently rely on the use of silicon as a substrate.[19-21] As a result, silanes tend to be frequently used to passivate the surface due to the improved adhesion with hydroxyl species. Silanes offer improved chemical stability over other surface passivation methods as the use of pristine/environmentally neutral processing environments are not needed in addition to an adjustable platform for a plethora of side and terminal groups. Unfortunately, silanes are mildly toxic should they detach from the silicon surface and react with the surrounding environment.[22] For sensors in harsh aquatic environments, the use of silicon results in biocompatibility issues due to leaching [23] and surface breakdown from harsh chemicals.[24] This is in addition to inefficiencies derived from an indirect band gap.[25] Hence the application of silicon is limited to controlled environments, even with the addition of passivating adlayers. To address the indirect band gap and its associated inefficiencies, II-VI and III-V semiconducting materials have gained significant attention due to both their

direct band gaps as well as varied energy band separations (see Table 1). The expanded repertoire of usable materials multiplies not only the bulk electrical characteristics, but also potential binding sites for adsorbates. This opens up another front for surface functionalization of semiconducting materials for new applications.

Table 1 Examples of II-VI and III-V direct band gap binary compounds and their associated band energies.

Compound	Band Gap (eV)
AlN	6.20 [24]
GaN	3.40 [26]
GaAs	1.40 [24]
GaSb	0.78 [27]
InN	0.76 [26]
InP	1.35 [28]
InAs	0.36 [27]
InSb	0.28 [28]
CdSe	1.74 [29]
CdsS	2.43 [30]
ZnO	3.35 [30]
ZnSe	2.67 [24]
ZnS	3.68 [30]
ZnTe	2.25 [30]

1.2 Dissertation Focus: GaN

Of the various semiconducting materials mentioned, GaN is the material of choice for a variety of reasons. Unlike other widely used III-V semiconductors such as InN or GaAs, GaN boasts a large band gap of 3.4 eV as opposed to 0.76 and 1.40 eV respectively. Indium is elementally scarcer than gallium (0.05 ppm versus 16.9 ppm), [31, 32] thus posing a

financial burden on device fabrication. InN is difficult to fabricate due to lattice mismatches in growth substrates and subsequent layering, thus resulting in large quantities of defects (10^8 cm^{-2} threading dislocations) throughout the material.[33] InN also suffers from thermal breakdown at elevated temperatures, which limits processing to low temperature/slow growth techniques.[34] GaAs fares much better than InN in that it is well studied, higher quality, easy to fabricate, and commercially available.[35] GaAs boasts the formation of a native oxide layer, which when introduced to aqueous environments tends to leach due to oxide instabilities. The leaching, though smaller than silicon, can prove toxic due to the use of arsenic, which prevents its use for biological applications.[36, 37] Recent advances in GaN fabrication are capable of yielding faster growth of low defect, high quality free-standing structures in addition to utilizing cheaper raw materials than other III-V semiconductors. Like GaAs, GaN produces an oxide layer that readily leaches into solutions of extreme pHs.[36] The oxide layer is not resistant to acidic/basic solutions; however, the use of GaN limits the exposure of biological environments to overly toxic components such as arsenic and indium.[36, 38] GaN remains resistant to many chemical attacks;[34] however, vulnerability to acidic solutions provides a means to alter topographical features. By increasing the surface area, additional dangling bonds are formed that can provide sites for chemical binding in addition to modulating bulk photoluminescence properties. This will be discussed in further detail in chapter 1.5 and 1.6. It is thus the focus of this dissertation to utilize acid assisted functionalization to explore unique optical and electronic properties of GaN.

1.3 Gallium Nitride Fabrication

GaN was first produced by Maruska and Tietjen in 1969, whereupon a thin layer of GaN was grown via hydride vapor phase epitaxy (HVPE).[39] Until then, GaN was only available in polycrystalline form, which limited its applications as a semiconductor due to high defect density and grain boundary formations. The advent of single crystalline GaN eventually enabled the formation of intense blue LEDs and other applications; however, many developments were required to move from the initial defect rich single crystalline specimen to what can be achieved with GaN today.[40]

1.3.1 Buffer Layers

Early GaN substrates suffered from high dislocation densities due to lattice mismatch between the GaN thin film and the sapphire substrate.[40] To correct for this, buffer layers were introduced to improve epitaxial formation through stress relaxation by utilizing similar lattice constants between substrate and epi-layer. Initial use of AlN by Yoshida in 1983 paved the way for buffer layers throughout GaN growth and development.[41] Additional buffer layers include ZnO,[42] AlGaN,[43], BN,[44] and a thin layer of GaN.[45] The use of buffer layers is contingent on the substrate being used, in addition to desired impurities (intentional or otherwise) to the GaN layer. In addition to closing the lattice mismatch, use of buffer layers promoted improved films due to decreased surface cracking resulting from diverse coefficients of thermal expansion.

1.3.2 Foreign Substrates

In addition to buffer layers, the types of foreign substrates used for growth was also explored. Sapphire was originally chosen due to physical stability within hot environments in addition to being chemically resistant to the ammonia, a precursor for GaN formation. Sapphire has a lattice mismatch of 14% relative to GaN and a thermal expansion mismatch of 25%.[46] Of the many viable foreign substrates, sapphire has one of the greatest lattice mismatches relative to GaN in addition to the discrepancy in thermal expansion.[47] Buffer layers were initially developed to overcome sapphire's limitations; however, other foreign substrates such as AlN,[48] SiC,[49] ZnO,[50] $ScAlMgO_4$,[51] $LiAlO_2$,[52] $LiGaO_2$,[53] Si,[54] GaAs,[55] and MgO [56] were explored concurrently. Of these foreign substrates, SiC is perhaps the most widely used substrate for GaN growth commercially due to its low lattice mismatch and high thermal conductivity.[57] It was not until 1997 when NEC Corp. utilized GaN as a native substrate for subsequent GaN growth.[58] The perfect matchup enabled a dramatic decrease in crystallographic defects by two to three orders of magnitude versus foreign substrate growth.[40]

1.3.3 Growth Processes

In addition to a wide range of substrates available, GaN production spans a plethora of growth environments. HVPE, as previously mentioned, was the first growth technique utilized for GaN fabrication within this dissertation. HVPE utilizes gaseous ammonia and gallium hydride (often GaCl) precursors for formation. HVPE benefits from high growth

rates, but risks propagating defects throughout the entirety of the structure to result in cracking.[59] Due to this, HVPE was largely neglected until better substrates and nucleation layers were developed.[47] Another form of vapor phase epitaxy called metal organic vapor phase epitaxy (MOVPE) renewed interest in HVPE by providing higher quality thin layers of GaN through reduced formation temperatures.[47] MOVPE replaces hydride bound gallium with organically bound gallium such as trimethylgallium.[60] The cost of the high quality GaN formation is significantly longer process times than HVPE. Prior to the development of MOVPE for improved GaN, molecular beam epitaxy (MBE) was used to produce very smooth layers.[40] MBE forms GaN via combining plasma from gallium and nitrogen sources and deposits onto a substrate.[61] Plasma free MBE also exists, where the use of a reactive ion beam forms the epitaxial layers.[47] Though MBE grown GaN is of higher quality than initial HVPE grown GaN, slow deposition limits its use to thin layers. A recent addition to GaN fabrication is ammonothermal growth, whereupon a supercritical bath of ammonia and solid polycrystalline GaN form additional layers upon a GaN seed layer.[62, 63] This method has shown promising results in terms of crystal quality and boule size; however, final product quality seems to be entirely dependent upon the quality of the seed layer.[62]

Formation of high quality GaN was first achieved with a technique called epitaxial lateral overgrowth (ELO). ELO was developed for GaN by Nam et al. in 1997 [64] following previous uses for high quality Si,[65] GaAs,[66] and InP.[67] ELO utilizes a lithographic approach of creating a mask layer of SiO_2 over a layer of grown GaN (utilizing improved

substates, buffer layers, and growth techniques mentioned before). GaN was then further grown from between the masked regions resulting in a pyramidal structure. Eventually after enough growth, the regions will coalesce over the mask and form a region of reduced threading dislocations. The pyramidal structures resulted from the formation of c-plane or (0 0 0 1) GaN that would grow through the mask defined by {1 1 -2 2} planes.[68] This can also be accomplished with other starting substrate orientations such as {1 1 -2 0}.[69] The orientation of GaN growing between masks depended upon the temperature and pressure of the growth chamber. The use of higher temperatures and lower pressures promotes the creation of rectangular formations that predominantly grow from the a-plane or {1 1 -2 0} planes.[70] Relaxation of stresses above the mask layer frequently produces voids, which is undesirable for high quality substrates.[69] Initial use of ELO was able to reduce the number of threading dislocations from 10^8 - 10^{10} cm^{-2} to 10^7 cm^{-2}.[68] Subsequent removal of the substrate and additional ELO techniques have allowed for improved substrates that have led to threading dislocations on the order of 10^6 cm^{-2}.[40]

1.3.4 Liftoff Techniques

In addition to ELO, free-standing epitaxial or bulk GaN substrates offer another method to provide homoepitaxial deposition substrates for subsequent GaN growth. Initial methods of producing free-standing GaN structures include polishing away or using reactive ion etching to remove the substrate and subsequent defect rich layers.[71] These methods provided free-standing layers of GaN; however, surface roughening from each technique was

detrimental to future applications. The use of a UV laser to promote thermal liftoff of the GaN layer from foreign substrates improved the quality of GaN closest to the substrate as well as decreased processing time required for liftoff.[71, 72] The use of laser liftoff provides a high quality GaN layer for subsequent GaN deposition, which is often augmented with additional processing steps of chemical-mechanical polishing (CMP). Thermal liftoff can result in thermally induced cracking, which can be mitigated by heating the substrate during liftoff. Homoepitaxial grown GaN on free-standing GaN substrates provides increased bulk fabrication capabilities via HVPE and ammonthermal growth not available under other bulk techniques utilizing extreme growth conditions.[73]

1.3.5 Crystallographic Orientations

Gallium nitride has two primary crystal structures: wurtzite and zinc blende.[34] Zinc blende is frequently seen for thin GaN structures such as nanowires;[74] however, due to thermodynamic instabilities associated with processing and the lack of high quality bulk structures, zinc blende GaN remains a challenging research endeavor. The wurtzite crystal structure as seen in Figure 1, is a hexagonal prism. The basal plane, termed c-plane or polar GaN (Figure 1 a), is terminated in either gallium atoms (0 0 0 1) or nitrogen atoms (0 0 0 -1). Polar GaN was the first structure studied due to its natural formation on sapphire and is mass produced for transistor and LED applications due to high crystal quality.[34] Though polar GaN is readily produced in large amounts, the separation of gallium atom planes from nitrogen planes produces an internal electric field. The internal electric field creates a

piezopolarization and quantum-Stark effect, which through separation of charge carriers decreases the overall emission efficiency and produces blue shifting for LEDs.[75] To mitigate this spontaneous piezoelectric effect, other crystallographic planes of GaN were investigated. A-plane (Figure 1 b) GaN and m-plane GaN utilize crystallographic planes that have equal numbers of gallium and nitrogen atoms present.[59] This eliminates the internal electric field; however, processing issues from heteroepitaxial growth promote poor crystalline quality. Growth and dicing of GaN boules along desired planes have shown a promising way of developing native free-standing nonpolar structures of high quality.[59] In addition to nonpolar planes, semipolar planes with varying degrees of an internal electric fields based upon atomic composition are available depending on the desired application.

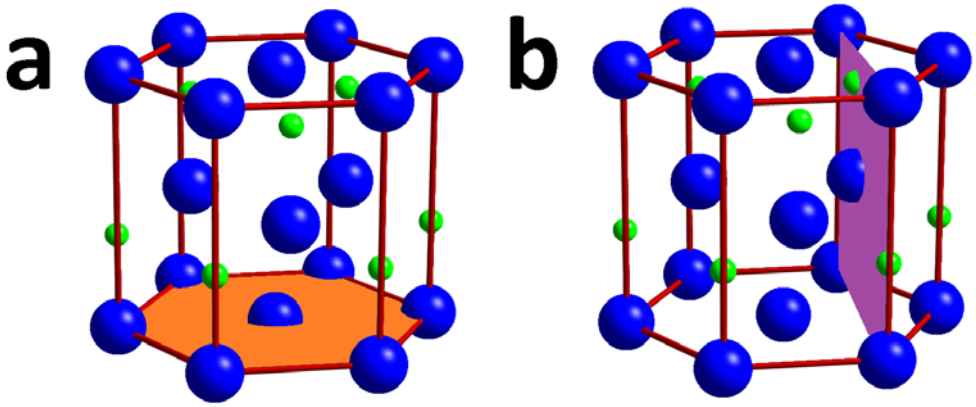

Figure 1 Representative wurtzite structures of c-plane (a) and a-plane (b) configurations for GaN. Blue represents gallium atoms while green represents nitrogen atoms.

1.3.6 Doping

Like most semiconductors, the electrical characteristics of the bulk material of GaN can be altered via doping species. Due to the foreign substrates being utilized for earlier heteroepitaxial growth, GaN was often unintentially doped with substrate species.[40] GaN frequently demonstrates background n-type doping, primarily from carbon contaminations within growth chambers as well as silicon incorporation from the use of silicon and SiC foreign substrates for growth.[34] N-type doping results primarily from shallow donors that have replaced nitrogen vacancies. The first reported instance of p-type doping for GaN was in 1989 with the use of magnesium.[76] Mg replaces gallium sites and by acting as an acceptor promotes the p-type carrier response within GaN. Better control of growth and purity allowed for deeper level dopants including Zn, Hg, Cd, Br, and Li.[34] Today, doping is routinely performed to create junctions for LEDs, transistors, and other applications.

1.4 GaN Defects

The majority of defects seen within GaN layers result primarily from the use of foreign substrates for growth. Two primary forms of defects occur from this interface: stacking faults (SFs) and misfit dislocations.[47] SFs form boundaries where the stacking order of planes of atoms is interrupted, thus creating stress from mismatched atomic spacings. Poor epitaxial quality is defined by SFs on the order of 10^5 cm^{-1} and frequently are found near basal planes.[77] Misfit dislocations are the manifestations of strain releases within the material through edge, screw, or mixed dislocations at the interface of an epitaxial

growth. Misfit dislocations are traditionally very difficult to identify, but their presence promotes decreased crystal quality of subsequently grown GaN.[47] Both interfacial defects pose challenges to final crystalline quality; however, the presence of threading dislocations is the greatest issue in terms of final device performance. Threading dislocations (TDs) are edge, screw, or mixed dislocations that permeate throughout the entirety of the crystal. TDs are choice spots for nonradiative recombination, which can limit performance for FETs, and LEDs. Most threading dislocations are composed of edge dislocations. Manifestations of threading dislocations within surface topography provide insight into misfit characteristics. For c-plane GaN, a hillock structure is the result of multiple screw dislocations, whereas a step-like structure is predominantly edge.[47] The use of MOVPE or MBE growth techniques can reduce the degree of screw dislocations to less than 10%. TDs on the order of 10^8 - 10^{10} cm^{-2} were common for initial GaN specimens, which has been cut to ~10^5 cm^{-2} in recent years.[47]

1.4.1 Surface Identification for C-Plane and A-Plane GaN

In addition to various underlying causes for a defect, the crystallographic orientation of GaN alters how a defect terminates. Surface topography is a convenient way to establish the types of defects, usually by techniques such as atomic force microscopy (AFM) or scanning electron microscopy (SEM).[78] As mentioned earlier, screw dislocations for c-plane GaN produce hillock structures, while edge dislocations result in a wave-like structure. Mixed dislocations are far more prominent in HVPE grown GaN than other growth processes

and form a mixed surface topography.[78] The surface topography of a-plane GaN is generally composed of facets throughout the structure.[79] Better processing techniques remove these facets; however, not all defects disappear. Defects frequently show up along c-plane directions within a-plane GaN.[80] Pits that would normally signify the termination of a dislocation for c-plane GaN are manifested as v-grooves along the surface.[81] Dislocations in a-plane GaN do not create hillock or step-like structures as within polar GaN; however, high defect densities can produce a wavy like structure. As high quality homoepitaxial a-plane GaN is developed, additional effects from basal plane stacking faults and prismatic/pyramidal stacking faults are seen from heteroepitaxial growth as jagged striations across the surface.[82] Collectively, they appear as lines and are not distinguished unless investigated by transmission electron microscopy (TEM).[82] M-plane GaN behaves similarly to a-plane GaN, but with an incorporated tilt. Semipolar GaN (such as r-plane) will not be discussed here as they were not utilized within this study.

1.5 Etching GaN

Semiconductor etching is frequently performed to expose regions of interest, whether they are areas for subsequent device fabrication or defect identification. In the case of device fabrication, chemical etching provides a means to remove material along specific crystallographic orientations while providing atomically smooth surfaces. Other methods of material removal such as mechanical polishing or reactive ion etching produce regions of

thermal and kinetic damage from friction.[83] In addition to higher quality surfaces, chemical etching is scalable for industrial environments whereas ion milling is not.

III-V semiconductor etching is challenging due to the natural resistance to chemical attack. Of the III-V semiconductors, GaAs was one of the first to be chemically etched, owing to its weaker overall chemical stability compared to other III-V semiconductors.[84] GaN is one of the most chemically stable III-V compounds, which limits etching to harsh chemicals such as molten potassium hydroxide (KOH), sodium hydroxide (NaOH), hot phosphoric acid (H_3PO_4), and sulfuric acid (H_2SO_4).[78] Additional etching techniques include UV-assisted etching, typically done with molten KOH or hot phosphoric acid.[85] The reaction of gallium nitride with water, utilizing the etchant as a catalyst, produces ammonia and gallium oxide.[85] Gallium oxide is soluble and unstable at both low and high pH values. Despite this, the nitrogen faces of GaN are less stable than gallium faces. This is observed in gallium terminated polar GaN. When exposed to etchants, the surface forms pits along the [0 0 0 -1] direction with nonpolar and semipolar facets.[86, 87] In the case of nitrogen terminated polar GaN, the reverse occurs: multifaceted pyramids form along nonpolar and gallium rich semipolar planes.[85] In the case of nonpolar GaN, v-grooves grow along the [0 0 0 -1] direction leaving semipolar {1 0 -1 1} facets behind.[86] In addition to providing a convenient way of identifying crystallographic polarity, chemical etching can be used to identify dislocations without the use of advanced microscopes like the TEM. Edge dislocations tend to form smaller pits for c-plane GaN than screw dislocations.

Mixed dislocations, being a mixture of both edge and screw, form pits of a medium size relative to either individual component.[78]

In addition to providing information on the material quality, etching enables additional benefits such as improved luminescent properties through increased surface area. The critical angle of escape for photons from GaN is 23.6° as described by Snell's Law.[85] By using smooth GaN, this angle is further decreased to as low as 4°, which limits the luminescence of the final device.[85] By etching along a c-plane threading dislocation, the subsequent critical angle increases and improves final luminescence. This has been shown in multiple studies for c-plane GaN.[85, 88] A-plane GaN does not benefit as much from this as continued etching produces line trenches that can eventually coalesce and limit the critical angle.[81, 86, 89] The increased surface area formed from etching enables additional binding sites by producing dangling bonds that are energetically unfavorable. Without capping dangling bonds unsatisfied carriers encourage charge annihilation through nonradiative recombination, which is detrimental for optical applications.[90]

1.5.1 Fabrication of High Aspect Ratio GaN Structures

Increasing the surface area beyond the limitations of 2D morphologies from above is achieved with aggressive etching techniques by utilizing higher temperatures, longer times, photo or electrical assistance, and/or multi-component etch processes. These extreme conditions accelerate the natural etching along specific orientations, particularly for defect rich substrates, which subsequently controls the number of features and subsequent

spacing.[78] Termed defect-assisted etching, high energy locations from terminating threading dislocations act as preferential etch sites as seen in Figure 2.[91] In this way, the final device morphology can be controlled by the aforementioned conditions. This allows the formation of nanorods,[92] nanopyramids,[93] nanowires,[78] and other morphologies that are otherwise unavailable. For applications, the high aspect ratios increases the number of potential binding sites that in the case of sensors, allows for significantly greater responses to environmental conditions and subsequent binding events.[94, 95]

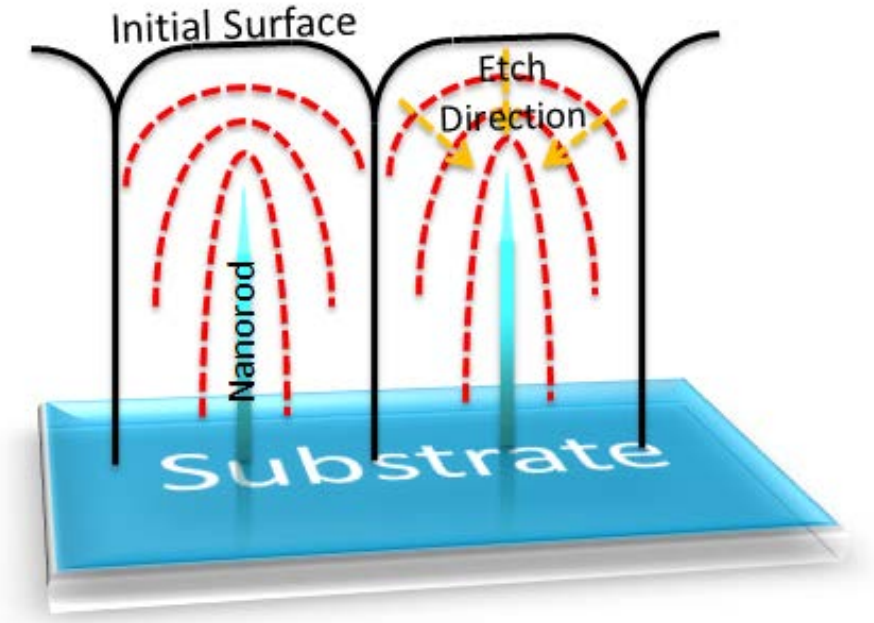

Figure 2 Schematic of defect-assisted etching for forming 3D GaN structures. Threading dislocations are shown as black lines connecting the substrate to the initial surface.

1.6 Surface Passivation of Semiconductors

Surface functionalization of semiconductors provides a convenient way to modify the surface optical and electrical characteristics without use of material or equipment intensive processing.[96] Though the bulk properties are controlled by overall quality of the crystal such as dopants used or defects present, the surface interface ultimately controls properties such as electrical conductivity, chemical selectivity, and optical recombination events. In the presence of a total vacuum, the surface would be covered with unsatisfied bonds. With the addition of atmosphere, these dangling bonds seek to lower their energy by reacting with surrounding molecules to create a passivated layer.[97] In the case of semiconducting materials, this is often the formation of an oxide layer, which with increased humidity can terminate the surface with hydroxyl or hydrogen species.[98] To improve device performance, uniform surface profiles are required to limit complications from undesirable adsorbates. In the case of optical properties, undesirable species and defects can lead to nonradiative recombination of charge carriers.[99] This limits the overall emission efficiency and produces unwanted heat. This is also seen electrically with higher sheet resistances from nonradiative recombination events [100] and high carrier recombination velocities.[101] For electrical interfaces of semiconductors the difference in work functions, controlled by the Fermi level within the bandgap, hinder device performance through charge trapping.[102] By controlling the surface chemistry, these properties can be manipulated to ensure desired function.

Organic based surface functionalization of semiconductors has seen significant developments due to desirable properties such as environmental stability, unique electrical and optical properties, secondary binding platforms, chemical selectivity, and simplified processing methods. Organic functional groups are composed of a binding group and a tail or terminal group as represented in Figure 3. The binding group determines the stability of adhesion whereas the tail and terminal groups control properties and assembling characteristics. For the most part, these molecules assemble themselves without the need for external coercion, which are termed as self-assembling molecules (SAMs). Many factors control the adhesion such as temperature, pressure, and solvent solution; however, these specific parameters allow for flexibility in device fabrication. Processing of SAMs usually takes the form of an evaporative process [103] or a lengthy soak [104] to encourage coverage; however, this dissertation focuses on a rapid immersive process that combines both functionalization and substrate etching into one.

Of the SAMs currently being investigated, only thiol and phosphonic acids were chosen for this study. By isolating two binding groups, the properties from unique terminal groups are explored in detail as will be discussed in future sections.

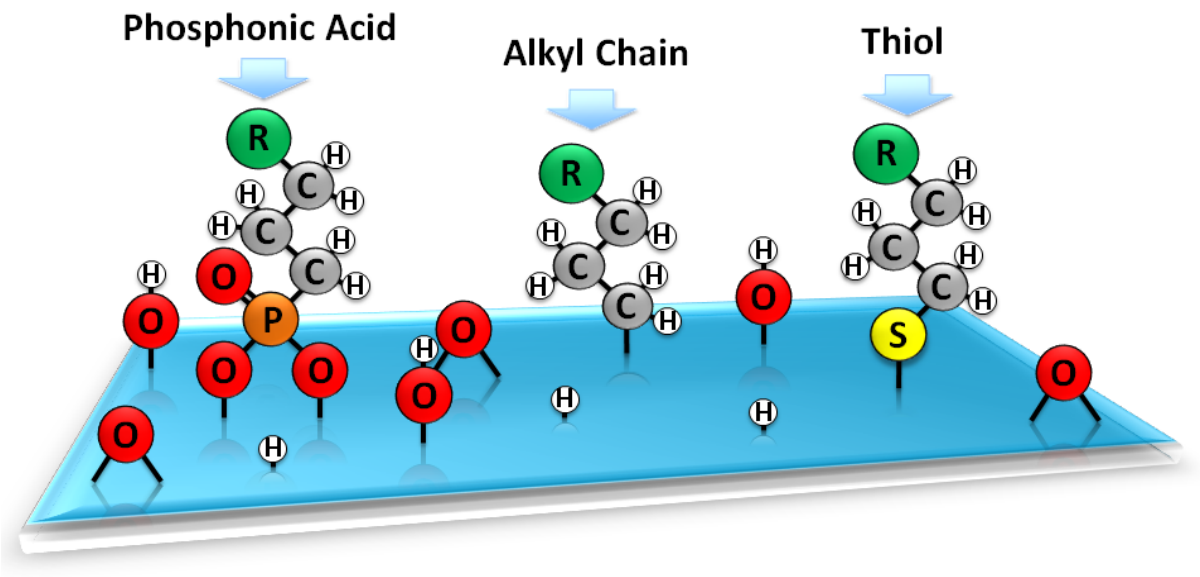

Figure 3 Representation of a few potential binding adsorbates for III-V semiconductors.

1.6.1 Surface Passivation with Thiols

Sulfur group adhesion to III-V semiconductors for simultaneous stability and electrical enhancement was first observed in 1987 on GaAs.[101] It wasn't until 1991 when organic sulfur functional groups were introduced to GaAs with a similar role.[105] In the years following, GaAs saw an explosion in surface functionalization primarily with octadecylthiol [106, 107] and similar long chained thiols.[108] Long chained thiols are well studied and consistently form monolayers. The adhesion of thiols depends entirely on the purity of the substrate surface. Thiols readily bind to noble metals due to minimal oxygen contamination as oxygen limits thiol adhesion due to charge repulsion. In the case of GaAs,

oxides must be removed prior to functionalization to ensure complete binding. This is performed with a series of oxide removal strategies such as HCl and HF.

Thiol functionalization of GaN was first explored in 2003 with 1-octanethiol.[109] Since then, GaN has remained an unexplored substrate for thiol functionalization. In light of recent research, cysteamine has shown many interesting properties as can be seen in Table 2. Cysteamine is a short double carbon backboned thiol with an amine terminal group that has been used as an agent for overdoses of paracetamol [110] as well as kidney protection by reducing cystine storage from cystinosis.[111] For this reason, cysteamine has garnered a lot of attention from the quantum dot community as a potential passivating agent to reduce cell necrosis but improve quantum dot uptake. For bulk materials such as GaAs and InAs, cysteamine has demonstrated the ability to limit oxide formation and control surface stability in a variety of environments.[112-114] The possibilities discussed have led to patenting of this passivation technique with the intent of forming biological sensors. [115] Cysteamine's amine group provides additional binding sites without the added toxicity from aromatic, aliphatic, or heterocyclic groups in addition to providing a dipole moment with a positive terminal group.[116] Unlike octadecylthiol, cysteamine does not always form a well ordered monolayer. It is a time and concentration sensitive functionalization process rather than a kinetic based process as discussed in future chapters.

Table 2 Thiol functionalization on various semiconductors and observed properties.

Substrate	Functionalization Process	Observed Properties	Ref.
InAs	1 hour full solution dip. Concentrations of 1, 10, 100 mM cysteamine in ethanol. Temperature not specified.	Cysteamine reduced formation of oxide.	[112]
InAs	30 minute full solution dip. Concentrations of 10 mM cysteamine in 1:9 NH4OH :ethanol. Performed at 55°C.	Simultaneous oxide removal and surface functionalization was observed with cysteamine.	[114]
GaAs	18 hours of full solution dip. 5 mM cysteamine in ethanol with 5% ammonia. Performed at 55°C	Cysteamine did not enhance passivation or PL intensity unlike longer chained thiols. Demonstrated hydrophobicity.	[113]
CdTe	2 hours full solution dip and sonicated. 0.24% cysteamine hydrochloride in water. Temperature not specified.	Cysteamine decreased metabolic cell rates at dose above 10 mg/mL but decreased fluorescence of QDs	[117]
CdS, ZnS	Time not specified. Cysteamine hydrochloride aqueous solution. Performed at room temperature.	Increased absorbance and blue shifted PL spectra. Reduced electrical resistance and capacitance.	[118]
CdTe	Time not specified. 2:4:1 CdCl2:cysteamine:NaHTe aqueous solution. Performed at 100°C.	Allowed for binding of single strand DNA to CdTe for improved fluoresce. Redshifted absorbance.	[119]
CdTe	25 minute reflux process. Cysteamine hydrochloride (2.64 mM) in NaHTe solution. Heated to reflux temperature.	Stable PL intensity in PBS and redshifted absorbance. Low uptake cysteamine treated QDs with human SH-SY5Y cells. Lowered mitrocondrial activity, but high uptake capability	[120]
ZnS coated CdSe	Time not specified. 1:1 cysteamine:thioglycerol solution. Temperature not specified.	No DNA damage observed with 4 μM solution for 12 hours.	[121]
CdTe, ZnS coated CdSe	Time not specified. 1:1 cysteamine:thioglycerol solution. Temperature not specified.	Lowered QD uptake with CdTe, but lowered luminescence and increased leaching for CdSe based QDs.	[122]

1.6.2 Surface Passivation with Phosphonic Acids

Surface passivation with phosphonic acids (also known as alkyl phosphonates) have seen use on metallic oxide formations such as TiO_2,[104] ZnO,[103] Ta_2O_5 [123] as well as semimetal oxides like SiO_2.[124] Similar to thiols, phosphonic acids have been explored as a way to pin the Fermi level to control properties such as surface recombination velocity and the work function. In applications such as solar cells, controlling the degree of band bending in electrode materials such as ZnO and TiO_2 is crucial in order to enhance overall device efficiency. Alkyl phosphonic acids boast unique features such as a customizable carbon backbone that can support a myriad of terminal and side groups that can alter surface properties.[18, 104, 125] In the case of dye-sensitized solar cells, charge recombination can be prevented through the use of phosphonic acids for better interfaces with sensitizer materials. Phosphonic acids differ from thiols in that adhesion utilizes a binding group with three oxygen atoms, which offers more binding mechanisms as seen in Figure 4. This subsequently offers a higher probability of surface passivation. Unlike thiols, phosphonic acids require a native oxide layer in order to bind. This benefits surface passivation techniques as ultra-pure processing environments are not necessary. With recent interest in environmentally stable interfaces for chemical and biological applications, phosphonic acids have seen use with materials such as ZnSe,[126] GaAs,[127] and GaN (seen in Table 3).

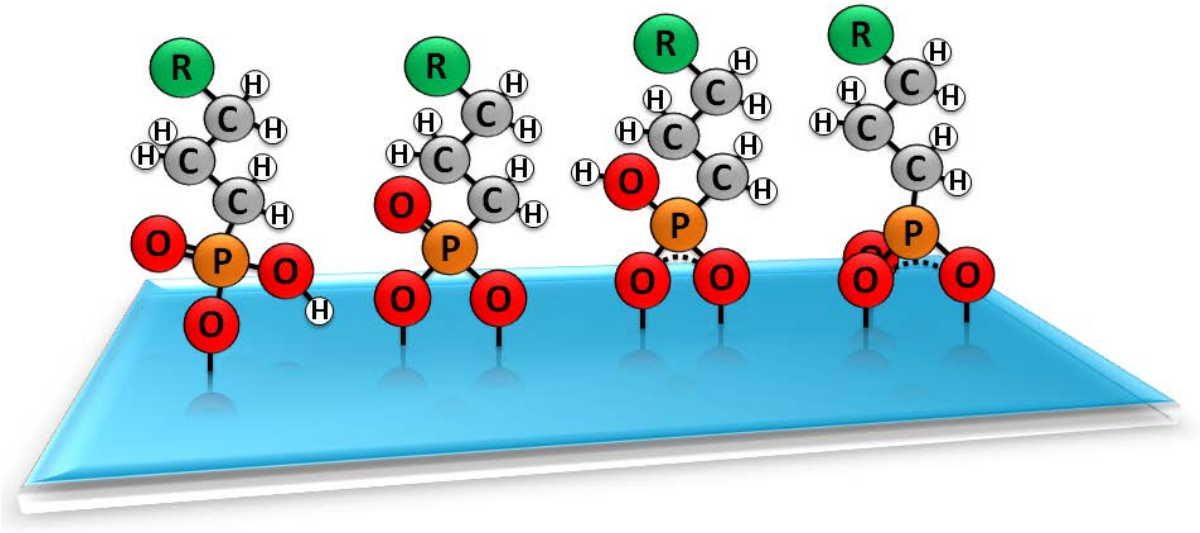

Figure 4 Potential binding mechanisms for phosphonic acids.

Table 3 Phosphonic acid functionalization of GaN and observed properties.

Chemical Name	Functionalization Process	Observed Properties	Ref.
Octadecyl-phosphonic acid (ODPA)	1-5 mM in tetrahydrofuran (THF) for unspecified time and temperature.	ODPA was hydrophobic while octadecanethiol (ODT) was not. ODPA survived one week, while ODT did not.	[128]
11-hydroundecyl phosphonic acid (HO-UDPA), octadecyl-phosphonic acid (ODPA)	1 mM ODPA in THF solution at 130°C for 48 hours. Sonicate for 30 minutes. Repeat with 50 µM HO-UDPA.	ODPA was more stable than HO-UDPA in pH 5 and 7, but not within a pH 9 solution. Thiol stable in pH 9 solution.	[129]
Octadecyl-phosphonic acid (ODPA)	5 mM ODPA in toluene for 17 hours. On set baked at 160°C at 0.6 torr for 24 hours.	ODPA induced hydrophobic behavior, with a slight increase in water contact angle for N-polar verses Ga-polar. Heat treatment improved adhesion in acidic and neutral environments only.	[130]
Octadecylphosphonic acid (ODPA) and 16-phosphonohexa decanoic acid (16-PHDA)	1 mM in toluene for 15 hours at room temperature. Rinsed in toluene and baked at 160°C for 72 hours.	16-PHDA reduced sheet resistance compared to control and ODPA treatment. Fermi level pinning was observed.	[131]
Diacetylenicalkyl phosphonic acid (DEAPA)	0.1 mM DEAPA in toluene for 17 hours. Baked at 160°C at 0.6 torr for 24 hours. Treated with UV light for various amounts of time.	DEAPA showed hydrophobicity; but desorbed without UV irradiation. Most hydrophobicity seen with 5 minutes of irradiation. Basic solution removed material and DEAPA.	[132]
Octadecyl-phosphonic acid (ODPA)	5 mM ODPA in toluene for 17 hours. On set baked at 160°C at 0.6 torr for 24 hours.	ODPA had water contact angles greater than other surface treatments. AFM revealed smooth treated surfaces. Good coverage.	[133]

1.6.3 Environmental Passivation

Though briefly touched on in the previous sections, environmental stability of semiconductors remains an ongoing research topic, particularly in the case of III-V semiconductors. For GaN, a thin (1-5 nm) amorphous oxide layer forms in ambient air and subsequently inhibits further growth of the oxide layer.[6, 134] Unlike a mono-species material such as Si that only produces SiO_2, GaN produces a myriad of oxides and sub-oxides that have varying electrical and chemical properties. For applications in aqueous environments, the pH and electric potential controls the stability of the surface and subsequent leaching species as seen in Figure 5. As GaN contains multiple species, the environmental stability is highly contingent on ratio of III to V species on the surface. Previous studies have shown that increased V content on the surface leads to increasing leaching characteristics, which is frequently seen for harsh conditions with etching.[135] This is a result of smaller dissociation energies required to break bonds for V species than for III species.[136, 137] For a device within an aqueous solution, it is therefore imperative to subsequently cap the surface (substrate and any formed oxides) to prevent additional leaching that might occur. Surface functionalization provides a mechanism to alter the optical and electrical properties as previously mentioned, but also a way to reduce unsatisfied bonds and stabilize surface oxides. To test the effectiveness of surface functionalization, GaP, a III-V semiconductor with an indirect bandgap of 2.26 eV,[138] will be compared to GaN as a way to identify the effectiveness of surface passivation as well as the stability of another III-V compound.

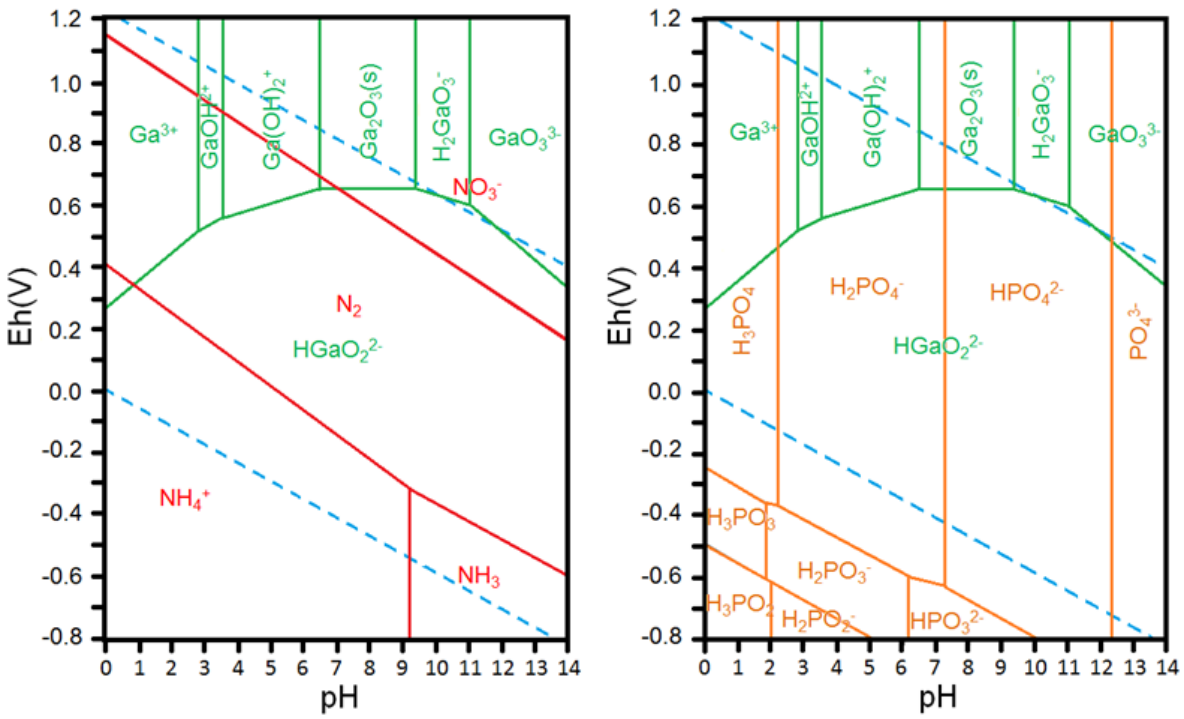

Figure 5 Soluble III-V species for GaN (left) and GaP (right) within various aqueous environments.[139]

1.7 Characterization Techniques

In an effort to characterize surface passivation effects, surface sensitive techniques such as X-ray photoelectron spectroscopy (XPS), water goniometry (also referred to as water contact angle), and atomic force microscopy (AFM) coupled with kelvin probe force microscopy (KPFM) are used to identify alterations to surface chemistry, hydrophobicity, topography, and electrical properties. Additionally, inductively coupled plasma-mass spectrometry (ICP-MS) and photoluminescence (PL) were utilized for aqueous particle concentrations and photoluminescence emission. Mentioned techniques will be discussed in

detail in the following sections. Other characterization methods that performed include X-ray diffraction (XRD) and optical microscopy; however, they will not be discussed due to their minor contributions to this dissertation.

1.7.1 X-ray Photoelectron Spectroscopy

XPS provides high resolution surface chemistry analysis through the photoelectron effect. Originally discovered in 1887,[140] the photoelectron effect operates by extracting electrons from a material via photon excitation. The orbital that the electron is removed from corresponds to a specific binding energy required to remove it from the atom. In the case of the modern XPS, which has been around since the 1950s,[141] x-rays are used to excite electrons to identify surface species through equation 1.[142]

$$h\nu = \mathrm{KE} + \mathrm{BE} - \Phi \quad (1)$$

The energy of the x-ray source is $h\nu$ and defined as 1486.7 eV for an Al Kα source or 1253.6 eV for a Mg Kα source. The kinetic energy (KE) is the energy that the electrons strike an electron analyzer with. The work function (Φ) of the spectrometer is a collection of energies from analyzer heating and other processes that account for no more than 2 eV.[143] Knowing the calibration of the instrument allows this term to be ignored. By knowing the KE and $h\nu$, the binding energy of an electron can be calculated, which is associated with a specific band within the material electron structure (see Figure 6). Each electron with a specific energy is summed up to produce an intensity profile within a given binding energy spectra.

Intensities of different binding energies are compared to one another, which allows for a qualitative analysis of chemical composition. Large survey scans are typically used to identify sources of contamination and other impurities. Survey scans utilize large pass

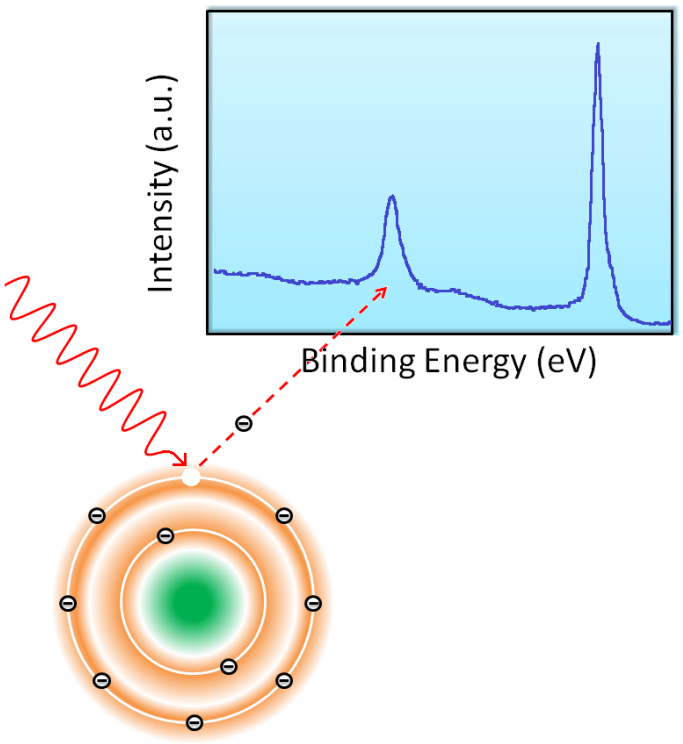

Figure 6 Interaction of x-ray with electron to form photoelectron effect and the resulting spectra.

energies, which limits the resolution. By decreasing the pass energy, region scans provide high resolution spectra of specific binding energies that allow for detailed analysis. Prior to analysis, charge calibration must be done to ensure the peaks are where they should be assigned. As XPS acts similar to a chemical fingerprinting technique, lack of calibration or

inappropriate calibration can skew interpretation. As advantageous carbon is present in all environments, calibrating the primary carbon 1s peak to 284.8 eV is both convenient and well expressed.[144] Other internationally accepted calibrations include Cu 2p3/2 at 932.62 eV, Ag 3d5/2 at 368.21 eV, and Au 4f7/2 at 83.96 eV according to the International Standards Organization.[145]

When analyzing a region, the observance of peak shifting indicates two things: potential charging effects associated with a nonconductive surface and/or the possibility of additional binding species on the surface. In the first case, charging is frequently seen for GaN, especially when using a monochromated source. Monochromated sources improve final resolution by interacting with a smaller surface area, through a shorter x-ray line width, and reducing noise due to bremsstrahlung radiation and satellite peaks.[142] The downside to a monochromated source is confined beam energy across a small area that results in thermal artifacts as well as charging. To account for this, a charge neutralizer plants lower energy electrons near the region of charging to dissipate energetic species. This is in addition to utilizing conductive sample mounting platforms to encourage charge dissipation, as well as decreased dwell time. Charging manifests as increased noise within survey scans as well as shifting of peaks to higher binding energies, hence calibration is used to account for these artifacts. In the second case, peak shifting implies binding associated with various unique elemental species. Based upon the materials being analyzed, this can move to higher or lower binding energies. As discussed in future chapters, the binding energies of GaN are associated with oxides (higher binding energies) and native metal bonding (lower binding

energies).[142] This is generally seen as more energy is required to remove an electron from an ionic bond than a metallic bond.

High resolution region scans also enable quantification. The areas produced under individual components contribute to a total signal area that when related to other species can identify atomic compositions. Care must be taken as overlap between bound species can occur, which also includes doublets and auger peaks. Auger peaks pose a problem for GaN as gallium auger peaks overlap N1s peaks with a Al Kα source [146] and overlap C1s peaks with a Mg Kα source.[147] As calibration was performed with C1s, gallium auger peaks were identified via peaks with broad full width half max (FWHM) almost twice the width of the primary N1s peak.

The use of quantification when performing angle resolved XPS allows for film thickness measurements. The spectra formed by tilting the sample can be used to characterize the degree of coverage for a monolayer in addition to identifying the depth of oxides and shallow elemental species. By exposing the surface to a greater surface section, the propensity for noisy signal increases with increasing take-off angle. Multiple scans of a given spot ensure an accurate intensity capture as well as reduced noise levels when averaged over the course of the scans.

1.7.2 Photoluminescence

PL is a frequently used nondestructive technique for understanding underlying contributions to the optical properties of materials. PL has existed since the late 1960s when

high powered lasers were being unveiled.[148] The general operating principle of PL is the excitation of charge carriers, the formation of an electron-hole pair known as an exciton, with a photon source with energy greater than the band gap. Because of this, PL is largely relegated to materials with a distinct band gap such as semiconductors and some insulators.[149] Following excitation, the exciton relaxes and the charge carriers migrate back across the band gap to recombine. Depending on the mode of relaxation, phonons (typically heat through nonradiative recombination) or photons (light through radiative recombination) are released. This nearly simultaneous process allows for the measurement of contributions to the optical properties by unveiling modes of recombination in the form of spectral intensity. Factors such as lattice parameters, defects, dopants, and many others contribute to the final radiative emission, which is the only observable signal.[149] In the case of direct band gap semiconductors, the number and type of contributions influence the final radiative radiation as seen in Figure 7. For band to band recombination, the shortest wavelength is released, indicating high purity and crystalline quality. The introduction of shallow donors and acceptors increases the emitted wavelength, which is only further increased with deeper level donors and acceptors.[149]

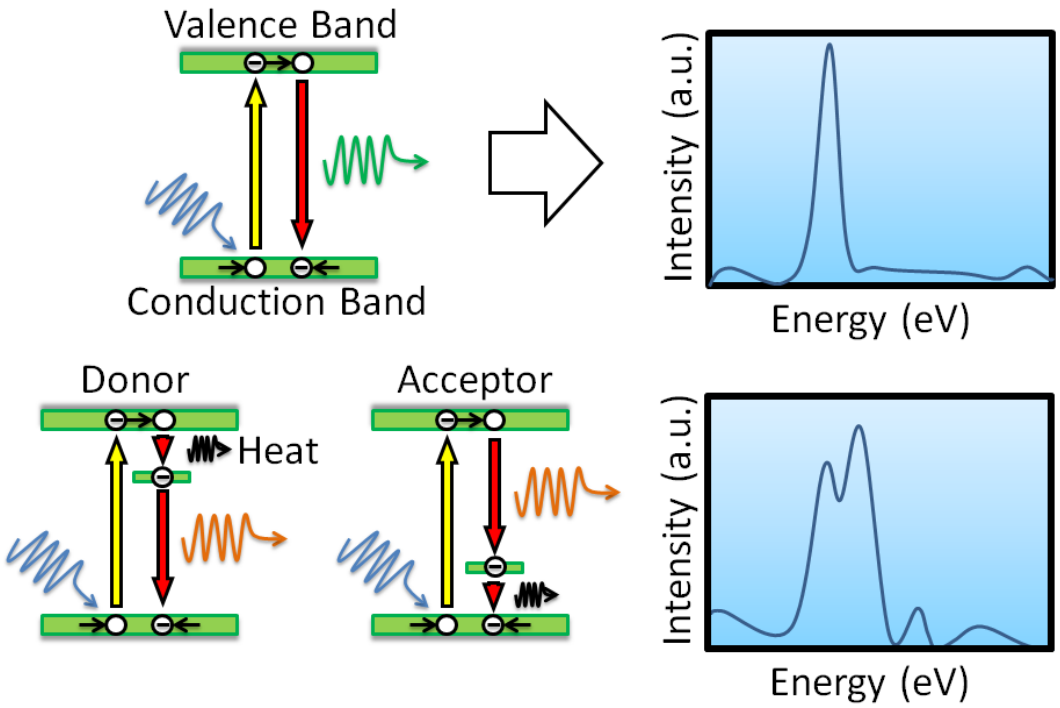

Figure 7 Example of PL recombination events for band to band (top) versus defect driven recombination from donors and acceptors (bottom) and resulting spectra.

By comparing a defect free material the degree of non-band to band recombination contributions can be estimated.[148] In the case of doping, this provides a reliable check for growth complications. The lack of a pristine material can limit this, especially when performed at room temperature. Reducing the temperature to liquid helium (~4 K) narrows the peak FWHM revealing individual band relaxation events.[149] This temperature dependent behavior is attributed to the density of carriers available, which will recombine at a slower rate at lower temperatures.[148] Cooling the material suppresses much of the nonradiative recombination events that contribute to wider FWHM and red-shifting for many semiconductors. For this dissertation, the quality of GaN was high enough to not require the

use of low temperatures to achieve discernable differences between treatments. Additionally, room temperature PL allowed for batch processing of samples to eliminate variance between laser output and focus. Another way of resolving recombination mechanisms is measuring the decay intervals between excitation. This can discern band overlap, especially when combined with lowered temperatures.[150]

Due to the excitation based response, the laser wavelength must be smaller than the band gap. By utilizing different laser sources such as HeCd or Ar, different penetration depths are possible, which provides flexibility for regions of interest. All PL performed throughout this dissertation utilized a 325 nm HeCd laser that penetrates a maximum depth of 40 nm.[149] This shallow profile allows greater analysis of the effects that surface species have on the final surface optical properties. Other factors that go into the final spectra include resolution, which is determined by the grating or separator within the detector. The focus of the laser and signal filtering contribute to final spectra output and only prevent detector saturation.

1.7.3 Atomic Force Microscopy

AFM is one of many surface characterization techniques available today. Unlike techniques such as SEM, AFM provides qualitative as well as quantitative data. AFM operates by reflecting a laser off of a cantilever that responds to interactions between a tip and the surface as seen in Figure 8. The reflected laser is detected with a quadrant photodiode that compiles images from each line scan. AFM boasts of a wide range of capabilities from

identifying binding events on a surface [151] to surface roughness,[152] potential,[153] magnetic fields,[154] and chemical identification.[155] To simplify the discussion, only surface topography and surface potential will be discussed. Developed in 1981, the first AFM utilized a current through the tip (also known as scanning tunneling microscopy) to image conductive atomic species.[156] It was not until later (1986) that the first contact mode was developed to identify insulating species by interaction with coulomb and van-der-Waals forces.[157] There exist two primary modes within AFM: noncontact and contact. Noncontact relies on the minute attractive forces between the surface and the tip. As these forces are on the order of pN-fN, very little interaction occurs between the tip and the surface.[158] This prevents tip blunting and the formation of artifacts frequently seen within contact based AFM; however, noncontact AFM requires the use of ultra-high vacuum as well as cryogenic temperatures to achieve resolvable data.[158] Noncontact modes are frequently carried out with soft materials due to delicate structures. On the other hand, contact mode utilizes strong repulsion forces to resolve topography. The stronger forces result in the physical deformation of AFM tips, which can produce artifacts and other defects.[156] As the tip geometry controls the final resolution, a sharper tip is required to achieve higher resolutions. By blunting the tip, the final resolution is limited to the new tip radius of curvature, which should the tip become excessively dull, facets from tip fabrication appears as either regular triangular or square-like features. Unexpected prismatic structures should not be confused with novel features for self-assembled or nanofabricated devices.

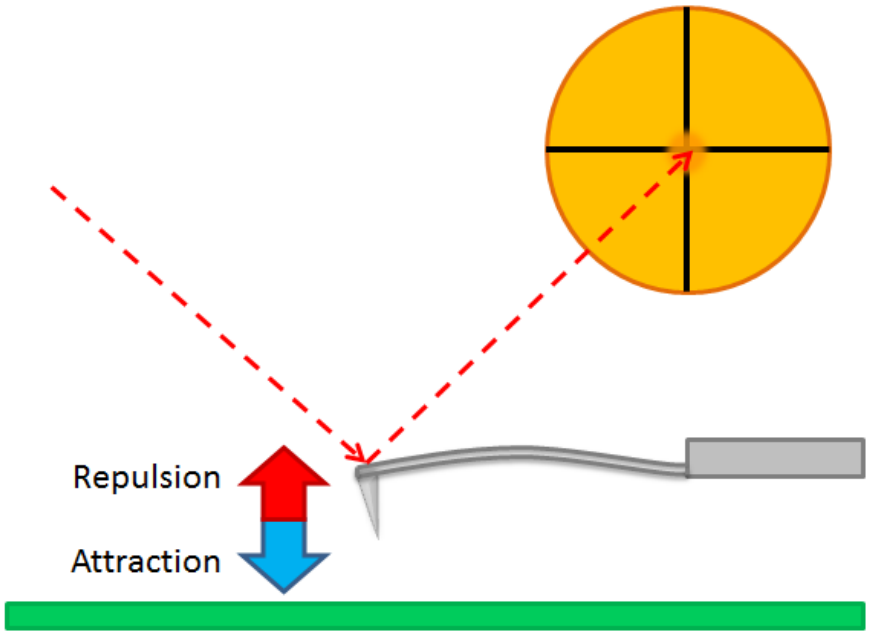

Figure 8 Schematic of AFM tip assembly and interaction with surface and photodiode.

Within contact mode, two additional modes exist: contact and tapping (or frequency) mode.[156] Contact mode utilizes AFM cantilevers with lower spring constants such as Si_xN. As this mode remains in constant repulsion with the surface, increased tip dulling as well as contamination adhesion frequently occurs. Tapping mode (used in this dissertation) pulses the cantilever with an AC current at a harmonic frequency according to its geometry and spring constant. Stiffer materials are frequently used as higher resonance frequencies are attainable, which improves topography tracking. With each oscillation, the tip comes in contact with the surface and is repelled. Each deflection is recorded and compiled to form the final micrograph. Tip dulling is reduced with decreased points per line, which corresponds to the final image resolution.

1.7.3.1 Kelvin Probe Force Microscopy

KPFM allows for the detection of surface charged species by charging the cantilever and detecting the forces between the tip and the surface.[159] The measured forces are in direct response to the capacitive cavity formed between the probe (referenced at 0 V) and the sample surface. In operation, KPFM produces both topographic and surface potential maps. This is done by rastering the tip across the surface in repulsion mode (topography) and following with a second raster at a user specified distance (typically between 1-40 nm) in an noncontact mode (surface potential). KPFM was first developed in 1991 to identify features that would go unnoticed with a traditional topography image.[159] The charge sensitive nature of KPFM allows for accurate identification of work functions with the use of reference electrodes or materials with known work functions such as pyrolytic carbon.[160, 161] In addition to identifying nanoscale particles, KPFM can identify surface defects due to resulting dangling bonds [162] as well as charged adsorbates used for electronic surface functionalization.[153] This latter feature is the focus for work within this dissertation as adsorbates can contain significant dipole structures.

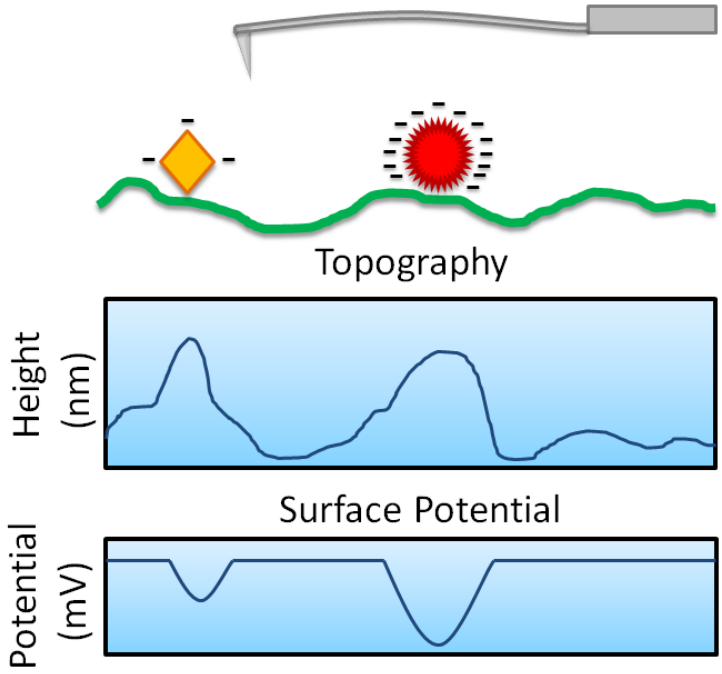

Figure 9 Schematic of KPFM operation and resulting profile scans.

1.7.4 Inductively Coupled Plasma Spectrometry

ICP-MS has been around since the 1980s.[163] ICP-MS offers another ultra-sensitive elemental analysis that can readily achieve resolutions on the order of ppb and sometimes ppt.[164] In comparison, XPS frequently reports concentrations (surface only) on the order of ppm to ppb.[142] Unlike XPS, ICP-MS is a destructive testing technique. This is done by stripping away electrons from atomic species with a plasma to form ions that then pass through an electric field and separate based upon charge and mass.[164] Because of this, subsequent repeat testing is not possible. Another ICP technique known as inductively coupled plasma-optical emission spectroscopy (ICP-OES) is also frequently used. Instead of

using an electric field from a quadrapole to separate masses, species are separated by color spectra.[165] As individual atomization is required to enter the plasma and form ions, materials must be in a gaseous form. Most accepted materials are in solution form to facilitate this. There have been studies utilizing ICP to etch away materials; however, for the purposes of spectroscopy the power required is too high to observe without detector damage.[166] Materials accepted within ICP-MS and ICP-OES tend to be metallic or semimetallic as these materials are more readily ionized. To improve sensitivity, solutions may be digested or significantly diluted to less than 0.1 M concentrations.[164] Care must be taken for sample solutions as certain digestion can interfere with quantification or chemically attack the equipment. For the purposes of this dissertation, ICP-MS was used in preference to ICP-OES as higher sensitivity was obtained with ICP-MS.[165] It should be noted that no samples tested throughout this dissertation required the use of digestion.

1.7.5 Water Goniometry

Water goniometry provides information on surface hydrophobicity, which is controlled by the degree of functional surface group coverage, contamination, and topography.[103, 167, 168] Fluid goniometry covers a wide range of solutions (oils, solvents, water, etc) in addition to various techniques for measurement (static drop, receding drop, advancing drop, bouncing, coalescence, etc).[169, 170] The final droplet size is controlled by the three interfacial energies in equation 2 as shown in Figure 10.

$$\gamma_{SV} = \gamma_{LV}\cos\theta + \gamma_{SL} \quad (2)$$

Equation 2, frequently referred to as Young's equation, relates the liquid-vapor interface (γ_{LV}) to the solid-liquid (γ_{SL}) and solid-vapor (γ_{SV}) interfaces. The angle between γ_{SL} and γ_{LV} is known as the contact angle (θ). The contact angle varies depending on the surfaces, fluids, environment, and approach. Techniques involving hyper dynamic (bouncing, splashing, etc) testing require the use of high speed cameras to capture the angles at point of impact. This is often to demonstrate environmental conditions that surfaces might experience in an outdoor environment. Other types of dynamic testing include advancing and receding contact angles. The slower motion by retaining the drop on the tip of the dispenser allows for detailed analysis of spreading on the surface with respect to the dispenser material. In other words, the angle is no longer between the liquid and the substrate. The benefit of these techniques is a decrease in error resulting from nonuniform surface coverage or contamination.[170] Static contact angle relies on equilibrium between all of the interfaces and does not require high speed cameras or other specialized equipment. Static contact angle provides a method of identifying interfacial energies when in contact for large amounts of time. For the purposes of this dissertation, fluid goniometry is limited to water and static measurements to identify surface group effects on hydrophobicity.

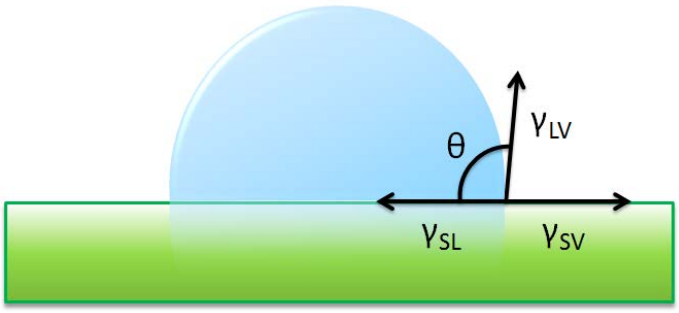

Figure 10 Diagram of droplet and interfacial forces acting on it.

1.8 Summary

The utilization of an acid etch in conjunction with a desired adsorbate provides a simplified process that is designed to alter the surface properties of a host material. Though surface functionalization is routinely done without etchants for many material systems, the use of an acid etch provides a simultaneous alteration to the surface topography as well as surface chemistry by inducing increased numbers of exposed bonds for potential binding sites. It is through this assistance that improved chemisorption of adsorbates takes place, which can lead to more complete surface coverage. The primary questions that this dissertation addresses are the roles GaN topography, crystallographic orientation, and surface terminations have on adsorbate binding events. The functional groups attached to organic adsorbates are used to alter the electrical and optical properties as well as chemical stability of GaN, which has been little explored to date. By choosing GaN, compatible binding groups and etchants are limited due to functionalization mechanisms and GaN's natural chemical resistance; however, it is the aim of this dissertation to explore these limitations with a

material that demonstrates excellent potential for future light emission, chemical sensing, and biosensing applications.

2. Effect of Etching with Cysteamine Assisted Phosphoric Acid on Gallium Nitride Surface Oxide Formation

Stewart J. Wilkins,[1] Tania Paskova,[1,2] Albena Ivanisevic[1,3]

[1]Department of Materials Science and Engineering, North Carolina State University, Raleigh, North Carolina, 27606, USA

[2]Department of Electrical and Computer Engineering, North Carolina State University, Raleigh, North Carolina, 27606, USA

[3]NCSU /UNC-CH Joint Department of Biomedical Engineering, North Carolina State University, Raleigh, North Carolina, 27606, USA

The following manuscript is reprinted with permission from S.J. Wilkins, T. Paskova, A. Ivanisevic, "Effect of etching with cysteamine assisted phosphoric acid on gallium nitride surface oxide formation," *Journal of Applied Physics*, **2013**, 114 (6), 064907.

2.1 Abstract

In-situ functionalization of polar GaN was performed by adding cysteamine to a phosphoric acid etchant in order to study its effect on photoluminescence and oxide formation on the surfaces. The functionalization was characterized by atomic force microscopy, x-ray photoelectron spectroscopy, photoluminescence (PL), and water contact angle measurements. Two sets of polar GaN samples with different dislocation densities were evaluated, thin GaN layers residing on sapphire and thick freestanding GaN separated from sapphire substrate aiming to reveal the effect of material quality on in-situ functionalization. The addition of cysteamine to the phosphoric acid solution was found to

result in: (i) decreased surface roughness, (ii) no change to hydrophobicity, (iii) decreased oxygen content especially at high-temperature treatments. The effect of the in-situ functionalization on the PL efficiency was more pronounced in the free-standing sample than in the film residing on the sapphire, which was attributed to a higher crystal quality free from strain.

2.2 Introduction

Nitride materials are III–V semiconductors characterized by a bandgap spanning wide ranges from 0.7 to 6.1 eV and [34] desirable for many optoelectronic applications, primarily blue and UV light emitting diodes (LEDs) as well as high frequency and power transistors.[171] In addition to its use in traditional semiconductor applications, GaN has been shown recently as a suitable candidate for biological interface applications due to GaN's chemical stability [172] and biological compatibility.[173] Polar GaN layers with (0001) surface orientation grown on sapphire substrates by hydride vapor phase epitaxy (HVPE) are often preferred templates for epitaxial growth of devices structures, aiming to avoid the low-temperature buffer, while the free-standing quasi-bulk GaN released from the substrates are the most desired substrate for homoepiatxial growth due to substantially lower defect density achieved in this material. The HVPE offers faster growth than processes such as metal organic vapor phase epitaxy (MOVPE) or molecular beam epitaxy (MBE).[59] This faster, high quality growth of polar GaN allows for thicker GaN with low amounts of threading dislocations and stacking faults that is common amongst heteroepitaxy deposition

techniques (growth of GaN on sapphire or silicon carbide).[59, 174] The very nature of polar GaN results in a spontaneous polarization due to specific packing of the wurtzite crystal structure with Ga or N atoms, which in turn affects doping capabilities,[175] carrier distributions,[176] and emission wavelength.[177] Aiming to modify the surface properties of GaN in a controllable way doping with various elements has been explored. Examples include Mg [178, 179] and Si [179, 180] for p- and n-type GaN, respectively. Alternatively, the surface can be etched (via heated KOH [85, 86, 88] or phosphoric/sulfuric [81, 85] acid) or coated with thiols,[109] or other molecules.[14, 129, 181-184] The etching and surface functionalization routes provide convenient ways to modify GaN surface properties without the need for intensive doping strategies that predominantly rely on hazardous chemicals.[180, 185] Etching adds the ability to alter both the surface morphology as well as composition through the formation of pitting structures, which cannot be accomplished by only chemi- or physisorbing compounds on the surface.[186] Etched polar GaN has shown increased luminescence over pristine GaN, which produces more efficient optoelectronic devices.[88] Etching processes are sensitive not only to the etchant being used,[180] but also to the temperature,[187] time,[187] and pressure,[188] hence pairing additives with etchants may result in unique properties not seen before. Phosphoric acid acts as the catalyst as well as solvent for dissolved gallium oxide during the etching process. We hypothesized that one can alter the amount of gallium oxide formed on the surface if a small organic molecule with an affinity for the GaN surface is added during the etching process. In this study, phosphoric acid and cysteamine ($NH_2CH_2CH_2SH$) were used to produce quantifiable in-situ

functionalization on the polar (0001) surface of GaN. GaN has been reported to etch in the presence of water and acid to form gallium oxide and ammonia.[189] The presence of the cysteamine during etching permits to cap the surface and control the amount of oxide reformation. The surface morphology was analyzed with atomic force microscopy (AFM) and water contact angle, while the chemical composition was analyzed with x-ray diffraction (XRD) and x-ray photoelectron spectroscopy (XPS). Photoluminescence (PL) provided a way to quantify changes in optical properties.

2.3 Experiment

2.3.1 Sample preparation

GaN samples were grown by HVPE at 1030°C utilizing 330-µm-thick c-plane sapphire wafers. Two sets of samples were used for this study: (i) thin GaN layers with thickness of 1.5 µm residing on sapphire with dislocation density of about 8 x 10^9 cm^{-2},[190] and (ii) thick GaN layer with thickness of about 1 mm, which was initially grown on sapphire substrates and self-separated from the sapphire substrates. After separation, the sample was polished on both sides and formed 374-µm-thick free-standing GaN sample with typical dislocation density in the range of 5 x 10^5–1 x 10^6 cm^{-2}.[190] The Ga- face surface of the free-standing sample was chemically mechanically polished before being dicing. Both types of samples were diced into 3 x 3mm^2 squares. The samples were cleaned in solvent baths of acetone and methanol before being rinsed with deionized (DI) water (18.2 MΩ*cm resistivity) and dried with nitrogen. A hot hydrochloric acid bath followed by a room

temperature hydrofluoric acid was used for etching, leading to the formation of native oxide. The samples were stored in a desiccator under low vacuum.

2.3.2 Etching

The two sets of GaN samples, thin layers residing on sapphire and thick free-standing samples, were each split in two subsets of samples, aiming to be treated either in phosphoric acid (Stock 95 vol.% phosphoric acid (Fisher Scientific)) or in phosphoric acid + cysteamine solution (95% phosphoric acid: 3mM cysteamine (Sigma-Aldrich)). Each set of samples was etched for 150 min at either 40°C or 100°C and evaluated after each treatment.

2.3.3 Characterization

Prior to etching, samples were analyzed using a Rigaku Geigerflex model D/Max IIA XRD with MDI DataScan4 software. A 20mA electron beam accelerated to 25 kV was used to excite a Cu Kα (hv = 8047.7 eV) source. Diffraction slits of 1° were used for the diffraction and scattering slits in conjunction with a 0.6mm receiving slit and a 0.8mm receiving slit monochromator. The Rigaku was calibrated to the 004 silicon reflection (69.13° 2θ). The XRD served primarily as a sample orientation verification method as both sample sets appeared transparent and of equal clarity. We recorded 2θ scans in the range of 30°-75° with a step of 0.008°. The spectra (not shown here) revealed, as expected, only two peaks related to 002 and 004 GaN reflections as expected and 0006 Al_2O_3 reflection for the sample residing on sapphire substrates. Surface topography images were taken with an

Asylum Research Cypher AFM. The images were recorded for each sample after cleaning and after etching. The samples were mounted to 12mm diameter 430 stainless steel discs. Three random locations on each sample were scanned using a 1Hz tapping mode performed over a 10 x 10 μm^2 area. The images were flattened with Igor Pro (Ver. 10.0) software and used to calculate root mean square (RMS) roughness values. Averages from all scans are reported.

Water contact angle was performed with a Ramé-hart Model 200-F4 goniometer equipped with a 28 ga. (AWG) needle. Each drop was captured at 2 frames per second for 5 s. The half-angle was then averaged to produce an average contact angle for that test. The samples were then dried with nitrogen and tested four times for consistency. The angles were captured with DROPImage (Ver. 2.4.07) software.

Surface chemistry was analyzed with a Kratos Axis Ultra XPS utilizing a monochromated Al Kα (hv = 1486.7 eV) source with charge neutralizer (2.0A filament current). Samples were mounted to an aluminum sample holder with copper tape. Pass energies of 160 and 20 eV produced survey and high resolution region scans (C1s, Ga2p, Ga3d, N1s, P2p, S2p) at 0° take off angle. Survey scans were performed once, while region scans are the average of 5 sweeps. All scans were performed at 3 x 10^{-8} Torr. Casa XPS (Ver. 2.3.16 PR) was used to deconvolute peaks after calibrating the C1s peak to 284.8 eV.[144] The full-width at half-maximum (FWHM) of the deconvoluted peaks was limited to the primary peak according to a Lorentzian fit. The background was removed with a Shirley approximation before surface quantification with Kratos provided atomic sensitivity factors.

Ga3d region was used to calculate atomic percentages rather than Ga2p due to greater depth profiling.[191] Ga auger peaks from the N1s spectra were not included in the calculation. All region scans were normalized following quantification.

Photoluminescence spectra were recorded at room temperature via a Horiba Jobin Yvon LabRam ARAMIS Ramen/PL setup utilizing a 325 nm HeCd laser excitation. The microscope was aligned to Teflon (middle Ramen peak of 1295 cm^{-1}) with 40x UV objective at a 2400 grating/min. resolution. The spectra were recorded from 330 to 700 nm utilizing a constant objective height from calibration. The RTD exposure time, accumulated exposure time, and number of accumulations were 5 s, 2 s, and 5, respectively. 30% filter was used to prevent signal cutoff for free-standing GaN. Each sample was spotted in five random locations.

2.4 Results and Discussion

2.4.1 Surface Morphology

Figure 11 shows AFM images taken from free-standing bulk GaN and thin layer GaN residing on sapphire before and after etching with phosphoric acid. The free-standing GaN surfaces (Figures 7(a) and 7(b)) show no increase in pit density, while a noticeable increase in surface contamination following treatment in etch containing cysteamine was seen (Figure 11(b)). This observation confirms qualitatively the Gaface character of the GaN surface, as no prominent pyramidal structures can be seen.[85, 88, 186, 187, 192] The RMS surface roughness for the free-standing bulk GaN surface was found to be 3.4 ± 1.2 nm, which

increased to 3.9 ± 1.1 nm and 9.1 ± 6.5 nm, respectively, after etching with phosphoric acid with and without cysteamine at 40°C. Increasing the temperature treatment to 100°C resulted in decreased roughness to 2.7 ± 0.9 nm after treatment with cysteamine, but increased roughness to 13.3 ± 6.9 nm after 100°C treatment without cysteamine. Comparing only the effect of treatment in solutions without cysteamine, the surface roughness increases with higher temperature. Comparing only the effect of treatment in solutions with cysteamine added, the surface roughness appears to remain the same within the range of standard deviation.

The AFM images of thin layer GaN residing on sapphire (Figures 7(c) and 7(d)) revealed hillock features, consistent with previous reports for HVPE grown GaN[179, 189, 193] that were not seen in the free-standing bulk GaN sample due to polishing processing. Figure 11(d) reveals the effects of etching in solution without cysteamine at 40°C. One can see a little change in the morphology features in addition to an increase of contaminants on the surface. The RMS roughness of 13.1 ± 16.3 nm following the cleaning decreased to 2.5 ± 0.8 nm and to 2.2 ± 0.5 nm after etching at 40°C with and without cysteamine additive, respectively. Elevating the solution temperature to 100°C led to higher roughness of 40.6 ± 20.8 nm and 90.0 ± 25.0 nm after etching with and without cysteamine, respectively. The surface of the thin GaN layer seems to suffer from increased acid sensitivity as compared to the surface of free-standing bulk GaN sample. Both sample surfaces performed similarly after treatment in solution utilizing only KOH as an etchant.[88] The use of cysteamine in both cases produced decreased surface roughness as compared to specimens etched with

stock phosphoric acid. This is expected if cysteamine interferes with gallium oxide formation and protects the surface from more aggressive etching, which has been observed previously with other III–V materials.[114, 194] All pitting defects are attributed to threading dislocations that are intersecting the sample surface. The different size of etched pits can be related to the different types of dislocations,[78, 195] as reported previously, but it is beyond the focus of this study.

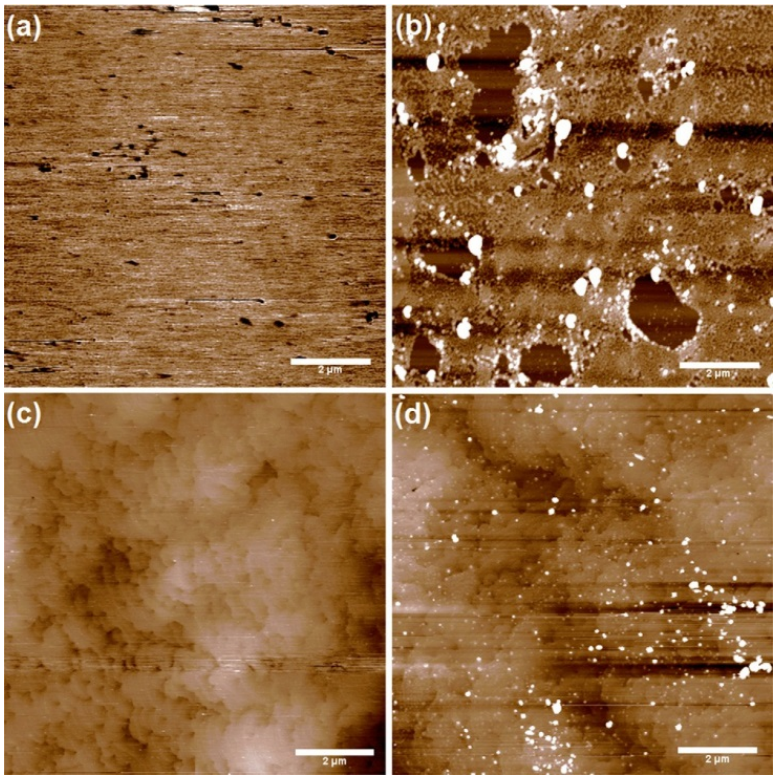

Figure 11 AFM images of free-standing bulk GaN sample (a) and (b) and thin layer GaN residing on sapphire substrate (c) and (d) before etching (a) and (c) and after etching (b) and (d). The height scales are 21 nm (a) and (b), 15 nm (c) and 11 nm (d).

Water contact angle measurements (Figure 12) show a changing of water angle with varying both etching solutions and temperature. For the free-standing bulk GaN, the initial contact angle was estimated to be 80.6° ± 4.6°. After etching at 40°C in phosphoric acid with and without cysteamine, the contact angles decreased to 65.5° ± 1.0° and 72.9° ± 6.1°, respectively. Elevating the treatment temperature to 100°C resulted in a further decrease of the contact angle to 30.6° ± 7.9° and 36.3° ± 9.1° with and without cysteamine, respectively. The surface of the thin layer GaN on sapphire showed a contact angle of 72.1° ± 2.7° before etching, which decreased to 68.1° ± 6.9° and 67.9° ± 1.0° after etching at 40°C in solution of phosphoric acid with and without cysteamine, respectively. Higher treatment temperature led to contact angles of 63.0° ± 6.6° and 52.7° ± 6.6° with and without cysteamine, respectively. The increased contact angle at 40°C is likely due to surface contamination that remained following the cleaning step, as the pristine III–V materials have hydrophilic characteristics.[196, 197] Comparing the effects of solutions with and without cysteamine, the water contact angle is about the same. This implies that there is not enough cysteamine on the surface to produce a hydrophobic monolayer.[172, 198, 199] The decreased hydrophobic character of the free-standing bulk GaN surface after treatment at 100°C as compared to that of the surface of thin GaN layer on sapphire is likely due to the formation of microchips on the surface. The increased surface area (as seen in Figure. 8) promoted increased water adhesion.

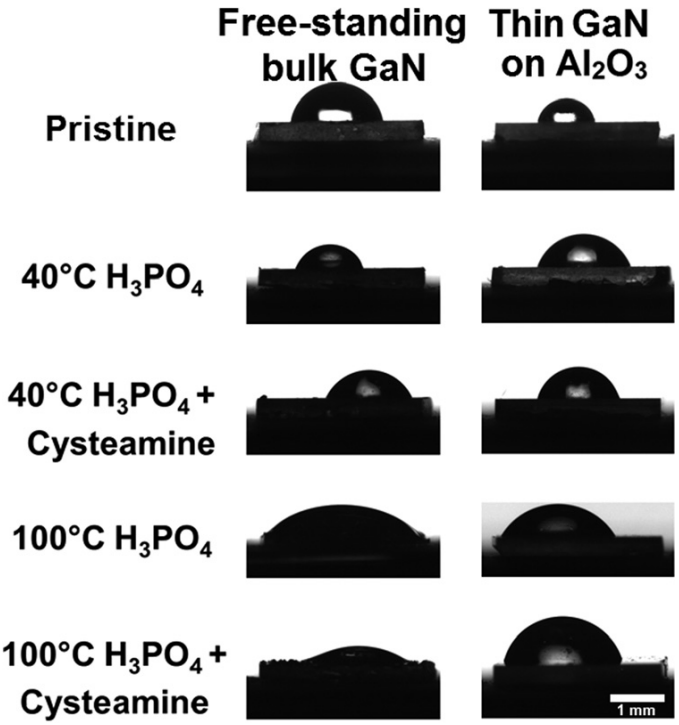

Figure 12 Water droplets images used for contact angle measurements on free- standing bulk GaN and thin layer GaN residing on sapphire at different stages of treatment.

2.4.2 Chemical Composition

XPS was used to identify chemical species on the surfaces of both sample sets throughout the various etch combinations. Figure 13 shows a high resolution Ga2p3/2 scan of both free-standing bulk GaN and thin layer GaN on sapphire (b) after peak normalization. Comparing the different treatments performed on the free-standing bulk GaN (Figure 13(a)), the pristine sample shows the rightmost peak shift to low binding energies. The sample treatment utilizing phosphoric acid at 40°C promotes peak shifting to higher binding energies, while the treatment in solution with added cysteamine to the phosphoric acid at the

same temperature shifts the peak to lower binding energies, although it remains at higher energy as compared to the peak in the spectrum from the cleaned sample. The same trend is seen in spectra from the samples treated at 100°C, but to a greater extent. The spectra from the thin GaN layer on sapphire (Fig. 9(b)) remain largely unchanged by the same treatments, although the treatment at 100°C in phosphoric acid with cysteamine led to a small shift of the peak by 0.1 eV, which is the maximum resolution of the XPS.

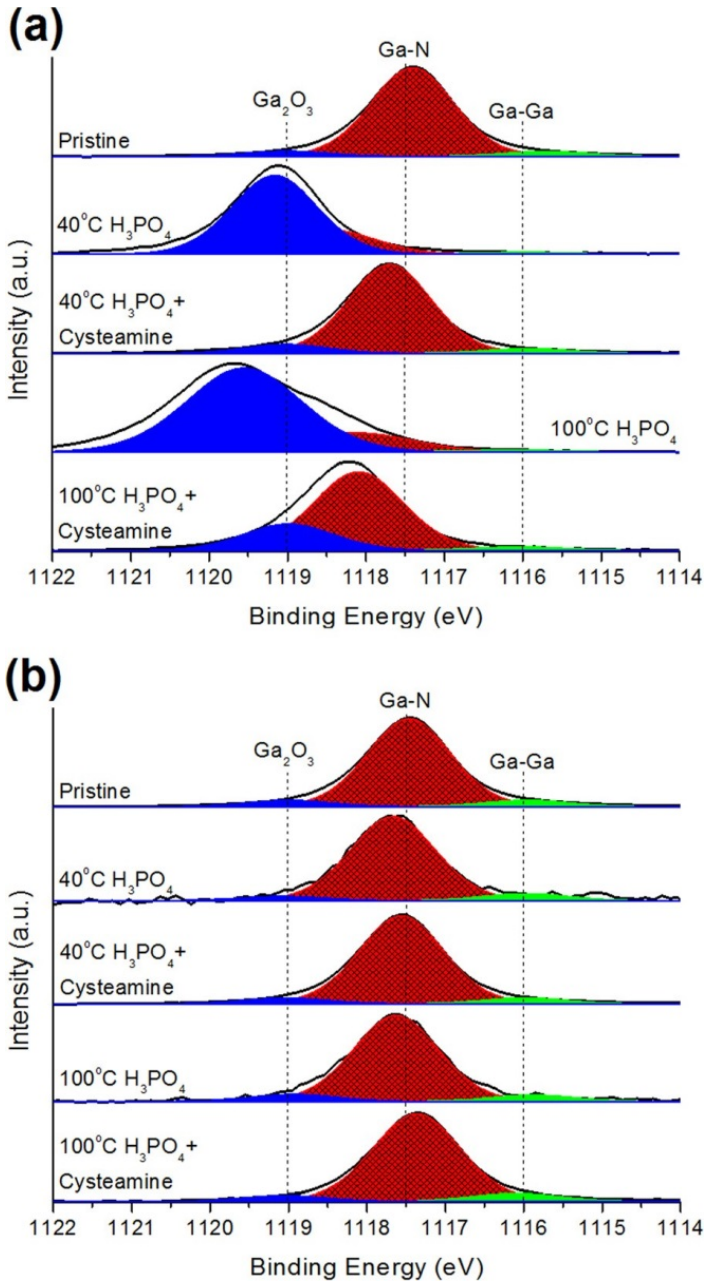

Figure 13 XPS Ga2p spectra of free-standing bulk GaN (a) and thin layer GaN residing on Al_2O_3 (b). The reported binding energies for Ga_2O_3, Ga-N, and Ga-Ga are indicated with dotted lines at 1119, 1117.5, and 1116 eV, respectively.

A deconvolution procedure of the spectra produced three distinct peaks associated with Ga-Ga bonding, Ga-N bonding, and gallium oxide (Ga_2O_3). The Ga-Ga bonding is cited at 1116 eV,[200, 201] the Ga-N bonding at 1117.5 eV,[202, 203] and the gallium oxide at 1119 eV.[204, 205] The deconvoluted peaks are limited to 60.5 eV of the respective binding energy to prevent peak overlapping. During the deconvolution procedure, each peak FWHM was controlled by the Ga-N peak, in such a way that an excessive broadening was prevented. In most of the spectra, the FWHM was found to vary no more than 0.2 eV across both sample sets' treatments. Only the spectrum from the free-standing bulk GaN sample treated in phosphoric acid at 100°C revealed a noticeably larger FWHM of 0.4 eV, which can be attributed to an increased oxide formation.[137, 206, 207] Analyzing the oxide formation for gallium oxide related peaks. It is difficult to resolve the Ga_2O peak from the Ga_2O_3 peak. It is widely assumed that most gallium tend to form Ga_2O_3 over Ga_2O due to the lower Gibbs free energy associated with Ga_2O_3 formation.[208] The gallium oxide is known to lead to a broadening of the peaks in addition to shifting the peaks to higher binding energies.[137] Both effects are observed in our spectra. However, the peak shift seen in the spectrum from the sample treated in phosphoric acid at 100°C (Fig. 9(a)) is beyond the expected binding energies of gallium oxide and does not correspond to any elements possibly related to the substrate or solutions used. We note that despite using a charge neutralizer, conductive copper tape, C1s peak calibration, and limited x-ray exposure, this sample appears to experience some measure of surface charging. This was likewise seen in other scans of the same sample, such as Ga3d and N1s, which are not shown.

A quantitative analysis of the surface composition was performed utilizing the Ga3d peak for gallium content. The Ga2p peak was not used for quantitative analysis as its electron attenuation length is shorter than that for the Ga3d (0.7 vs. 2.2 nm),[137, 181] although it provides superior surface qualification. The areas from pre-normalized spectra (Ga3d, C1s, N1s, P2p, O1s, S2p) were used to identify surface atomic percentages of both free-standing bulk GaN and thin GaN layer on sapphire. The results are shown in Tables 4 and 5, respectively. The gallium auger peaks within the N1s spectra were left out of the quantification.

Analyzing the data in Table 4 for the free-standing bulk GaN, one can see that increasing the solution temperature led to a decreased amount of carbon, while the amounts of oxygen and phosphorous increased. Adding cysteamine to the solution, regardless of the temperature, led to increased amounts of both nitrogen and gallium. The sample treated in phosphoric acid at 100°C was determined to experience ~2/3 of its surface covered by oxygen. Such an amount of oxygen has the potential to shift the Ga2p peak well beyond the typical binding energies, which may negate some of the charging effects discussed above. Analyzing the data for the thin GaN layer on sapphire (Table 5), one can see that higher treatment temperature resulted only in increased amount of phosphorous on the sample surface. The surface of the sample treated in solution with cysteamine exhibited a lower carbon content, while nitrogen and gallium contents increased. The oxygen content on the sample surfaces remained largely unchanged throughout the different treatments as was seen from Figure 13(b). A comparison of the two samples reveals that the addition of cyteamine

led to higher nitrogen and gallium contents. The temporary binding of cysteamine is believed to inhibit oxidation by forming an hydrophobic surface that prevents the contact of water with gallium,[209] and thus, the GaN surface is passivated and further oxide formation is halted.[189, 209] We expected that cysteamine may show up in the S2p spectra as the thiol group readily attaches to the surface.[109] Our inability to observe sulfur is likely due to low amounts on the surface, which are below the detection limits.

Table 4 Atomic % of surface species on free-standing bulk GaN samples calculated from XPS data.

Treatment	C	O	N	P	Ga
Cleaned	11.2%	49.7%	15.5%	0.0%	23.6%
40°C H_3PO_4	36.9%	46.8%	5.1%	2.4%	8.9%
40°C H_3PO_4 + Cysteamine	33.2%	47.8%	6.2%	2.5%	10.2%
100°C H_3PO_4	10.4%	66.1%	2.6%	16.3%	4.6%
100°C H_3PO_4 + Cysteamine	18.8%	54.5%	8.6%	4.1%	14.1%

Table 5 Atomic % of surface species on thin layer GaN residing on sapphire calculated from XPS data.

Treatment	C	O	N	P	Ga
Cleaned	13.5%	14.8%	29.0%	0.0%	42.8%
40°C H_3PO_4	60.1%	27.6%	4.0%	0.0%	8.3%
40°C H_3PO_4 + Cysteamine	40.1%	19.2%	14.7%	1.4%	24.6%
100°C H_3PO_4	61.4%	18.5%	3.4%	1.1%	5.7%
100°C H_3PO_4 + Cysteamine	50.9%	19.2%	9.9%	2.3%	17.7%

2.4.3 Optical Properties

Photoluminescence was used to identify the effect of different etching procedures on the optical properties as a result of surface modification. PL spectra taken in the nearbandgap region (free exciton emission) after each treatment of the free-standing bulk GaN (Figure 14(a)), revealed that the PL intensity of the sample treated in phosphoric acid at 40°C increased the most. Subsequent treatment at the higher temperature of 100°C led to a decrease of the PL intensity. The treatments in solutions with added cysteamine led to the same results, at both temperatures of 40°C and 100°C. PL spectra taken after each treatment of the thin GaN layer on sapphire (Figure 14(b)) led to a reversed effect, namely the PL intensities were the most increased in samples treated at the higher temperature of 100°C.

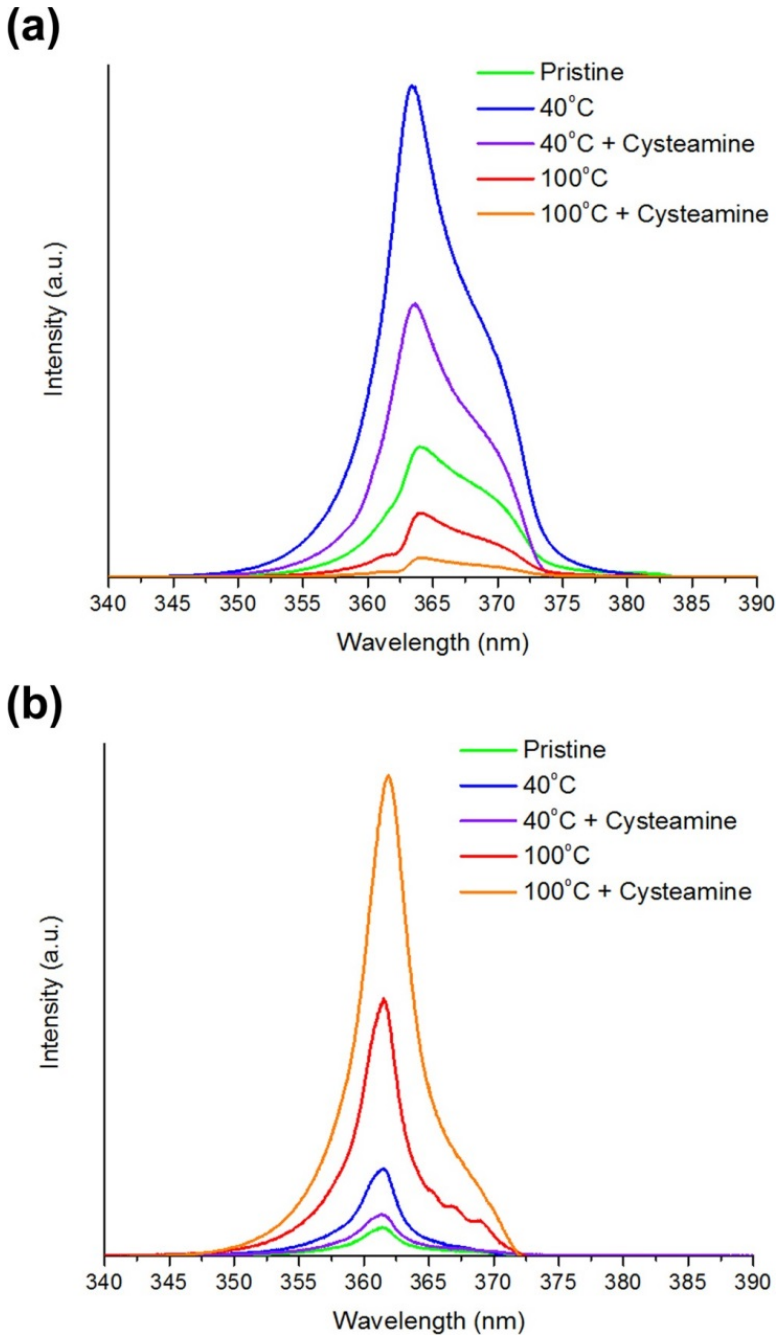

Figure 14 PL spectra of free-standing bulk GaN (a) and thin layer GaN residing on sapphire (b) after performing different treatments, as indicated.

A bar-graph comparison of the PL modifications with changing surface roughness is surmised in Figure 15. In both types of samples, the addition of cysteamine to the treatment solution generally limits the total increase in photoluminescence intensity as the amount of catalyst (phosphoric acid) is decreased (Figure 15(b)). This is consistent with the effect of the addition of cysteamine on the surface roughening decrease, as revealed by the AFM images and seen in Figure 15(a), reducing the light extraction and hence decreasing the PL emission. For thin layer GaN on sapphire, the larger increase in PL response was seen with greater surface roughening at higher temperature. The concentration of cysteamine on the sample surface was determined to be low enough to avoid photon adsorption that has been seen with other surface modifications.[14] What does change is the temperature of phosphoric acid required to maximize photoluminescence in the different types of samples. It has been shown that etching increased the photoluminescence as the surface roughness increases the critical angle for photon escape;[85, 86] however, there is an upper limit as over etching can produce light scattering and device degradation.[86] The addition of cysteamine at 100°C prevents over etching, while maximizing photoluminescence for thin GaN layer on sapphire.

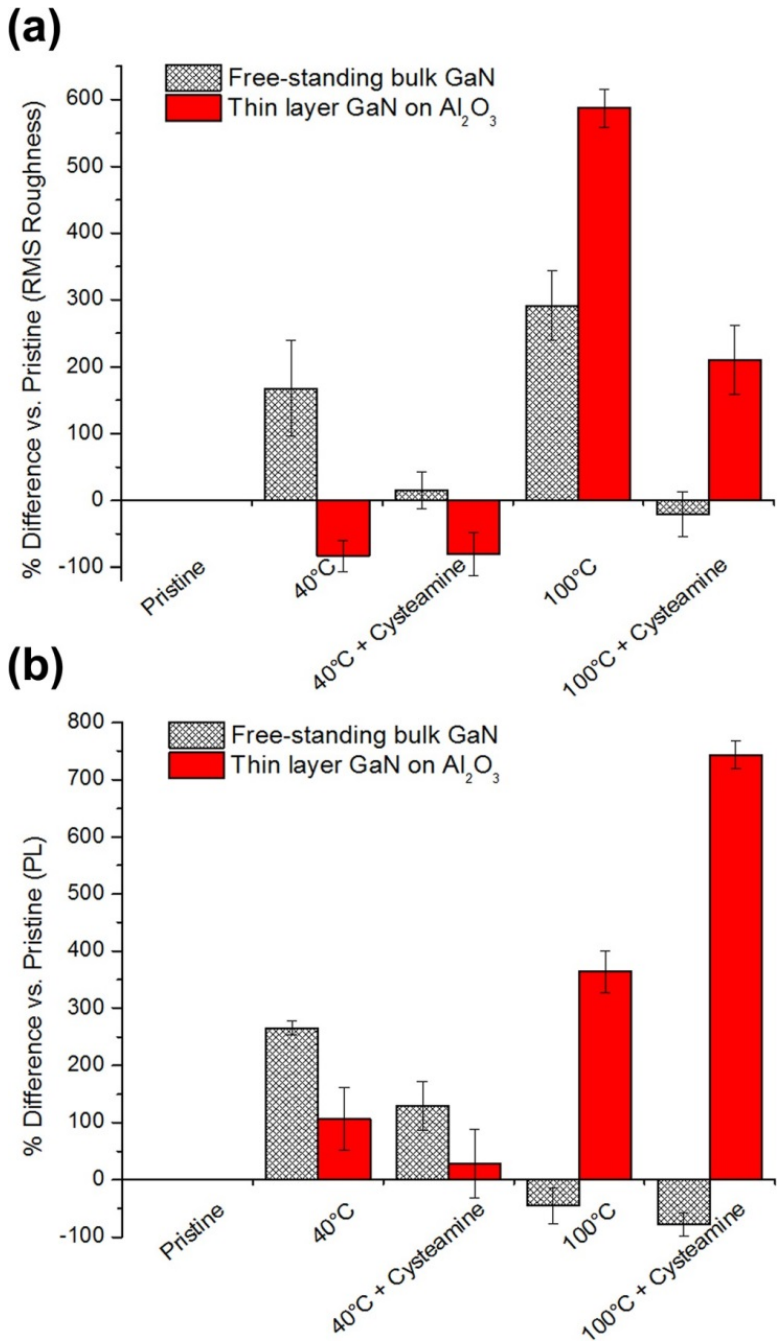

Figure 15 Calculated % difference from RMS roughness (a) and from maximum PL intensities in Figs. 10(a) and 10(b) versus pristine substrates (b).

The free-standing bulk GaN appears to be more sensitive to etching than the thin GaN layer on sapphire. The etchant solution treatment at 40°C resulted in higher PL intensity than that of the sample treated with 100°C solutions. In addition, the PL intensities from the free-standing bulk GaN sample experienced three times stronger PL intensity than those from the thin GaN layer on sapphire, which is related to higher crystal quality of the bulk GaN manifested by the lower dislocation density.[59, 210] We note that all the spectra from the bulk GaN, in addition to the free exciton emission, also exhibit a shoulder on the low energy side, which is the longitudinal-optical (LO) phonon replica of the main exciton emission, usually visible in the room temperature spectra of high-quality GaN.[211] The peak positions of the free exciton emission from the thin GaN layer on sapphire show a slight blue shift with respect to the peak position in the free-standing sample due to typical strain related effect in such thin layers.[212, 213] In addition, the PL spectra of both types of samples also demonstrated yellow band emissions (not shown), which are characteristic for the presence of point defect related deep levels in the bandgap in this material.[14, 59, 214]

2.5 Conclusion

In this study, the in situ functionalization of freestanding bulk GaN and thin layer GaN residing on sapphire with phosphoric acid and cysteamine was analyzed by several techniques: AFM, water contact angle, XPS, and PL. The effect of the addition of cysteamine to the etching solution treatment at two temperatures, 40°C and 100°C, resulted in a decreased surface roughness as compared to the surface morphology of the samples treated in

solutions of stock phosphoric acid. No significant change was seen in the water contact angle with adding cysteamine, although the bulk GaN was hydrophilic in nature at increased solution temperatures. The poor hydrophobic nature of the freestanding bulk GaN revealed low cysteamine concentration, which still increased the gallium and nitrogen surface concentration compared to etchant alone. The free-standing bulk GaN demonstrated hypersensitivity to stock phosphoric acid, which produced increased levels on oxide formation and stronger PL emission. Our results demonstrate that the addition of cysteamine promotes increased photoluminescence efficiency, while decreasing the amount of oxide formation.

3. Modulated Optical Properties of Nonpolar Gallium Nitride via Surface In-Situ Functionalization with Cysteamine Assisted Phosphoric Acid

Stewart J. Wilkins,[1] Tania Paskova,[1,2] Albena Ivanisevic[1,3]

[1]Department of Materials Science and Engineering, North Carolina State University, Raleigh, North Carolina, 27606, USA

[2]Department of Electrical and Computer Engineering, North Carolina State University, Raleigh, North Carolina, 27606, USA

[3]NCSU /UNC-CH Joint Department of Biomedical Engineering, North Carolina State University, Raleigh, North Carolina, 27606, USA

The following manuscript is reprinted with permission from S.J. Wilkins, T. Paskova, A. Ivanisevic, "Modulated optical properties of nonpolar gallium nitride via surface in-situ functionalization with cysteamine assisted phosphoric acid," *Applied Surface Science*, **2014**, 295, 207-213.

3.1 Abstract

In-situ functionalization of nonpolar a-plane gallium nitride (GaN) surface was achieved by adding cysteamine to phosphoric acid, aiming to modulate its optical properties. The emission properties and oxide formation were explored through surface characterization with atomic force microscopy (AFM), X-ray photoelectron spectroscopy (XPS), photoluminescence (PL), and water contact angle. Nonpolar a-plane bulk GaN sample sliced from a GaN boule and nonpolar a-plane GaN thin layer heteroepitaxially grown on r-plane sapphire were used to elucidate the effects of in-situ functionalization of identical surface

orientation of GaN crystals with different defect ensembles. The addition of cysteamine to the phosphoric acid solution was found to result in: (i) increased surface roughness, (ii) no change to hydrophobicity, (iii) decreased oxygen content at high solution temperatures and increased gallium and nitrogen content versus phosphoric acid solutions at similar temperatures without cysteamine. The in situ functionalization resulted in enhanced PL intensity from the nonpolar bulk GaN, while the PL intensity from the nonpolar heteroepitaxially grown GaN layer on sapphire was significantly reduced. The opposite PL modulation was explained by the effects of different defects present in the two samples on the nonradiative recombination.

3.2 Introduction

Group-III nitrides have seen use in applications such as blue and UV light emitting diodes (LEDs),[75, 215, 216] and UV detectors [217] due to the easily modified band gaps in wide spectral range (0.7–6.1 eV). Most of the currently developed nitride-based devices are grown along the [0 0 0 1] (c-axis) wurtzite crystallographic direction due to the optimized high-quality growth on c-plane sapphire (Al_2O_3) and silicon carbide (SiC) developed over the years. The major drawback of heterostructures grown along the polar [0 0 0 1] direction is the presence of the internal polarization-induced electric field which spatially separates the carriers and reduces the emission efficiency of the LEDs.[75, 218] This problem can be avoided if the structures are grown in directions perpendicular to the c-axis (so-called a- or m- directions).[218, 219] Nonpolar (a- or m- plane) GaN can be grown heteroepitaxially on

r-plane sapphire, a- or m-plane SiC, and γ-LiAlO2, or produced from a GaN boule grown along the [0 0 0 1] direction by cutting perpendicular to the a- or m- directions.[77] The heteroepitaxial approach usually leads to a high density of stacking faults (SFs) (~5 x 10^5 cm^{-1}) which together with a common high density of threading dislocations (TDs) (~10^9 cm^{-2}) significantly deteriorates the structural quality of the material.[77, 219] On the other hand, nonpolar GaN sliced from boules possesses a threading dislocation density in the range of 5 x 10^5 – 3 x 10^6 cm^{-2} with no SFs. Such bulk GaN substrates have been previously shown to exhibit better structural and optical properties over heteroepitaxially grown GaN nonpolar templates, which ensures improved radiative recombination and overall better efficiency of the light emission devices.

In addition to improvements in GaN crystal quality, surface modifications were employed to increase device optical properties through techniques such as focused ion beam (FIB) milling, dry plasma etching, laser assisted grooving, and wet chemical etching.[220] Though FIB, dry plasma etching, and laser assisted grooving improve final device performance, thermal damage from plasma and laser techniques [83, 221] as well as kinetic damage from FIB [222, 223] limit performance and require further processing to remove structural damage. Wet chemical etching lacks surface damage caused by ablation techniques and can be employed en masse for scalable production.[220] Wet chemical etching is often paired with photon assistance from UV sources to improve etching characteristics. [89, 224] To date, wet chemical etching has been reported for polar GaN [85, 88, 186] and some nonpolar heteroepitaxial thin layers GaN.[86, 89, 220, 224] For example, hot potassium

hydroxide (KOH) was shown to preferentially etch along c-plane directions and increase optical efficiency for both current injection and photoluminescence for polar GaN [85, 88] as well as thin layer of nonpolar GaN. [89, 224] Phosphoric acid (H_3PO_4) is also known to produce etching effects for polar GaN, [85, 186] but little has been reported for nonpolar GaN.[81] As etching processes are sensitive to temperature, pressure, time, and concentration, we hypothesize that the addition of small organic molecules attracted to GaN will produce unique properties through surface functionalization and control of gallium oxide (Ga_2O_3) formation.

In this study cysteamine ($NH_2CH_2CH_2SH$) and phosphoric acid were used to produce quantifiable in-situ functionalization of the surface of nonpolar (1 1 -2 0) GaN. GaN has been reported to etch in the presence of water and a catalyst (phosphoric acid), forming gallium oxide and ammonia. [189] The manifestation of cysteamine during etching permits control of oxide reformation through surface capping. The surface morphology was analyzed with atomic force microscopy (AFM) and water contact angle, while the crystallographic orientation was analyzed with x-ray diffraction (XRD). The chemical composition was analyzed via x-ray photoelectron spectroscopy (XPS). The optical properties and their modulation upon different treatments were quantified with photoluminescence (PL).

3.3 Materials and methods

3.3.1 Sample Preparation

The GaN samples were grown by hydride-vapor phase epitaxy (HVPE). Two sets of nonpolar (1 1 -2 0) GaN samples were used for this study. The first set of samples was prepared from a heteroepitaxial grown GaN layer along the [1 1 -2 0] direction on (1 1 0 -2) plane sapphire in a conventional horizontal reactor at 1080°C on metal organic vapor phase epitaxial GaN template layers.[225] The second set of GaN samples was prepared from a nonpolar bulk wafer grown by HVPE at Kyma Technologies. Boules with 2 in. diameter and thickness up to 7–8 mm were grown in the [0 0 0 1] direction. Then rectangular bars with sizes of about 10 mm × 6 mm were sliced parallel to the (1 1 -2 0) plane, followed by polishing of both sides to form ∼420-μm-thick nonpolar bulk GaN substrate. This was finished with one-side chemical mechanical polishing (CMP).[225]

Each of the two sets contains five samples with a similar 3 mm × 3 mm square-shape. All specimens were pretreated with solvent baths of acetone and methanol before being washed with deionized (DI) water (18.2 MΩ *cm resistivity) and dried with nitrogen. A 100°C hydrochloric acid bath followed by a room temperature hydrofluoric acid bath was used for oxide removal. The samples were kept in a desiccator under low vacuum.

3.3.2 Etching

Both sets of GaN samples, thin layer GaN residing on sapphire and bulk GaN samples, were each split in two subsets, which were treated either in phosphoric acid (Stock 95 vol.% phosphoric acid (Fisher Scientific)) or in 1:1 phosphoric + cysteamine solution (95% phosphoric acid: 3 mM cysteamine (Sigma–Aldrich)). All samples were etched for 150 min at the two temperatures of 40°C or 100°C and characterized after each treatment.

3.3.3 Characterization

Before etching, samples were analyzed using a Rigaku Geigerflex model D/Max IIA XRD with MDI DataScan4 software. A Cu K_ (hv = 8047.7 eV) source was excited with an electron beam of 20 mA accelerated to 25 kV. 1° diffraction slits were used for the diffraction and scattering slits in union with a 0.6 mm receiving slit and a 0.8 mm receiving slit monochromator. A (0 0 4) silicon peak (69.13° 2θ) was used to calibrate the Rigaku. The XRD served primarily as a sample orientation and verification method as both sample sets appeared transparent. The free-standing GaN samples were distinguished from thin layer GaN on sapphire by a faint yellow tint. XRD 2θ scans in the range of 30–75° were captured with a step height of 0.008°. The spectra (not shown here) revealed, as anticipated, a (1 1 0) GaN reflection, as well as the (2 -2 4) Al_2O_3 reflection for the samples residing on the r-plane sapphire.

An Asylum Research Cypher AFM was utilized to take topography images for each sample after cleaning and after etching. 12-mm-diameter 430 stainless steel discs were used

to mount samples during imaging. Three random 10 µm x 10 µm locations were imaged on each sample using a 1 Hz tapping mode. All images were flattened using Igor Pro (Ver. 10.0) software and averaged to calculate root mean square (RMS) roughness values.

A Ramé-hart Model 200-F4 goniometer equipped with a 28 ga. (AWG) needle was used to perform water contact angle. Water drops were captured at 2 frames per second for 5 s. The half-angle was then averaged to produce an average contact angle, which was performed four more times to produce a total sample average. After each test samples were dried with nitrogen. The water contact angles were captured with DROPImage (Ver. 2.4.07) software.

A Kratos Axis Ultra XPS utilizing a monochromated Al K_ (hv = 1486.7 eV) source with charge neutralizer (2.0 A filament current) was used to analyze surface chemistry. A conductive copper tape was used to mount samples to an aluminum sample holder. Small energy passes were made for high resolution region scans for C1s (276 - 296 eV), Ga2p (1110 - 1130 eV), Ga3d (10 - 30 eV), N1s (384 - 408 eV), O1s (524 - 544 eV) P2p (123 - 143 eV), S2p (152 - 172 eV). These scans were swept 5 times to form average region scans with a maximum resolution of 0.1 eV. Survey scans were produced by scanning 0 - 1200 eV and were only scanned once. All scans were performed at 3 x 10^{-8} Torr and at a 0° take off angle. Casa XPS (Ver. 2.3.16 PR) was used to deconvolute peaks after calibrating all XPS spectra to the C1s peak to 284.8 eV, which is associated with adventitious carbon.[144] Adventitious carbon naturally occurs due to contamination from atmospheric exposure, which provides a convenient charge reference to identify peak shifting in other species. The

full-width at half-maximum (FWHM) of deconvoluted peaks was limited to the primary peak according to a Lorentzian fit after removing the background with a Shirley approximation. Kratos provided atomic sensitivity factors were utilized for surface quantification. The Ga3d region area was used to calculate atomic percentages rather than Ga2p due to greater depth profiling.[191] Ga auger peaks from the N1s spectra were not included in the surface quantification. All region scans were normalized following quantification.

A Horiba Jobin Yvon LabRam ARAMIS Ramen/PL setup, utilizing a 325 nm HeCd laser excitation, was used to record photoluminescence spectra at room temperature. The microscope was aligned to Teflon (middle Raman peak of 1295 cm^{-1}) with a 40x UV objective at a 2400 grating/minute resolution. The objective height was locked from calibration to capture spectra from 330 nm to 400 nm. The real time data (RTD) exposure time, accumulated exposure time, and number of accumulations were 1, 1, and 5, respectively. 90% filter was used to prevent signal cutoff for the PL of the nonpolar bulk GaN samples. Each sample was spotted in five random locations to account for surface variances.

3.4 Results and Discussion

3.4.1 Surface morphology

Figure 16 displays AFM images taken from a nonpolar bulk GaN and a thin layer GaN residing on sapphire before and after etching with phosphoric acid and cysteamine at 40°C. The bulk nonpolar GaN surface (Figure 16(b)) demonstrates pit formation upon

treatment with phosphoric acid. The pits (Figure 16(b)) are random in size and shape (no uniform structure), which is consistent with previous reports in the literature. [86, 89] Qualitatively, the lack of a smooth surface with symmetric hexagonal pits (associated with gallium terminated polar structures) as well as hillock or pyramidal features (characteristic of nitrogen terminated polar GaN) confirms the presence of a uniform surface without polar orientation. [226-228] For the bulk GaN, the RMS roughness of a cleaned sample was 3.0 ± 1.2 nm, which remained unchanged (2.7 ± 0.1 nm) after etching with phosphoric acid without cysteamine at 40°C but increased to 5.8 ± 1.2 nm with cysteamine at 40°C. Using a higher temperature solution of 100°C phosphoric acid, however, led to a significant increase of the surface roughness up to 23.2 ± 10.9 nm and 22.0 ± 17.7 nm without and with cysteamine, respectively. The addition of cysteamine was seen to have increased the roughness for the 40°C etchant solution; however, no changes were discernible at higher temperature. The elevated temperature did increase the overall roughness versus a pristine and lower temperature treated sample, which confirms active etching at these conditions.

Figure 16(c) and (d) shows AFM images of thin layer a-plane GaN on r-plane sapphire substrate before and after etching. Qualitatively there is little difference between the pristine sample (Figure 16(c)) and an etched sample (Figure 16(d)). Triangle-shaped pits have been previously reported for the heteroepitaxial nonpolar GaN layers on r-plane sapphire, and the etching produced better defined facets (Figure 16(d)). The surface roughness of the heteroepitaxial nonpolar layer (93.0 ± 12.0 nm) was more than an order of magnitude higher than that of the bulk nonpolar GaN (3.0 ± 1.20 nm) and only slightly

increased (103.3 ± 82.3 nm) upon treatment with phosphoric acid without cysteamine at 40°C. However, adding cysteamine increased the surface roughness by a factor of 2 up to 174.6 ± 36.1 nm, which replicated a similar response from the nonpolar bulk GaN. Interestingly, increasing the etchant temperature led to an opposite effect, namely a decrease of the surface roughness by an order of magnitude to 18.6 ± 6.2 nm and 42.2 ± 7.8 nm for phosphoric acid treatment without and with cysteamine, respectively. The addition of cysteamine again produced a rougher surface, but the increased etchant temperature produced a flattening effect. At low temperatures, both sample types show increased sensitivity to cysteamine addition, which is more likely a result from contamination agglomeration than any actual increase in pit formation. At elevated temperatures, the etching of the bulk nonpolar GaN produced an expected increase in surface roughness that is associated with pit formation. [86, 89] The thin heteroepitaxial nonpolar layer GaN on sapphire behaved differently due to increased defect density on the untreated sample surface.[80, 229] This type of thin heteroepitaxial nonpolar layers of GaN has been previously shown in numerous reports to possess a significant increase in stacking faults (SFs).[79, 225, 230, 231] These thin nonpolar layer GaN demonstrates increased sensitivity to etching as the phosphoric acid preferentially reacts with defects. Though the nonpolar surfaces lack the formation of hexagonal pits or polygonal pyramids seen from gallium or nitrogen terminated polar surfaces, these nonpolar GaN surfaces showed nonsymmetrical pits characteristic of v-grooves formed along polar directions.[81, 232] Additional etching with KOH and

phosphoric acid has been shown to produce preferential etching along polarv-groove pits,[81, 86, 89] which, however, was not observed in our experiments.

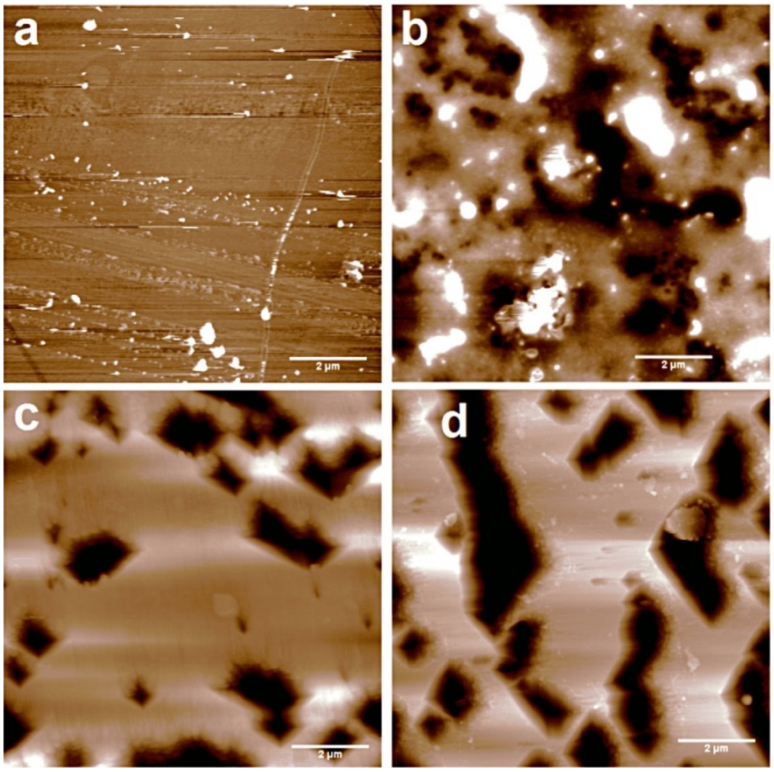

Figure 16 AFM images of nonpolar a-plane bulk GaN sample (a and b) and thin heteroepitxaial a-plane layer GaN residing on r-plane sapphire substrate (c and d) before etching (a and c) and after etching with 40°C phosphoric acid and cysteamine (b and d). The height scales are 14 nm (a), 17 nm (b), 410 nm (c), and 450 nm (d).

In addition to atomic force microscopy, water contact angle was performed to understand surface topography through changes in hydrophobicity upon treatments with varying etching temperatures and solutions. For the bulk nonpolar GaN (Figure 17), the initial water contact angle following cleaning was 90.0 ± 5.1°. With the use of a 40°C

phosphoric acid solution the contact angle decreased to 78.2 ± 4.7° and 67.3 ± 6.4° without and with cysteamine, respectively. Utilizing higher-temperature 100°C solution treatments without and with cysteamine decreased the water contact angle to 67.8 ± 4.6° and 72.9 ± 8.5° respectively, which is similar to the effect of 40°C solution treatments. The thin heteroepitaxial nonpolar layer GaN on r-plane sapphire demonstrated a similar response. In a pristine state, the thin layer GaN produced a water contact angle of 92.9 ± 3.0°. With 40°C phosphoric acid without cysteamine the water contact angle was found to be 84.3 ± 6.1°, whereas the addition of cysteamine produced a similar 85.8 ± 4.8° water contact angle. Using the 100°C phosphoric acid without and with cysteamine formed contact angles of 71.8 ± 4.0° and 65.1 ± 5.4°respectively. In both cases (bulk GaN and thin layer GaN on sapphire), the use of an etchant (both with and without cysteamine) decreased the hydrophobicity. It is well known that clean III-V materials demonstrate hydrophobic characteristics.[196, 197] The increased roughness, as revealed by AFM imaging (Figure 16), represents an increase in the surface area of pits and hence, regions for water to flow into. However, the decrease in RMS roughness for the thin nonpolar layer GaN on sapphire etched with 100°C solutions does not correspond to an increase in water contact angle. This is most likely due to the surface flattening through an increased number of pits, whereas the 40°C etchants expanded existing pits. The use of cysteamine produced no difference (within the standard deviation) between etchant solutions at identical temperatures and did not increase hydrophobicity that is seen at high cysteamine concentrations in agreement with previous studies.[172, 198, 199]

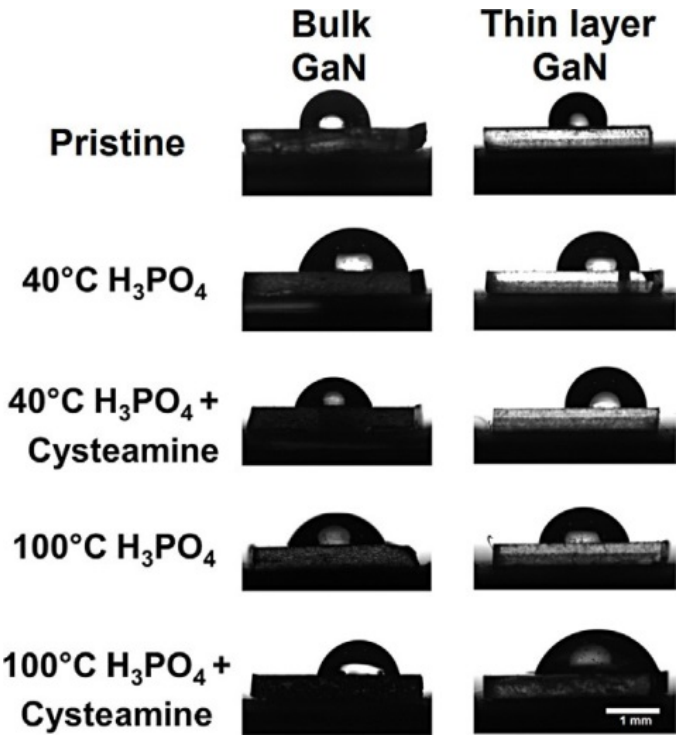

Figure 17 Water droplets images used for contact angle measurements on nonpolar a-plane bulk GaN and thin heteroepitaxial a-plane layer GaN residing on r-plane sapphire at different stages of treatment.

3.4.2 Chemical composition

Figure 18 shows high resolution $Ga2p_{3/2}$ spectra of both bulk nonpolar GaN (a) and thin heteroepitaxial a-plane layer GaN on r-plane sapphire substrate (b) after peak normalization. Comparing only the bulk nonpolar GaN species, the pristine sample (Figure 18(a)) exhibited the right-most shifted peak toward lower binding energies (black line). The use of phosphoric acid treatment promoted increased peak shifting to higher binding energies at both 40°Cand 100°C solutions with greater shift at 100°C. The addition of cysteamine also led to a shift of the peaks to higher binding energies, as compared to the peak position in the

spectra from the pristine, but not to the extent of the pure phosphoric acid treatment effect. The 100°C phosphoric acid with cysteamine solution treatment produced a similar effect of increase in binding energies as the treatment in 40°C phosphoric acid with cysteamine. A similar trend is seen for thin nonpolar GaN layer on sapphire (Figure 18(b)). The treatment at 40°C solution without cysteamine led to a greater shift to higher binding energies than the etchant solution treatment with cysteamine. Unlike the bulk nonpolar GaN, the 100°C solution treatments did not lead to as large of a shift as their 40°C counterparts, although the trend of lower binding energy with cysteamine vs. without cysteamine remained consistent. Other than 40°C phosphoric acid with cysteamine for the bulk GaN, the binding energy was increased as compared to the pristine stage. For the treatment with 40°C phosphoric acid with cysteamine, the peak shift was found less than the spectral resolution of the XPS (0.1 eV).

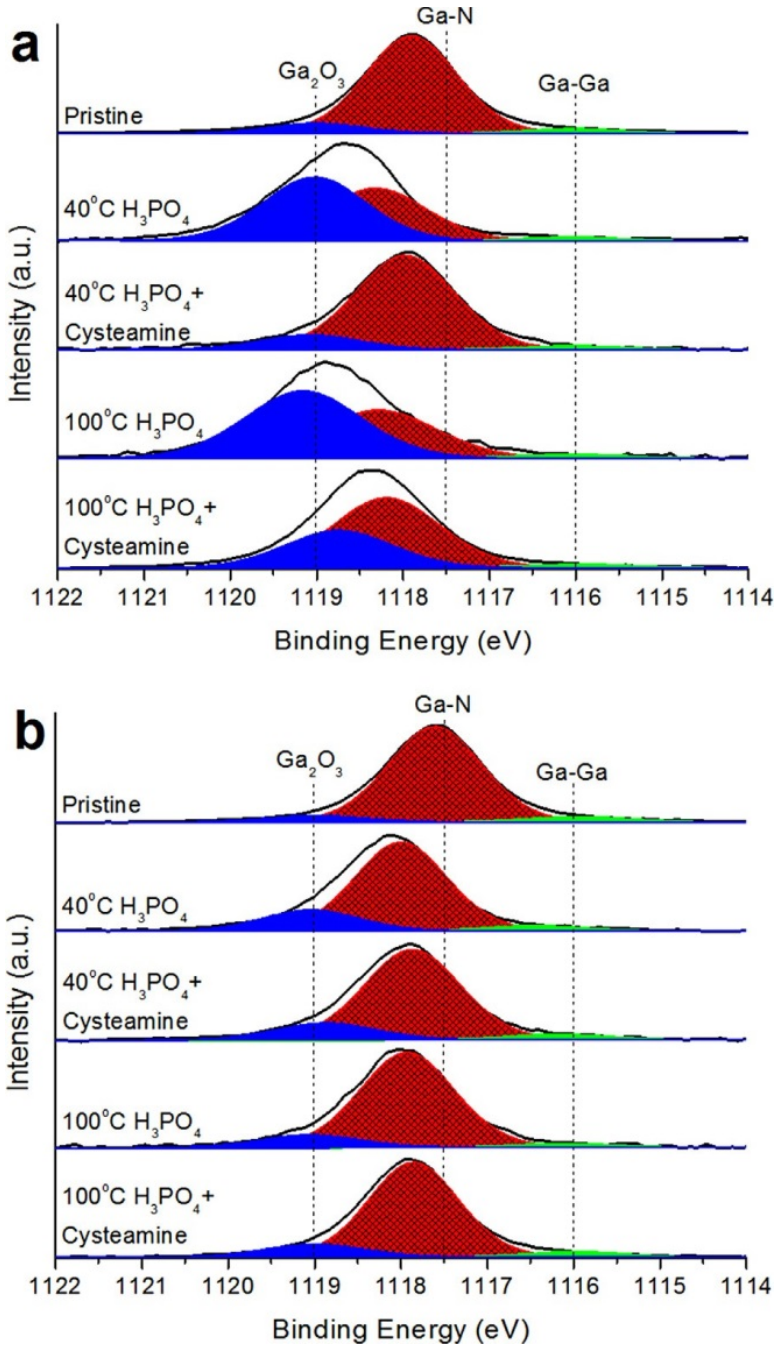

Figure 18 XPS Ga2p spectra of nonpolar a-plane bulk GaN (a) and thin heteroepitaxial a-plane layer GaN residing on r-plane Al2O3 (b). The reported energies for Ga2O3, Ga-N, and Ga-Ga are indicated with dotted lines at 1119.0, 1117.5, and 1116.0 eV respectively.

Three distinct peaks associated with Ga-Ga bonding, Ga-N bonding, and gallium oxide formation (Ga_2O_3) were identified by deconvolution of the $Ga2p_{3/2}$ peak in the XPS spectra. Gallium oxide (blue) is reported to have a binding energy of 1119.0 eV,[204, 205] the Ga-N bonding (red) is reported to be at 1117.5 eV, [59, 209] and the Ga-Ga bonding (green) is reported to reside around 1116.0 eV. [200, 201] A potential formation of additional gallium oxide species (Ga_2O) could not be resolved from the dominant Ga_2O_3 peak but the Ga_2O formation is less likely as the Ga_2O_3 has a lower Gibbs free energy of formation and thus appears to be the more stable species.[208] The FWHM of the deconvoluted peaks were controlled by the FWHM of the primary Ga-N species peak to prevent unreasonable broadening. The FWHM of the peaks from the bulk nonpolar GaN had a maximum variance of 0.34 eV, while the FWHM of the peaks from the thin nonpolar layer GaN on sapphire showed a maximum variation of 0.13 eV. The formation of gallium oxide is known to cause a peak broadening as well as a peak shift to higher energies.[137, 206, 207] In addition to controlling the FWHM, the energies were bound to less than ± 0.5 eV from the reported binding energies in order to prevent peak overlapping and thus, avoiding imaginary peaks.

A quantitative analysis of surface composition after various treatments in phosphoric acid solutions with and without cysteamine was performed and the results are shown in Tables 6 and 7. The $Ga2p_{3/2}$ peak provides excellent surface qualification; however, the shorter attenuation length (0.7 nm) limits a holistic understanding of chemical composition.[137, 181] Hence the Ga3d peak (with an attenuation length of 2.2 nm) was utilized for atomic % calculations. [137, 181] Along with the Ga3d peak, the amount of

carbon, oxygen, sulfur, phosphorous, and nitrogen were calculated with areas from pre-normalized C1s, O1s, S2p, P2p, and N1s peaks with gallium auger peaks from the N1s spectra being excluded.

For the bulk nonpolar GaN samples (Table 6), the use of any etchant led to an increase of the amount of carbon contamination due to environmental exposure and handling. The treatment in 40°C solutions with adding cysteamine led to increased amount of surface oxygen, while decreasing the amount of surface nitrogen and gallium. The 100°C phosphoric acid without cysteamine treatment produced both higher amounts of oxygen and carbon, but decreased amounts of nitrogen and gallium. For the thin nonpolar layer GaN on r-plane sapphire (Table 7) the treatments led to similar responses as for the bulk nonpolar GaN at both solution temperatures. In addition, both etchants with and without cysteamine decreased the amount of oxygen, increased the amount of gallium, and increased (or equaled, as in the case for 40°C solution) the amount of nitrogen. The bulk nonpolar GaN demonstrated a higher sensitivity to oxide formation (Figure 18(a)) as compared to that of the thin nonpolar layer GaN. The use of etchants in both cases decreased the surface nitrogen and gallium content, which is expected via the formation of surface oxides and contamination via carbon or residual phosphoric acid. The use of cysteamine reduced the amount of oxide formation for all solutions except for the case of 40°C etching of the bulk nonpolar GaN. As the surface roughness remainedunchanged upon treatment, no measurable amount of etching took place, which prevented surface passivation by cysteamine.[189, 209] The atomic % of sulfur was not shown as the amount of cysteamine on the surface was below the detection limits of the

XPS. This is consistent with the results from water contact angle measurements, showing no increase of hydrophobicity with the addition of 3 mM of cysteamine to the etchant solutions.

Table 6 Atomic % of surface species on nonpolar a-plane bulk GaN samples calculated from XPS data.

Treatment	C	O	N	P	Ga
Pristine	24.7%	39.3%	15.8%	0.0%	20.2%
40°C H_3PO_4	44.7%	44.0%	4.3%	0.8%	6.2%
40°C H_3PO_4 + Cysteamine	31.3%	55.8%	2.4%	6.8%	3.8%
100°C H_3PO_4	48.2%	39.9%	3.0%	3.9%	4.9%
100°C H_3PO_4 + Cysteamine	39.2%	38.6%	6.2%	3.7%	12.2%

Table 7 Atomic % of surface species on thin heteroepitaxial a-plane layer GaN residing on r-plane sapphire calculated from XPS data.

Treatment	C	O	N	P	Ga
Pristine	39.3%	19.9%	16.1%	0.0%	24.8%
40°C H_3PO_4	49.7%	26.9%	7.9%	3.1%	12.5%
40°C H_3PO_4 + Cysteamine	55.1%	21.3%	7.9%	2.3%	13.4%
100°C H_3PO_4	65.1%	17.9%	4.8%	2.8%	9.4%
100°C H_3PO_4 + Cysteamine	53.3%	17.3%	10.1%	3.4%	15.9%

3.4.3 Optical Properties

Photoluminescence spectra were taken in the near-bandgap region, dominated by free exciton emission at room temperature, which aimed to identify the effects of different etching methods on optical properties. For the bulk nonpolar GaN all surface treatments resulted in an increase of the PL intensity as seen in Figure 19(a). The 100°C treatments resulted in a greater increase in photoluminescence intensity as compared to that of the sample treated in the 40°C solutions. The addition of cysteamine to the etching solution led to increased photoluminescence at both temperatures as compared to the pristine, although the pure phosphoric acid solution etching showed stronger relative increase. Surprisingly the treatments of the thin nonpolar layer GaN on r-plane sapphire (Figure 19(b)) demonstrated the opposite effects in all cases. The treatments in both phosphoric acid solutions with and without cysteamine led to a decrease of the photoluminescence intensity with stronger effectat higher temperature. In all tests, the addition of cysteamine led to a reduced effect on the PL intensity as compared to the effect of etching without the cysteamine.

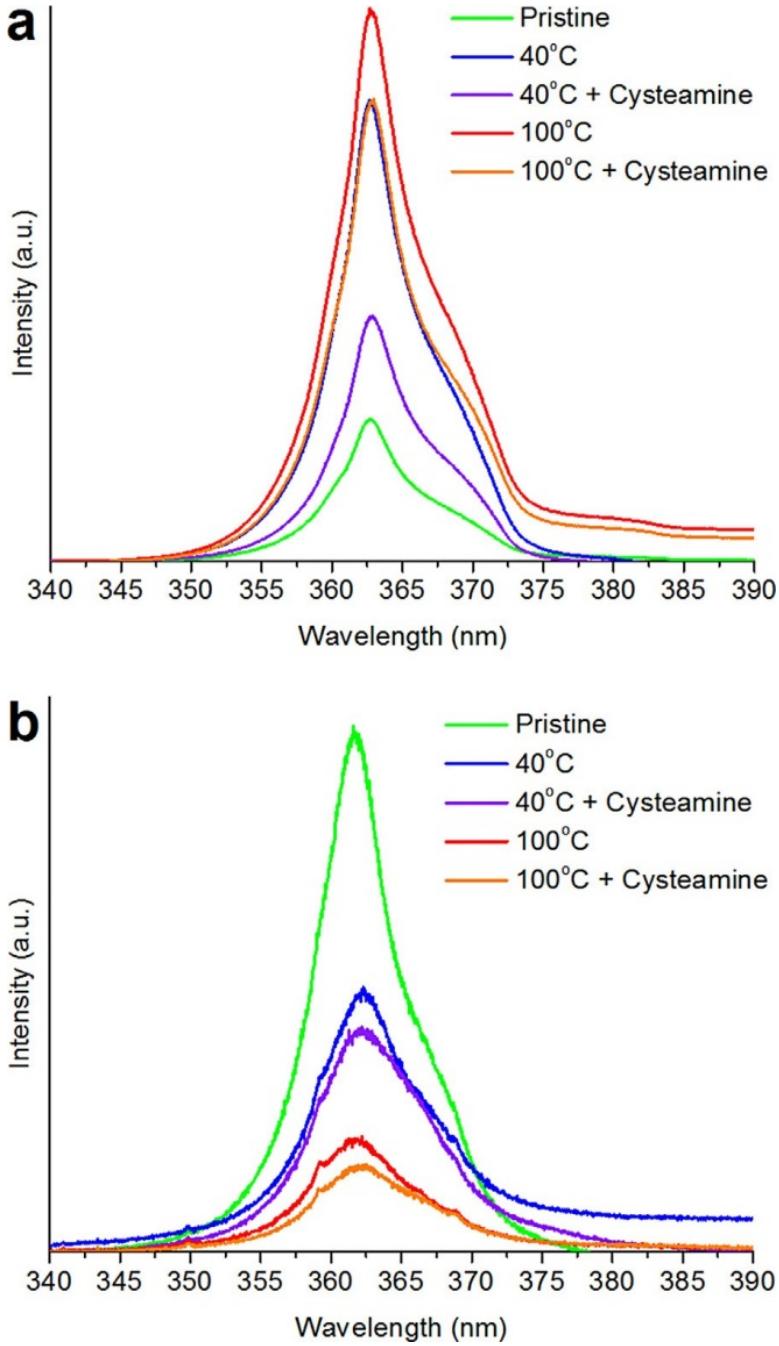

Figure 19 PL spectra of nonpolar a-plane bulk GaN (a) and thin heteroepitaxial non-polar a-plane layer GaN residing on r-plane sapphire (b) after performing different treatments, as indicated.

Figure 20 shows a bar-chart representation of PL intensities modulation compared to the respective non-etched samples. One can clearly see the opposite treatments effects on the optical properties of the bulk nonpolar GaN (as shown by the gray bars) and of the thin heteroepitaxial GaN layer (as shown by the red bars). The limited effects of adding the cysteamine can also be seen for both samples and for any respective treatment without the cysteamine. In addition, the modulation of the PL intensity of the bulk nonpolar GaN by all the treatments was significantly stronger (50–300%) than the PL modulation of the thin nonpolar layer (20–45%).

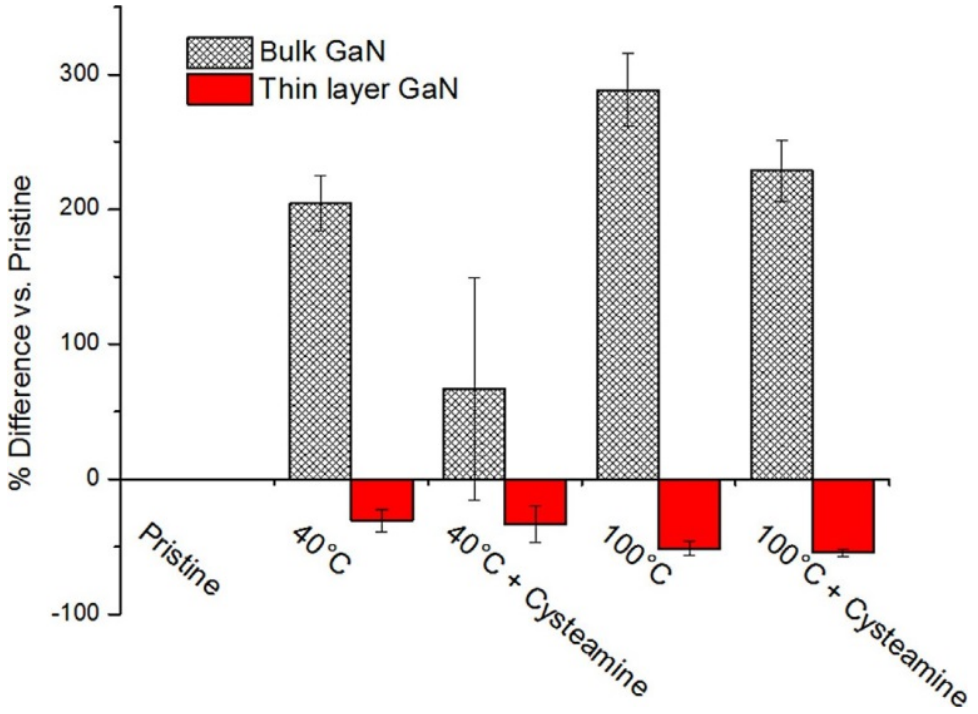

Figure 20 Calculated % difference from maximum PL intensities in Figure 19 (a and b) versus pristine substrates.

It is also important to point out that the PL intensities of the bulk nonpolar GaN was significantly stronger than the intensities in the PL spectra from the thin nonpolar layer GaN, and had to be controlled with a filter. The stronger signal response and sensitivity to treatments stems from the higher crystal quality of the bulk GaN manifested by significantly smaller amounts of dislocations related to nonradiative recombination.[59, 233] The high quality of the bulk GaN is confirmed by the shoulder on the lower energy side of the exciton peak (Figure 19(a)) that is characteristic of longitudinal-optical (LO) phonon replicas seen at room temperature PL.[211]

The thin nonpolar GaN heteroepitaxially grown on r-plane sapphire is characterized by rougher morphology (as shown in Figure 16(c)), high dislocation density in the range of 10^9 cm^{-2} and high SF density in the range of 10^5 cm^{-1}. The SF defects are characteristic only for the nonpolar heteroepitaxial thin layer and not for the bulk nonpolar sample.[225] Considering the identical modulation effects of the chemical treatments of the two samples with respect to the chemical composition and oxide formation it is clear that the opposite effects on the PL response is related to the specific defects on the surface and near-surface region of the thin layer exposed to the laser excitation. All of the defects listed above contribute to nonradiative recombination. The etching treatment is known to be more effective in the vicinity of the dislocations intersecting the surface and the pit with facets of different orientations. This enhanced etching results in increasing the defect areas and thus the density of the nonradiative recombination centers. The cysteamine adding to the etching solutions contributes to the surface passivation of some of the surface donor/acceptor centers

and thus, depresses the nonradiative surface recombination which partly compensates for the etching effect. While the etching effect in vicinity of high defect density seems to be the dominating effect in thin nonpolar GaN layer, this effect is much less evident in the bulk GaN sample in absence of such prominent defects.

We also stress on the fact that despite the different effect of the chemical treatments on the optical response in the two types of samples, they both are significantly pronounced. Our results clearly demonstrate the modulation of optical properties by the in-situ functionalization with phosphoric acid with or without cysteamine, due to the high sensitivity of the GaN nonpolar surfaces toward these chemical spices and have the potential to be utilized in variety of sensing approaches.

3.5 Conclusion

In this study AFM, water contact angle, XPS, and PL were utilized to characterize in-situ functionalization with phosphoric acid and cysteamine of nonpolar bulk GaN and heteroepitaxial thin layer GaN residing on sapphire. Cysteamine added to phosphoric acid solutions at 40°C and 100°C resulted either in no change or a slight increase in surface roughness compared to samples treated with stock phosphoric acid solutions. As only 3 mM of cysteamine was used, no significant change in the water contact angle was observed versus solutions without cysteamine. The change in water contact angle did decrease with increasing solution temperatures. The low amount of cysteamine was confirmed with the inability to detect sulfur from the thiol group in the XPS spectra. Despite the low

concentration, cysteamine added did decrease the amount of oxygen formed at high temperatures and improved the amount of surface gallium and nitrogen species. The in-situ functionalization was shown to modulate the PL response of both types of nonpolar GaN due to high sensitivity of this surface to the chemical exposure. The enhanced PL intensity from the nonpolar bulk GaN, observed after all the treatments, was explained by the depressed nonradiative recombination due to oxide formation, while the reduced PL intensity from the nonpolar GaN layer heteroepitaxially grown on r-plane sapphire was explained by the higher density of defects present in this type of material and their enhanced effect on the nonradiative recombination upon chemical treatments.

4. In Situ Chemical Functionalization of Gallium Nitride with Phosphonic Acid Derivatives during Etching

Stewart J. Wilkins,[1] Michelle Greenough,[2] Consuelo Arellano,[3] Tania Paskova,[1,4] and Albena Ivanisevic,[1,5]

[1]Department of Materials Science and Engineering, North Carolina State University, Raleigh, North Carolina 27606, United States

[2]Department of Chemistry, Wagner College, Staten Island, New York 10301, United States

[3]Department of Statistics, North Carolina State University, Raleigh, North Carolina 27695, United States

[4]Department of Electrical and Computer Engineering, North Carolina State University, Raleigh, North Carolina 27606, United States

[5]NCSU/UNC−CH Joint Department of Biomedical Engineering, North Carolina State University, Raleigh, North Carolina 27606,
United States

The following manuscript is reprinted with permission from S.J. Wilkins, M. Greenough, C. Arellano, T. Paskova, A. Ivanisevic, "In situ chemical functionalization of gallium nitride with phosphonic acid derivatives during etching," *Langmuir*, **2014**, 30 (8), 2038-2046.

4.1 Abstract

In situ functionalization of polar (c plane) and nonpolar (a plane) gallium nitride (GaN) was performed by adding (3-bromopropyl) phosphonic acid or propyl phosphonic acid to a phosphoric acid etch. The target was to modulate the emission properties and oxide formation of GaN, which was explored through surface characterization with atomic force

microscopy, X-ray photoelectron spectroscopy, photoluminescence (PL), inductively coupled plasma−mass spectrometry, and water contact angle. The use of (3-bromopropyl) phosphonic acid and propyl phosphonic acid in phosphoric acid demonstrated lower amounts of gallium oxide formation and greater hydrophobicity for both sample sets, while also improving PL emission of polar GaN samples. In addition to crystal orientation, growth-related factors such as defect density in bulk GaN versus thin GaN films residing on sapphire substrates were investigated as well as their responses to in situ functionalization. Thin nonpolar GaN layers were the most sensitive to etching treatments due in part to higher defect densities (stacking faults and threading dislocations), which accounts for large surface depressions. High-quality GaN (both free-standing bulk polar and bulk nonpolar) demonstrated increased sensitivity to oxide formation. Room-temperature PL stands out as an excellent technique to identify nonradiative recombination as observed in the spectra of heteroepitaxially grown GaN samples. The chemical methods applied to tune optical and physical properties of GaN provide a quantitative framework for future novel chemical and biochemical sensor development.

4.2 Introduction

Surface functionalization of III−V semiconductors has gained recent attention due to the ability to tailor optical [13, 234-236] and electrical responses [236, 237] as well as physical properties [130, 237, 238] and chemical signatures of semiconducting materials with tailored surface chemistry.[129, 130, 239] The tunable band gaps and unique crystallographic

features provided by III−V semiconductors paired with distinctive surface platforms offers the ability to form a wide array of sensing applications through the binding and release of analytes from surface groups. Examples include functionalized transistors for the detection of ions through a lipid bilayer [240] or DNA/protein detection via bound gold nanoparticles.[241] GaN has shown unique properties such as high chemical stability [172] and biocompatibility,[173] particularly over gallium phosphide [242] and gallium arsenide,[243] which make it a prime candidate for biological sensors.[179] GaN can be grown along different crystallographic orientations to provide variable sets of binding locations. Polar GaN (c plane within a wurtzite crystal structure) is defined by either a gallium or nitrogen terminated surface that is readily grown using a variety of substrates and techniques. Due to the offset of gallium and nitrogen atoms, an internal polarization-induced electric field is formed, which has been shown to reduce device emission efficiency due to the spatial separation of charge carriers.[75] To address this, GaN has been grown along different crystallographic orientations such as a or m planes to eliminate spontaneous polarization. These planes are termed nonpolar and are characterized with an equal number of surface gallium and nitrogen atoms. This in turn prevents the formation of polarization-induced electrical fields. Other orientations exist (known as semipolar), which possess varying degrees of spontaneous polarization.

Though the crystal orientation provides exciting potential for tunable properties, growth of high quality substrates, particularly for orientations not in the [0001] direction, is associated with unique challenges. Traditional growth of nonpolar GaN relied on

heteroeptixial growth of thin layers of GaN on r plane sapphire, a or m plane SiC, or γ-LiAlO2,18 which leads to high stacking fault densities and partial dislocations from lattice mismatch. In order to reduce defects, GaN substrates are grown in thick layers and cut according to desired orientation. Through this growth and slice process, threading dislocations have been decreased 3 - 4 orders of magnitude compared to thin-layer heteroepitaxial nonpolar GaN. This method provides a high-quality surface for device fabrication by the absence of stacking faults, pits, and other defects.[77] Due to these challenges associated with the growth of the high-quality material, any additional strategies that permit modulation of the GaN properties can be of use for applications such as sensing.

In this study, in situ functionalization of polar (c plane) and nonpolar (a plane) GaN was achieved by adding (3-bromopropyl) phosphonic acid ($BrC_3H_6PO(OH)_2$) or propyl phosphonic acid ($C_3H_7PO(OH)_2$) to a phosphoric acid (H_3PO_4) etch, which aimed to modulate the optical properties of GaN. Wet chemical etching provides an efficient method to modulate bulk properties such as surface roughness and luminescence.[86] Etchants of GaN include phosphoric acid, potassium hydroxide, and sulfuric acid, which preferentially attack regions of high energy such as surface defects.[85] GaN is known to react to etchants through the formation of gallium oxide: $2GaN + 3H_2O \rightarrow Ga_2O_3 + 2NH_3$. The etchant (phosphoric acid) acts as the catalyst through which water reacts with gallium and removes gallium oxide into solution.[85] The concentration, time, pressure, and temperature all control the degree of etching, which was limited to concentration and temperature for this study. The addition of phosphonic acid serves to stabilize the surface, alter the optical

properties, and promote functionalization sites.[130] Phosphonic acid has been used in biosensing for pesticide detection [244] as well as a carbon dioxide quantification.[245] By adding phosphonic acid to phosphoric acid, we seek to modify the optical properties of GaN, while simultaneously controlling the degree of oxide formation to avoid over etching. This one-step approach promises to reduce device fabrication time by combining both etching and functionalization processes into a single step for future sensor applications. We believe this to be the first study performed utilizing short-chained phosphonic acids as a means to modify the GaN surfaces. The emission properties and oxide formation were explored through surface characterization (atomic force microscopy (AFM) and water contact angle), chemical characterization (X-ray photoelectron spectroscopy (XPS) and inductively coupled plasma−mass spectrometry (ICP-MS)), and optical characterization (photoluminescence (PL)). In addition to observing phosphonic acid functionalization on GaN, the effects of crystal orientation and growth related factors such as defect density in bulk GaN versus thin GaN films residing on a sapphire substrate were also investigated.

4.3 Experimental Methods

4.3.1 Sample Preparation

Polar (0 0 0 1) and nonpolar (1 1 -2 0) GaN was grown by hydride vapor phase epitaxy (HVPE). Two types of polar GaN samples were studied, thin heteroepitaxial GaN layer and bulk free-standing GaN. The thin polar GaN layer with a thickness of ~1.5 μm was grown on 330 μm thick sapphire. This type of GaN material is characterized with a high

dislocation density of about 8 x 10^9 to 1 x 10^{10} cm^{-2}.[190] The bulk free-standing polar GaN was grown to approximately 1 mm thickness and separated from the sapphire substrate before undergoing polishing on both sides to achieve a 374 μm thick free-standing GaN sample with a dislocation density around 5 x 10^5 to 1 x 10^6 cm^{-2}.[190] The as-grown Ga face was subjected to chemically mechanically polishing (CMP) prior to dicing. Two sets of nonpolar GaN samples were also evaluated: a heteroepitaxial thin layer and a bulk sample. The thin a plane nonpolar GaN layer was grown at 1080°C on a metal organic vapor phase epitaxial (MOVPE) (1 1 -2 0) GaN template on r plane (1 1 0 -2) sapphire. The bulk a plane nonpolar GaN sample was diced from a thick GaN boule grown on 2 in. diameter sapphire wafers to a thickness of 7 - 8 mm in the [0 0 0 1] direction.[225] Rectangular bars of 10 × 6 mm^2 were diced perpendicular to the boule surface, parallel to the (1 1 -2 0) plane, and were polished on both sides to form ∼420 μm thick nonpolar bulk GaN substrates.[225] CMP was performed on one side only.

All samples were diced into 3 x 3 mm^2 squares, degreased in solvent baths of acetone and methanol, and rinsed with deionized (DI) water (18.2 MΩ*cm resistivity). Samples were then dried with nitrogen before being dipped into a 100°C 50/50 vol % H_2O/hydrochloric acid (Fisher Scientific, 35−38 vol %) solution for 10 min to remove native oxide, rinsed, dried, and dipped into hydrofluoric acid (Sigma Aldrich, 48 vol %). Once rinsed and dried, samples were stored in a desiccator under low vacuum.

4.3.2 Etching

Each of the four types of GaN samples were split into three groups for different chemical treatments: (i) phosphoric acid (Fisher Scientific, 95 vol %); (ii) a 1:1, v/v phosphoric acid/3 mM (3- bromopropyl) phosphonic acid (Sigma−Aldrich, 97%) solution; and (iii) a 1:1, v/v phosphoric acid/3 mM propyl phosphonic acid (Sigma−Aldrich, 95%) solution. All samples were etched for 150 min at the temperatures of 40 or 100°C and characterized after each treatment.

4.3.3 Characterization.

A Rigaku Geigerflex model D/Max IIA X-ray diffraction (XRD) system with a Cu Kα (hv = 8047.7 eV) source was used to verify crystal orientation and configuration. It was equipped with 1° diffraction slits on both diffraction and scattering sides in conjunction with a 0.6 mm receiving slit and a 0.8 mm receiving slit monochromator. A (0 0 4) silicon peak (69.13° 2θ) was used for calibration. XRD 2θ scans in the range 30 - 75° were captured with a step size of 0.008°. The spectra (not shown here) revealed, as anticipated, only two peaks ((0 0 2) and (0 0 4)) for bulk free-standing polar GaN but an extra peak associated with (0 0 6) sapphire reflection for the thin-layer heteroepitaxial polar GaN spectra. For nonpolar samples, the (1 1 0) GaN reflection was seen as well as the (2 -2 4) Al_2O_3 reflection for the samples residing on the r plane sapphire. All the spectra were analyzed using MDI DataScan4 software. The control groups were characterized before and after etching using the following techniques.

A Cypher AFM by Asylum Research was employed to take topography images for each sample with Veeco aluminum-coated SiN tips. 12 mm diameter 430 stainless steel discs were used to mount samples during imaging. Three random 10 x 10 μm^2 locations were imaged on each sample using a 1 Hz frequency. All images were flattened via Igor Pro (v. 10.0) software and averaged to calculate root mean-square (rms) roughness values.

A model 200-F4 goniometer by Ramé-hart was equipped with a 28 ga. (AWG) needle to perform water contact angle measurements. Water drops were captured at 2 frames per second for 5 s. This was performed five times per sample. The half angles were averaged together and then averaged across the repeated tests to produce a cumulative sample average. Nitrogen was used to dry the samples after each test. The water contact angles were captured with DROPImage (v. 2.4.07) software.

An Axis Ultra XPS by Kratos utilizing a monochromated Al Kα (hv = 1486.7 eV) source with charge neutralizer (2.0 filament current) examined surface chemistry. Copper tape was used to mount samples to an aluminum sample holder. Pass energies of 20 eV produced high resolution region scans (Br3d, C1s, Ga2p, Ga3d, N1s, O1s, P2p, and S2p) that were swept five times to form final average region scans. Survey scans were produced with 160 eV pass energies and were only scanned once. All scans were performed at 3×10^{-8} Torr and at a 0°, 45°, and 60° take off angles. Deconvolution of high-resolution region scans were performed with Casa XPS (v. 2.3.16 PR) after calibrating the C1s peak to 284.8 eV.[144] The full-width at half-maximum (FWHM) of deconvoluted peaks was limited to the strongest peak according to a Lorentzian fit after removing the background with a Shirley

approximation. Kratos provided atomic sensitivity factors were utilized for surface quantification. The deconvoluted Ga2p peaks were used to calculate atomic percentages (average of the three take off angles) rather than Ga3d due to more surface sensitive depth profiling.[191] Nitrogen content was quantified after removing contributions from Ga auger peaks from the N1s spectra. All region scans were normalized following quantification.

A Jobin Yvon LabRam ARAMIS Raman/PL setup by Horiba was used to record photoluminescence spectra at room temperature with a 325 nm HeCd laser. The microscope was calibrated to Teflon (Raman peak of 1295 cm^{-1}) with a 40x UV objective at 2400 grating/min resolution. The objective height was locked from calibration to capture spectra from 330 to 400 nm. The real time data (RTD) exposure time, accumulated exposure time, and filters were varied to prevent signal cutoff. The RTD, exposure time, and filter were 5, 2, and 30% for polar bulk free-standing GaN; 5, 2, and 0% for thin-layer polar GaN; 1, 1, and 90% for bulk nonpolar GaN; and 1, 1, and 0% for thin-layer nonpolar GaN.

An 820 ICP-MS spectrometer by Varian was used to identify leaching of gallium from four individual bulk free-standing polar GaN samples. Samples were functionalized with 40 °C (3-bromopropyl) phosphonic acid in phosphoric acid and steeped in 1.5 mL of DI water, physiological saline solution (0.9 g NaCl/100 mL H_2O), physiological saline solution with 10 vol % H_2O_2, and 0.1 M sodium acetate (pHs 7.9, 4.7, 3.8, and 5.0, respectively) solutions for 7 days. Samples were removed from solution, cleaned as previously described, etched in 40 °C phosphoric acid, and dunked into fresh solutions for 7 days. Gallium

concentration calibration was performed via monitoring gallium 69 with a linear fit against random samplings.

4.4 Results and Discussion

4.4.1 Surface Morphology

Topography images of GaN were taken to qualitatively assess the effects of etching and functionalization. Thin polar GaN layer residing on sapphire shows a hillock structure that lacked surface pits (see the Supporting Information).[189] Free-standing bulk polar GaN on the other hand has multifaceted pit formation, which is associated with nonfully coalescent intentionally introduced pits at the interface, aiming to reduce to strain and to assist the self-separation.[233] Throughout the treatments, little changes in surface topography are seen other than surface contamination. This was confirmed with surface rms roughness data (Supporting Information), revealing almost no morphology difference between treatments with and without phosphonic acid additives.

The nonpolar bulk GaN displays a smooth surface relative to that of thin-layer heteroepitaxial GaN, which is characterized by pits. Unlike the free-standing bulk polar GaN, the nonpolar GaN surface of the thin layer is characterized by deep diamond shaped pits and v-grooves, which are characteristic of stacking faults manifesting themselves through partial dislocations along polar directions.[79, 81, 225] These grooves are essentially a side view of uniformly shaped polygonal pits seen from the polar GaN.[246] No correlation is discernible between etchant temperatures or composition, as treatments resulted in relatively smooth

surfaces. As evaluation spots were selected randomly across the sample, it is likely that images may show unusual smooth regions. It should be noted that the v-grooves and pits did not increase in length as treatments were relatively mild (not long enough or hot enough) to promote preferential etching as seen elsewhere.[81, 86, 89] The thin heteroepitaxial nonpolar GaN layer demonstrated a greatest surface roughness due to a higher density of stacking faults and associated partial dislocations that is common with this growth technique.[225]

Due to the large standard deviation across the sample sets, no clear correlation can be made regarding the effect of the phosphonic acid attachment on the surface roughness. Longer chained phosphonic acids altered a smooth solid gallium surface by only 0.06 nm; hence, any significance is likely lost in the noise as short-chained phosphonic acid groups were utilized within this study.[237]

4.4.2 Hydrophobicity

Water hydrophobicity is used as a measurable quality for surface functionalization of materials. For GaN, an oxide-deficient surface demonstrates hydrophobic characteristics, while hydrophilic characteristics reveal an oxide layer.[130] Additionally, self-assembled monolayers bestow hydrophobic properties upon a surface with sufficient coverage. The nonpolar GaN samples (Supporting Information) demonstrate hydrophobic characteristics that have been reported for cleaned gallium compounds.[196, 197, 238] The polar GaN produces a comparable degree of hydrophobicity to that reported for nonpolar GaN and solid gallium but fall short of the degree of hydrophobicity seen from polar GaN samples within

this study.[237] Pristine samples show water contact angles larger than those on samples following 40 and 100°C treatments without phosphonic acid additives, which is consistent regardless of sample orientation or quality. This indicates the formation of an oxide layer, formed during the etch process. The addition of phosphonic acids to phosphoric acid resulted in contact angles more similar to those on pristine samples, which were greater than the angles seen on samples having only been treated with 40°C phosphoric acid. Further increasing the etchant temperature to 100°C led to a similar effect to that of 40°C solution treatment but not always. The use of 3 mM short alkyl chained phosphonic acid groups for a maximum 150 min at high temperature may result in a limited formation of uniform layer on the surface. Other reports have shown that increased time [237] and decreased temperature [238] resulted in larger contact angles. In comparison to the literature, shorter alkyl chains are less likely to form complete monolayers due to decreased van der Waals interactions between the chains and decreased steric hindrance between the water molecules and the substrate surface.[130] The formation of phosphonic-based monolayers requires water as a base for surface hydroxyl ions, water molecules, and oxides that assist in the formation of the monolayers.[129, 131, 239, 247]

4.4.3 Chemical Composition

To identify the surface species contributing to the changes in hydrophobicity, XPS was employed. The technique allowed us to probe the surface with high sensitivity. Figures 17 and 18 show high-resolution Ga2p spectra of polar and nonpolar GaN samples,

respectively. The deconvolution of XPS spectra provides a way to examine individual species formed within a single peak that is lost with peak shifting interpretation. This was performed by breaking the $Ga2p_{3/2}$ peak into three distinct regions associated with Ga-Ga bonding, Ga-N bonding, and gallium oxide formation (Ga_2O_3). The Ga-Ga bonding was reported to have binding energies around 1116.0 eV,[200, 201] the Ga-N bonding was reported to reside near 1118.0 eV,[248, 249] and the gallium oxide peak was reported to reside near 1119.5 eV.[248] The three respective peaks are colored green, red, and blue to better distinguish each species, while the black line represents the raw signal. In order to avoid the individual peaks from overlapping, additional constraints were placed. Hence, each deconvoluted species binding energy was given a limited ± 0.25 eV tolerance to ensure no unusual shifting. This agrees with values seen within the literature. An additional gallium oxide species (Ga_2O) is known to form during reactions but could not be resolved from the dominant Ga_2O_3 peak. As the Ga_2O formation is less thermodynamically stable, it is unlikely to be the dominant gallium oxide signal due to its instability.[208] The FWHM of the deconvoluted peaks was controlled by the FWHM of the primary Ga-N species peak to prevent unreasonable broadening. The FWHM of the peaks from bulk free-standing polar GaN showed a maximum variance of 0.336 eV, 0.053 eV for thin-layer polar GaN, 0.131 eV for bulk nonpolar GaN, and 0.273 eV for thin nonpolar layer GaN on sapphire. The entire FWHM analysis can be seen in the Supporting Information. The formation of gallium oxide is known to cause a peak broadening as well as a peak shifting to higher energies; however, it is distinguishable from other species.[137, 206, 207]

Figure 21a,b shows high-resolution $Ga2p_{3/2}$ spectra of freestanding bulk polar GaN and thin heteroepitaxial c plane layer GaN on sapphire, respectively. The bulk free-standing polar GaN demonstrated higher sensitivity to the treatments, as compared to that of the thin GaN layer, manifested by a significant shifting of the XPS peaks toward higher binding energies (resulting from the formation of oxide species represented in blue). The 100°C phosphoric acid treatment led to the greatest amount of oxide formation while a clean substrate demonstrated the least amount of oxide for bulk polar GaN. By adding phosphonic acid, the amount of oxide formation was decreased at both treatment temperatures with (3-bromopropyl) phosphonic acid having a greater effect than that of the propyl phosphonic acid. This trend was not seen for thin-layer heteroeptixial polar GaN, which demonstrated minimal shifting to higher binding energies. Propyl phosphonic acid assisted phosphoric acid solutions treatment led to minor shifting at high temperatures and no shifting at lower temperatures.

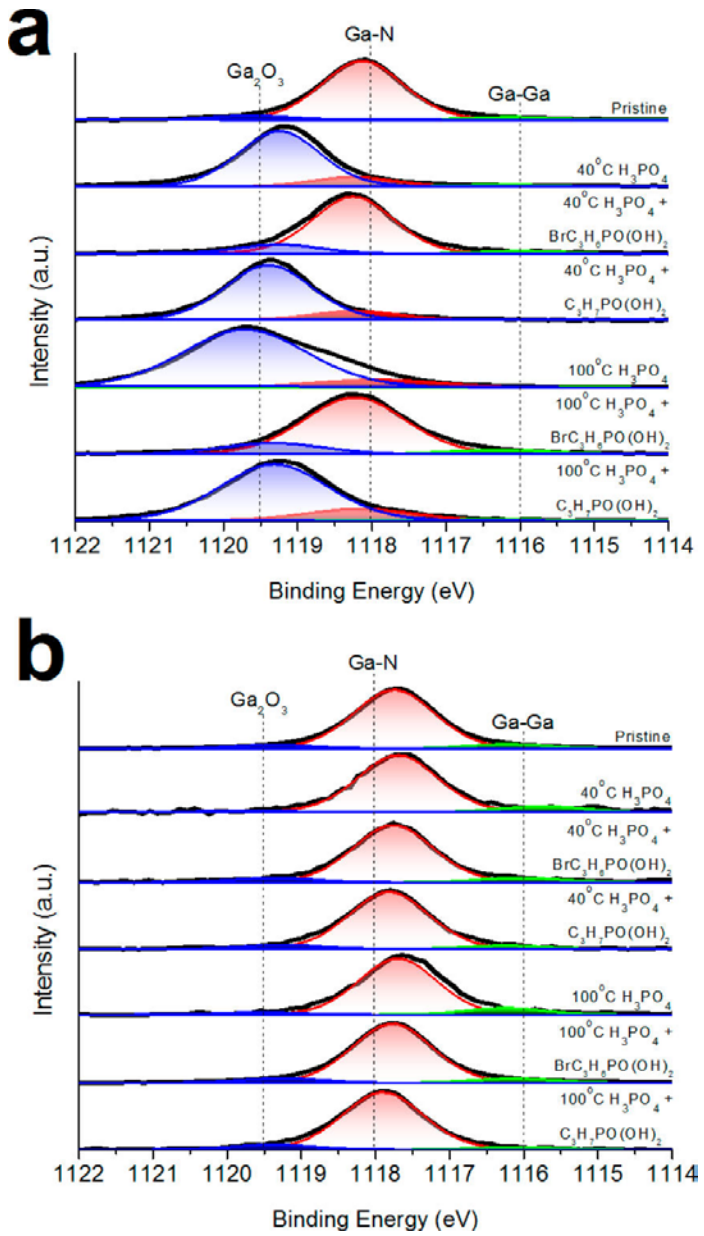

Figure 21 XPS Ga2p spectra of (a) polar c plane free-standing bulk GaN and (b) thin heteroepitaxial c plane layer GaN residing on c plane Al_2O_3. The reported binding energies for Ga_2O_3, Ga-N, and Ga-Ga are indicated with dotted lines at 1119.5, 1118.0, and 1116.0 eV, respectively.

High-resolution $Ga2p_{3/2}$ spectra for nonpolar GaN samples, shown in Figure 22, display similar characteristics to those shown for polar samples in Figure 21. Treatments with phosphoric acid only promote increased gallium oxide formation, while the addition of phosphonic acid to the phosphoric acid etch limits this formation. Similar to the spectra from the thin polar GaN layer, minimal shifting was seen for other treatments. Overall, nonpolar bulk GaN demonstrates a decreased sensitivity to oxide formation than polar bulk GaN, while the thin-layer versions remain relatively unresponsive to different treatments. The increased gallium content for the polar bulk GaN may be responsible for this increased oxide formation as there are more gallium atoms readily available for reactions. The indifference of the thin-layer GaN versions is likely to be a result from the substrate interaction and stabilization on the GaN film. It should be noted that peak shifting is limited to the 0.1 eV resolution of the XPS.

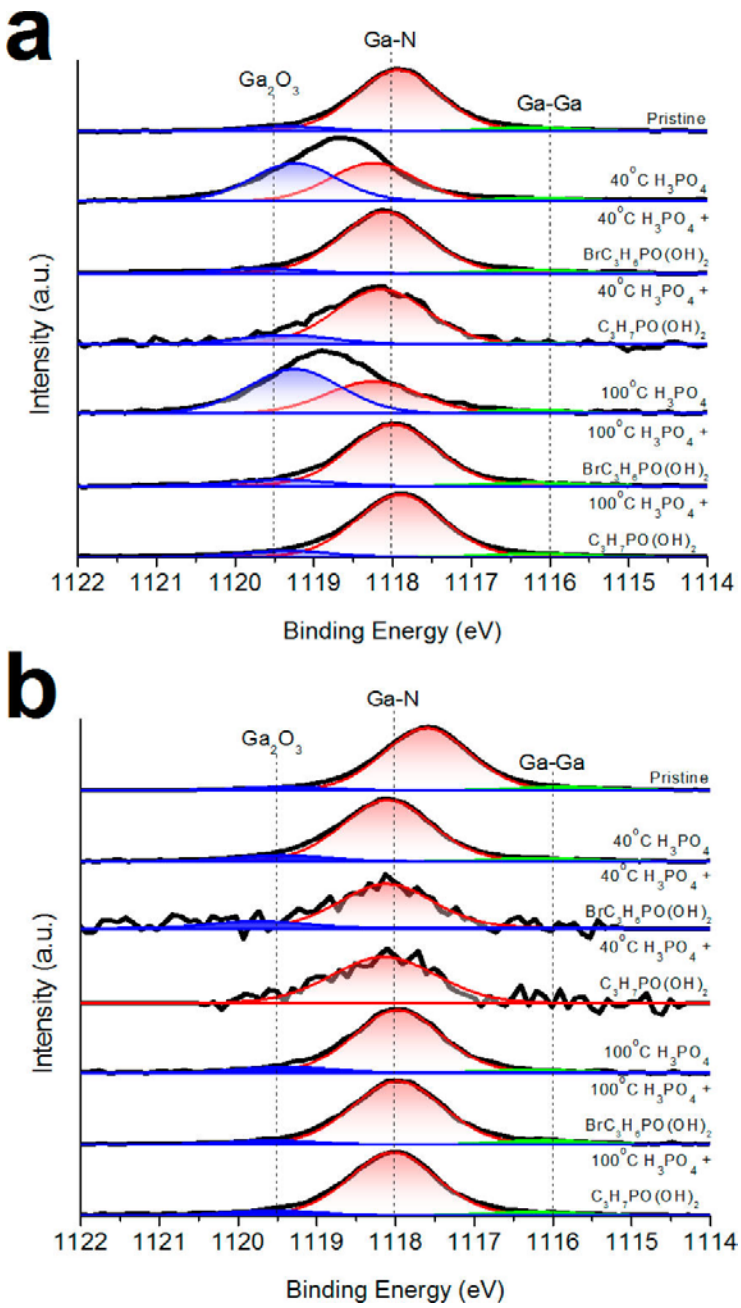

Figure 22 XPS Ga2p spectra of (a) nonpolar a plane bulk GaN and (b) thin heteroepitaxial a plane layer GaN residing on r plane Al_2O_3. The reported binding energies for Ga_2O_3, Ga-N, and Ga-Ga are indicated with dotted lines at 1119.5, 1118.0, and 1116.0 eV, respectively.

Quantitative analysis of the ratios of gallium oxide to other species can be seen in Table 8, represented by the ratio of the respective peak integral area. For the polar bulk free-standing GaN, treatments in 40 and 100°C phosphoric acid led to the most gallium oxide to other gallium binding species. This is consistent with previous studies where unprotected gallium nitride surfaces undergo extensive oxidation.[208] The addition of phosphonic acid limits the formation of additional oxide layers as binding of phosphonic acid prevents subsequent attack of gallium to form more gallium oxide. This can be seen when comparing the Ga2p to Ga3d Ga/O ratio (Supporting Information), with the exception of 40°C phosphoric acid for bulk free-standing polar GaN. Without an oxide layer, phosphonic acid cannot bind to a surface,[129, 246] which in turn limits the stability of the oxide layer under harsh environments. Direct phosphonic acid attachment was manifested by a wide oxide peak appearance in the O1s spectra (not shown). The wide oxide peak is composed of a primary peak at 533 eV and a secondary peak at 531 eV, which is characteristic for phosphonic acid (taken in powder form). The 531 eV is associated with hydroxyl groups that readily react to form a monolayer. The stronger this peak is, the greater the likelihood phosphonic acid groups have attached to the surface.[103] The surface treated with phosphonic acid demonstrated greater amounts of carbon content (Supporting Information) than the nonfunctionalized surfaces, which is attributed to the alkyl chains of the phosphonic acids. The change in surface chemistry, as shown by XPS, confirms that the change in hydrophobicity (a useful indicator of bulk properties) was not solely due to oxide or topography changes from the etchant but from surface modification due to phosphonic acid

groups as well. Furthermore, statistical analysis via a t test was performed (Supporting Information) in order to determine differences between the crystallographic directions upon similar treatments. The latter revealed that only the 100°C (3-bromopropyl) phosphonic acid proved significant among the treatments (no difference between substrates). Unlike thiol based functionalization that requires a pristine surface to directly bind to, phosphate groups are more stable under a variety of conditions when used in conjunction with an oxidized surface.[130] Both nonpolar bulk GaN and thin-layer GaN demonstrated this effect similar to polar free-standing bulk GaN. Such a trend was not observed for thin-layer polar GaN, likely due to a region of inhomogeneous oxide coverage.

Table 8 Ratios of the integral areas of the peaks related to G-N and Ga-Ga divided by that of the Ga_2O_3 related peak for the different sample sets and treatments. - signifies insignificant gallium oxide for ratio calculation.

	Polar		Nonpolar	
	Free-standing Bulk	Thin Layer	Bulk	Thin Layer
Pristine	8.9	14.0	19.8	-
40°C H_3PO_4	0.3	19.0	1.1	4.4
40°C H_3PO_4 + $BrC_3H_6PO(OH)_2$	8.4	14.1	18.4	-
40°C H_3PO_4 + $C_3H_7PO(OH)_2$	8.7	11.0	18.4	-
100°C H_3PO_4	0.5	12.8	1.1	7.1
100°C H_3PO_4 + $BrC_3H_6PO(OH)_2$	11.2	14.1	29.0	14.4
100°C H_3PO_4 + $C_3H_7PO(OH)_2$	5.4	5.0	19.9	15.1

In addition to identifying the surface composition, the reactivity of GaN surfaces (functionalized and nonfunctionalized) to different liquid environments was investigated via

ICPMS. GaN has shown potential as a biologically compatible material;[173] hence, a few solutions corresponding to fluids found within a body (with the exception of DI water) were selected for our study. Only the treatments at 40°C were tested in order to utilize the sensitivity of the polar free-standing bulk GaN toward oxide formation observed. A temperature of 40°C was chosen so as to avoid overetching that occurred at higher temperatures. As can be seen from Table 2, the 40°C phosphoric acid treatment led to a magnitude greater gallium leach within DI water, saline solution, and 0.1 M sodium acetate solution as compared to the treatment at the 40°C with 3 mM (3-bromopropyl) phosphonic acid in phosphoric acid. This result demonstrates the protective quality of the phosphonic acid treatment that prevents increased leaching of gallium through retained oxide formation. Phosphoric acid was seen to produce larger quantities of gallium oxide, which confirms the mechanisms associated with etching GaN. The addition of 10 vol % hydrogen peroxide was used to simulate altered physiological saline solution as in the case of environments containing macrophages.[167, 242] In that particular case, we observed halting of gallium leaching from the samples treated with phosphoric acid at 40°C. Hydrogen peroxide readily forms intermediate hydroxyl surface radicals, which promotes rapid oxide formation.[250] This rapid oxide formation promotes a more uniform passivation layer not achieved with atmosphere and water alone. Additionally, phosphonic acids provide passivation better at lower pH solutions,[129] which was seen in Table 9.

Table 9 Gallium concentration (ppb) measured by ICP-MS after 7 days in different solutions (horizontal rows) verses two different etchants treatments (vertical columns).

Treatment/Gallium Concentration (ppb)	40°C H_3PO_4	40°C H_3PO_4 + $BrC_3H_6PO(OH)_2$
DI H_2O	168.8	37.7
H_2O + NaCl	182.4	17.8
H_2O + NaCl + H_2O_2	8.5	11.1
H_2O + CH_3COONa	179.4	34.5

4.4.4 Optical Properties

Room-temperature PL provided an effective technique to identify the effects of etching, acid attachment, and crystal quality. Figure 23a,b shows representative PL spectra in the near-band-edge (NBE) region of pristine surface of free-standing bulk polar GaN and thin-layer heteroepitaxial GaN, respectively. Comparative analysis of the averaged intensities of the NBE emission from the pristine surface reveals stronger emission from the bulk free-standing polar GaN with a high signal-to-noise ratio. The PL spectrum from the thin-layer GaN on the other hand showed increased jagged signal quality, lending itself to increased signal obstruction from nonradiative recombination from increased defect density.[59, 233] By analyzing the PL wavelength, it was observed that the NBE peak from the thin-layer polar GaN was blue-shifted relative to the emission wavelength from the freestanding bulk GaN as a consequence of the biaxial induced strain due to the lattice and thermal expansion coefficient mismatch between the GaN and c plane sapphire.[212, 213] In addition to peak shifting, the PL spectrum from the thin-layer GaN lacked the manifestation of longitudinal-

optical (LO) phonon replicas from the primary exciton emission in contrast to the well-pronounced LO-related shoulders seen in the freestanding bulk GaN. LO phonon replicas are frequently seen in room-temperature PL spectra from high-quality, low-defect density GaN samples.[251]

Wet chemical etching is used as a way to modify optical properties in an efficient and inexpensive way.[88] A schematic comparative diagram of the altered NBE emissions integral intensity for the two sets of polar GaN samples are shown in Figure 23c. The PL intensity of the thin-layer GaN on sapphire was the most enhanced after the sample was treated with 40°C (3-bromopropyl) phosphonic acid assisted phosphoric acid. Enhancement of the PL signals to a less extent was also seen in the spectra from the samples treated with 40°C propyl phosphonic acid in phosphoric acid and with 100°C phosphoric acid solutions. The PL emission form the freestanding bulk GaN samples treated at 40°C with (3-bromopropyl) phosphonic acid assisted phosphoric acid and with propyl phosphonic acid assisted phosphoric acid showed only moderate PL enhancement. Both polar free-standing bulk GaN and thin-layer GaN demonstrate sensitivity to the temperature and the composition of the chemical solution treatment. The emission from the free-standing bulk polar GaN is the most sensitive to the temperature treatment most likely related to the formation of large pits with additional crystallographic facets. On the other hand, the PL spectra from thin-layer polar GaN demonstrate increased PL intensity after low-temperature phosphonic acid assisted phosphoric acid treatments as well as phosphonic acid free high-temperature phosphoric acid. The diminished PL signal degradation as compared to that of the PL spectra

from the bulk polar GaN samples treated with phosphoric acid only is explained by the adherence of phosphonic groups, which also limited the formation of oxides.

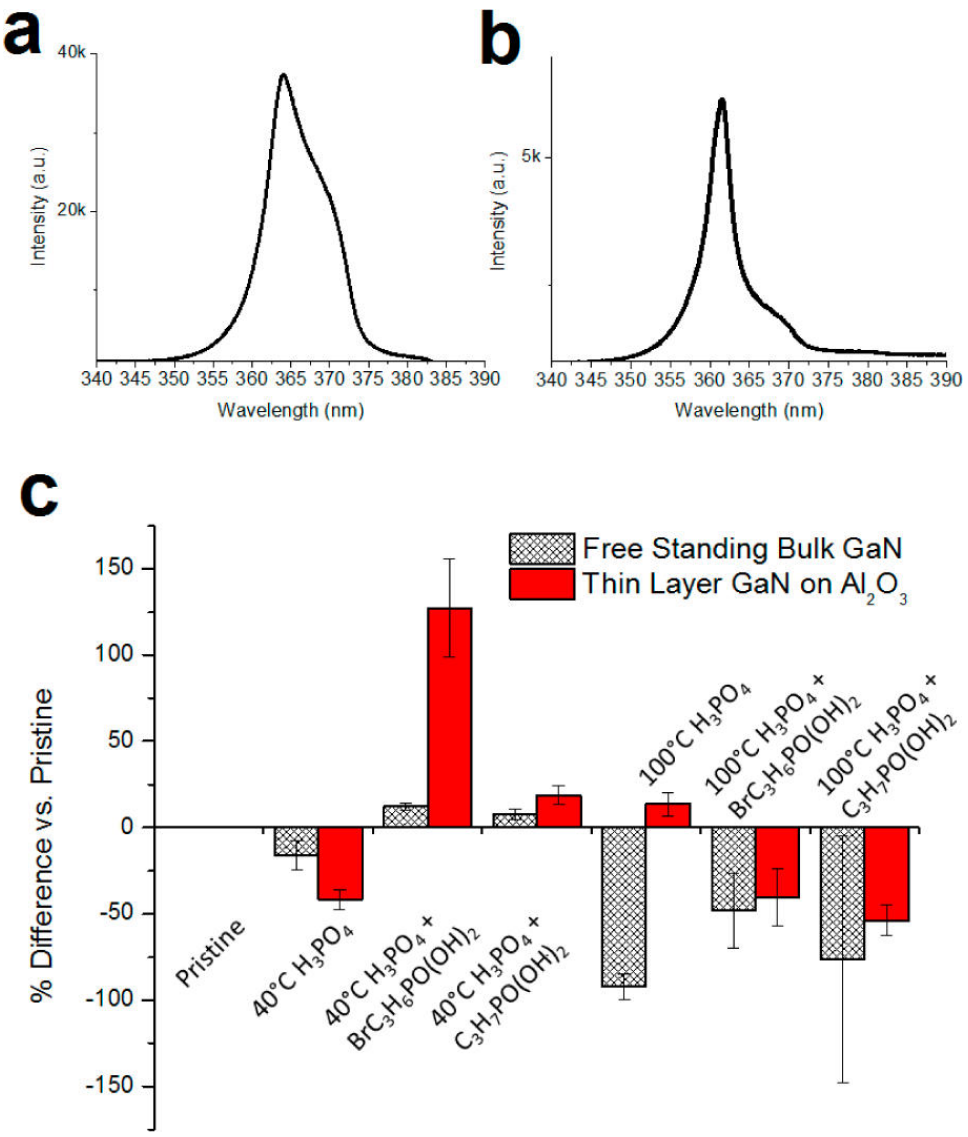

Figure 23 PL spectra of (a) a pristine polar c plane free-standing bulk GaN sample, (b) a thin heteroeptiaxial layer polar GaN sample, and (c) a comparison of averaged maximum PL intensities relative to pristine samples.

The effect of different treatments on the optical properties of the nonpolar samples was also evaluated, and the results are summarized in Figure 24. The PL spectrum from the bulk nonpolar GaN (Figure 24a) was similar to that from the bulk free-standing polar GaN, possessing similar strong intensity with high signal-to-noise ratio along with a similar phonon related replica. This is an expected result for samples of similar high crystalline quality. The PL spectrum from the nonpolar thin-layer GaN (Figure 24b) however reveals diminished intensity with noticeable noise and broader NBE emission related to the high defect density, partial dislocations, and stacking faults, typical for this material as seen from AFM. The larger broadening in this case is most likely due to enhanced exciton-defect scattering that leads to inability to resolve the zero-phonon line and the phonon line. In this case, strain related shifting was not observed despite the fact that such a thin layer is not likely to be strain-free. This was previously explained by the anisotropic character of the three strain components in the a plane GaN, which allows for a certain combination of the in-plane components a zero shift of the bandgap emission.[252, 253] The effect of the different chemical treatments on the emission intensity was similarly summarized in Figure 24c. The PL intensity of the bulk nonpolar GaN was enhanced the most after the treatment with 100°C phosphoric acid followed closely by treatment with 40°C phosphoric acid. The PL intensity from the thin nonpolar layer GaN on sapphire was also enhanced after the treatment with 40°C phosphoric acid but remained largely unchanged with other treatments. The PL spectrum from the bulk nonpolar GaN showed enhancement as well after treatment with (3-bromopropyl) phosphonic acid assisted phosphoric acid at both 40 and 100°C. Comparing

the PL spectra from the two types of nonpolar GaN samples with noticeably different defect densities, one can see that the emission from the bulk nonpolar GaN is significantly stronger due to enhanced exciton-related emission being less affected by defect scattering in higher quality material. Comparing the PL spectra from all four types of GaN, one can identify that the PL from the polar GaN (both freestanding bulk and thin layer) was less affected by all the chemical treatments than the PL from the nonpolar samples. We attribute this observation to the highest chemical resistivity of the Ga face of the polar material. This leads us to a conclusion that the optical properties of the nonpolar GaN, with an equal number of gallium and nitrogen atoms, appear more sensitive to chemical variations and the material can be used as a more optically sensitive interface for chemical sensor applications.

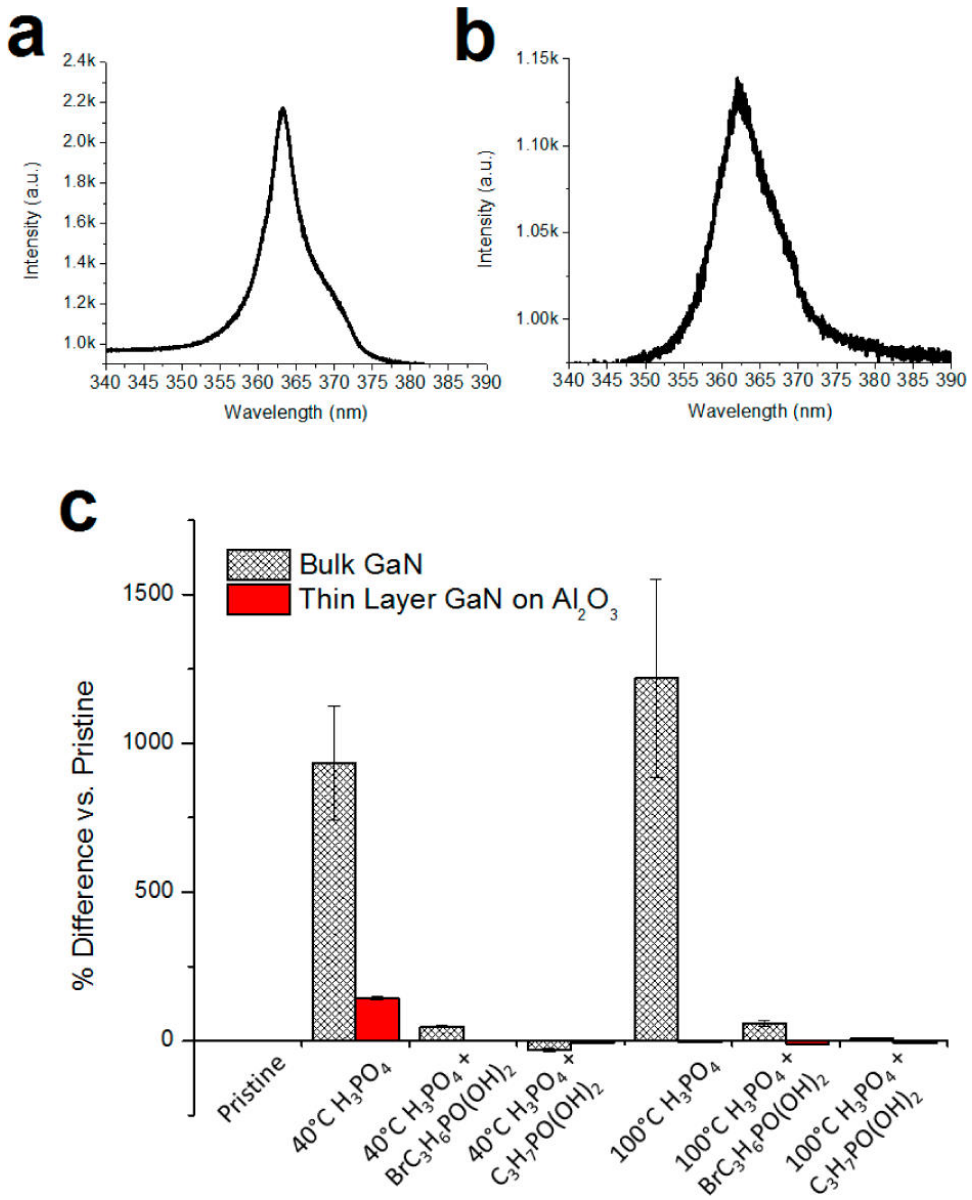

Figure 24 PL spectra of (a) a pristine nonpolar a plane bulk GaN, (b) a thin heteroepitaxial nonpolar a plane layer GaN residing on r plane sapphire, and (c) a comparison of averaged maximum PL intensities relative to pristine samples.

4.5 Conclusions

In this study, AFM, water contact angle, XPS, ICP-MS, and PL were utilized to characterize functionalization of GaN with various crystal qualities and surface orientations upon treatments with phosphoric acid, (3-bromopropyl) phosphonic acid, and propyl phosphonic acid. The addition of phosphonic acids to phosphoric acid did not lead to a noticeable change in the surface roughness of the various GaN samples. Etchant solutions containing phosphonic acids promoted hydrophobic behavior for all GaN samples at low temperature and for most samples at higher etchant temperature. The use of (3-bromopropyl) phosphonic acid and propyl phosphonic acid in phosphoric acid led to lower amounts of gallium oxide formation, which is associated with phosphonic group attachment to the surface as a result of surface passivation. Bare GaN exhibited decreased hydrophobicity and greater oxide formation as a result of treatment with only phosphoric acid. Phosphonic groups were identified through decreased oxide formation (greater hydrophobicity and decreased gallium oxide formation) as well as increased carbon content from phosphonic acids. In addition to providing passivation, phosphonic acid assisted phosphoric acid treatment resulted in enhanced PL emission from both thin layer and bulk freestanding polar GaN at low temperatures and bulk nonpolar GaN at 40 and 100°C (3-bromopropyl) phosphonic acid assisted etching solutions. High-quality GaN (both freestanding bulk polar and bulk nonpolar) demonstrated increased propensity to oxide formation, which in turn affected the chemical stability of the PL signal. The combination of etching and functionalization provide a potential avenue for future sensor fabrication.

5 Modified Surface Chemistry, Potential, and Optical Properties of Polar Gallium Nitride via Long Chained Phosphonic Acids

Stewart J. Wilkins,[1] Tania Paskova,[1,2] Albena Ivanisevic[1,3]

[1]Department of Materials Science and Engineering, North Carolina State University, Raleigh, North Carolina, 27606, USA

[2]Department of Electrical and Computer Engineering, North Carolina State University, Raleigh, North Carolina, 27606, USA

[3]NCSU /UNC-CH Joint Department of Biomedical Engineering, North Carolina State University, Raleigh, North Carolina, 27606, USA

The following manuscript is reprinted with permission from S.J. Wilkins, T. Paskova, A. Ivanisevic, "Modified surface chemistry, potential, and optical properties of polar gallium nitride via long chained phosphonic acids," *Applied Surface Science*, **2015**, 327, 498-503.

5.1 Abstract

Surface potential, chemistry, topography, and optical properties were modulated utilizing the attachment of phosphonic acids (11-Mercaptoundecylphosphonic acid, 1H,1H,2H,2H-Perfluorooctanephosphonic acid, and 1,8-Octanediphosphonic acid) with phosphoric acid to polar (c-plane) GaN. These changes were identified using x-ray photoelectron spectroscopy (XPS), atomic force microscopy (AFM) with kelvin probe force microscopy (KPFM), photoluminescence (PL), and water contact angle. The results indicated that the attachment of phosphonic groups to gallium nitride strongly depends on the formation of a native oxide layer and subsequent passivation. It was seen that a fluorine

terminated phosphonic acid increased the overall surface oxide versus other groups, as well as reduced the surface potential and improved the photoluminescence relative to other treatments. Sulfur terminated phosphonic acid demonstrated a similar reduction in surface potential and oxide formation to fluorine based phosphonic acid; however, improvements of optical luminescence on the same scale were not achieved.

Keywords: In-situ functionalization, polar, gallium nitride, x-ray photoelectron spectroscopy, kelvin probe microscopy.

5.2 Introduction

Surface functionalization of gallium nitride (GaN), a III-V semiconductor, provides unique properties such as increased water hydrophobicity,[92, 128, 133] extra binding sites,[254] and modified optical properties.[152] GaN has gained significant attention due to its electrical and optical properties that are dependent on crystallographic orientations,[59] but also improved chemical stability[172] and biocompatibility[173] over other semiconducting platforms such as GaAs[243] or GaP.[242] This has enabled new applications for GaN such as chemical and biological sensors.[255] To date, surface functionalization of GaN has been performed using carboxylic,[133] thiol,[92] and phosphonic groups.[131] In terms of surface stability, phosphonic acids produce the strongest surface bonding and improve performance with increased oxide coverage. Thiols and carboxylic groups require pristine surfaces for adhesion, which in turn requires the use of highly controlled environments. The exposure to aqueous environments replaces thiol groups

with hydroxyl and oxide groups, thus limiting the effectiveness of thiol treatments on GaN.[128, 133] Short and long chained alkanephosphonic acid functionalization of GaN have been explored previously;[128, 130, 131, 133] however, the use of phosphonic acids with terminal groups of high electronegativity has not been reported. The use of benzyl phosphonic acids and terminated alkanephosphonates has been shown for materials such as TiO_2,[104] indium tin oxide (ITO),[125, 247, 256-259] and ZnO.[103, 260, 261] Phosphonic acids provide not only a change in surface chemistry, but also in electrical characteristics such as improved charge injection for $TiO_{2[104]}$ and removal of midgap surface states through band bending for ZnO.[260] In the case of organic dye sensitized solar cells and organic light emitting diodes (OLEDs), matching the electrical structure across interfaces is crucial for improved device efficiency.

In-situ functionalization of polar (c-plane) free-standing bulk GaN via phosphonic acids altered surface electrical and chemical signatures as well as produced quantifiable changes to optical properties. This was performed by altering the concentration of phosphoric acid and adding 11-Mercaptoundecylphosphonic acid (MUDPA), 1H,1H,2H,2H-Perfluorooctanephosphonic acid (PFOPA) , and 1,8-Octanediphosphonic acid (ODPA) to various treatments. Phosphoric acid is known to catalyze with regions of high energy within GaN, such as defects, with water to form gallium oxide and ammonia.[85] The formation of gallium oxide (Ga_2O_3) alters the surface optical properties as the band gap shifts from 3.4 eV (GaN) to approximately 5.0 eV.[262, 263] In addition to producing gallium oxide, aqueous solutions increase the amount of surface hydroxyl groups, with subsequent attachment of

additives via condensation reactions. By attaching groups to the thin oxide layer, additional chemical attacks are lessened by stabilizing this oxide layer, which additionally provides unique surface properties and additional secondary reaction platforms.[130] X-ray photoelectron spectroscopy (XPS) was utilized to identify changes to the surface chemistry, while atomic force microscopy (AFM) and kelvin probe force microscopy (KPFM) identified alterations to the surface topography and potential. Optical properties and water hydrophobicity were observed via photoluminescence (PL) and water contact angle.

5.3 Materials and Methods

5.3.1 Sample Preparation

Polar (0001) free-standing GaN with a dislocation density in the range of $5x10^5$-$1x10^6$ cm^{-2} was manufactured by hydride-vapor phase epitaxy (HVPE).[190] The sample was approximately 1.2 mm thick prior to being separated from a sapphire substrate and chemical-mechanically polished on the gallium terminated side. 3 x 2 mm^2 rectangles were formed from dicing and were pretreated with solvent baths of acetone and methanol before being washed with deionized (DI) water (18.2 MΩ*cm). Nitrogen was used to dry the samples before being placed in a 100°C 50/50 vol.% hydrochloric acid (Fisher Scientific 35-38% vol. %)/water solution for 10 minutes. The samples were rinsed with DI water for 2 seconds, immediately dried with nitrogen and were held in a desiccator under vacuum for storage.

5.3.2 Sample Treatment

A total of 5 samples were treated with various solutions of phosphoric acid (Fisher Scientific, 95%) and phosphonic acid additives: (i) 95% phosphoric acid; (ii) 50/50 vol.% water/phosphoric acid; (iii) 50/50 vol.% 3mM 11-Mercaptoundecylphosphonic acid (Sigma-Aldrich, 97%)/phosphoric acid; (iv) 50/50 vol.% 3mM 1H,1H,2H,2H-Perfluorooctanephosphonic acid (Sigma-Aldrich, 95%)/phosphoric acid; and (v) 50/50 vol.% 3mM 1,8-Octanediphosphonic acid (Sigma-Aldrich, 97%)/phosphoric acid. All the samples were treated for 150 minutes at 40°C, rinsed with DI water for 2 seconds, dried with nitrogen, and characterized.

5.3.3 Characterization

The samples were examined with a Kratos Axis Ultra XPS within two hours from treatment to safeguard purity. The surface chemistry was analyzed with a monochromated Al Kα (*hv* = 1486.7 eV) source with charge neutralizer (2.0 A filament current). Copper tape was used to mount samples to an aluminum sample holder. Three random spots were taken on each specimen at 0°, 45°, and 60° photoemission angles per spot. 5 sweeps of 20 eV pass energies were averaged to produce high resolution region scans of C1s, Ga2p, Ga3d, N1s, P2p, S2p, F1s, and O1s. Survey scans were formed with 160 eV pass energies and were only scanned once. All scans were recorded at pressures at or below 3×10^{-8} torr. Casa XPS (Ver. 2.3.16 PR) software was used for peak deconvolution following charge correction using C1s (284.8 eV).[144] The XPS is calibrated to Ag (368.21 eV) according to ISO TC/201.[145]

The full-width at half-maximum (FWHM) of deconvoluted peaks was limited to the primary peak according to a Lorentzian fit after removing the background with a Shirley approximation. Kratos provided atomic sensitivity factors were utilized for surface quantification. Ga3d region was used to calculate atomic percentages rather than Ga2p due to its greater depth profiling.[191] Ga auger peaks from the N1s spectra were not included in the surface quantification. The Ga2p region scans were normalized for presentation.

Room temperature photoluminescence was recorded with a Horiba Jobin Yvon LabRam ARAMIS Raman/PL setup utilizing a 325 nm HeCd laser excitation source. The microscope was aligned to Teflon (middle Raman peak of 1295 cm^{-1}) with a 40x UV objective at a 2400 grating/minute resolution. The objective height was locked following a calibration to capture spectra from 330 to 400 nm across all samples. The real-time display (RTD) exposure time, accumulated exposure time, and number of accumulations were 1 second, 1 second, and 5 respectively, with a 60% signal filter. Each sample was evaluated in five random locations to account for surface variances.

Surface roughness and potential were taken using an Asylum Research Cypher AFM following the PL measurements. Three random 5 x 5 um^2 locations were imaged on each sample using a 1 Hz scan rate under the Surface Kelvin Probe Microscopy (SKPM) setup within the Igor Pro (Ver. 10.0) software. This utilizes a tapping mode protocol that produces both topographic and surface potential images simultaneously. No stage bias was used in this setup. Asylum Research AC240TM tips were used for all samples, with Asylum Research ASYELEC-01 tips used for data verification. All images were flattened within Igor Pro and

averaged to calculate root mean square (RMS) roughness and surface potential values. Statistical significance for both PL and AFM/KPFM was performed utilizing a t-test within SAS (Ver. 9.4 TS) software.

Water contact angle was studied with a Ramé-hart Model 200-F4 goniometer equipped with a 28 ga. (AWG) needle using DI water. Water droplets were formed by placing one drop on the surface and slowly retracting the needle. Once retracted, water drops were captured at 2 frames per second for 5 seconds. The half-angle was averaged to produce an average contact angle for each test, which was performed four more times to produce a total sample average. Following each drop, nitrogen was blasted on the surface to ensure a dry surface. The water contact angles were captured with DROPImage (Ver. 2.4.07) software. Optical microscopy images were captured with a Zeiss Axiovert 40 MAT microscopy with a Zeiss Epiplan 10x objective lens.

5.4 Results and Discussion

Material interfaces play a crucial role in the electrical properties of organic based devices. For example, in the case of dye sensitized solar cells, the ability to match the work function of the electrode and sensitizer enables improved efficiency as the mid gap band bending between materials is decreased. This provides a greater customizability for materials selection for organic electronics. Alkanephosphonic acids have demonstrated the ability to alter physical properties such as surface roughness and water hydrophobicity, but only by adding additional side/terminal groups do the phosphonates provide beneficial electrical

properties. Among the available phosphonic acids, MUDPA, PFOPA, and ODPA (Figure 25) were selected due to their unique terminal groups that promote unexplored packing and properties on GaN.

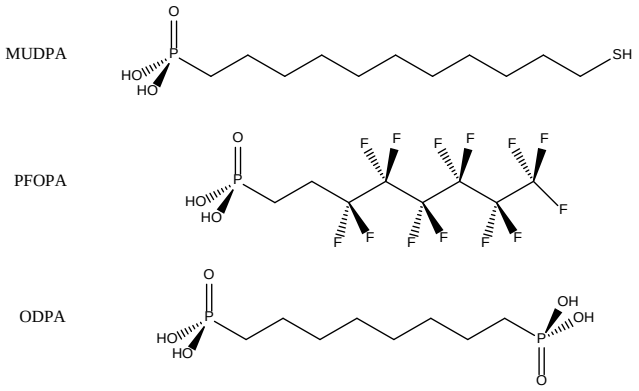

Figure 25 Chemical structure of phosphonic acids added to phosphoric acid solutions

5.4.1 Surface Homogeneity

Different scanning probe modes were utilized to assess the changes on the GaN interface after in situ-functionalization with the three different phosphonic acid molecules. The surface topography images (Figure A.1) of GaN display a wavy structure that has been previously observed on other thick c-plane GaN substrates.[264] Though the surface does not display the traditional pit formation[233] associated with polar GaN or hillock structure seen on HVPE grown substrates,[179] crack and finger-like formations can be seen in some of the images, which is likely to be the coalescence of multiple pits. The wavy texture typically appears as striations across the surface in optical microscopy, which was observed

(Figure A.1).[264] The surface RMS roughness (Figure 26) of a bare substrate was 2.65 ± 0.36 nm. The treatment with phosphoric acid and subsequent phosphonic acid solutions increased the roughness by a minimum of 0.56 nm assuming extremes in the standard deviation (AFM data in Table A.1). No significant difference in roughness could be distinguished between individual treatments. The star and double star in Figure 26 indicate statistical difference in quantities that did not transfer throughout the subset of treatments; however, the ODPA treatment provided a notable change in the surface roughness with respect to that of the cleaned substrate (P value of 0.02).

Mapping of charge distribution on materials for photovoltaics and solar cells is necessary when trying to assess the homogeneity of the interface between an organic molecular layer and a solid support. KPFM was used to identify changes to surface electrical characteristics with the three phosphonic acid derivatives. As seen in Figure 26, the surface potential for a freshly cleaned substrate closely resembles the potentials (within standard deviation) after all treatments except for those containing MUDPA and PFOPA. The cross (MUDPA and PFOPA) versus double cross (phosphoric acid) symbol in Figure 26 indicates exclusive statistical difference. As has been reported for other material surfaces such as ITO[125, 257] and ZnO,[260] the adhesion of phosphonic acids results in a change of the surface charge by modulating the work function. The ODPA treatment demonstrated a significantly different surface potential than that of both MUDPA and PFOPA treatments, likely due to various conformations that it may take (laying down due to binding on both ends versus standing up on one end group). In that way, the surface charge modifications

behave in unpredictable ways and results in a similar output to that of the phosphoric acid solution. This is the first reported surface potential measured on GaN following a phosphonic acid attachment. Many oxide materials (ZnO, ITO, TiO_2, etc.) have been characterized with respect to their surface electrical properties following phosphonic acid attachment, but in this work we report for the first time a similar analysis on GaN. The quantitative information in Figure 26 allows one to compare how topography and solution processing of the chosen GaN surface correlate with the homogeneity of their electrical properties. As expected, treating the surface with a concentrated etchant (H_3PO_4) in absence of organic adsorbates produces the largest heterogeneity in the surface potential properties. As predicted the adsorbates bound through a single terminal group (one phosphonic acid linkage), results in a more homogeneous surface as compared to surfaces treated with adsorbates with multiple surface binding groups. These results demonstrate that one can produce homogeneous interfaces using organic molecules on GaN. The latter has a significant practical importance because GaN has been proposed as an alternative material for dye-sensitized solar cells. The band alignment of GaN and the dye molecule is more favorable as compared to that of TiO_2. Prior studies have shown the superior stability of GaN surfaces and devices in solutions, and now we demonstrate improved homogeneity of the surface potential after the covalent attachment of MUDPA and PFOPA to the semiconductor surface.

The surface hydrophobicity (Figure A.2) not only demonstrated a native oxide formation that resulted in a large water contact angle, but also revealed that the use of phosphonic acids with phosphoric acid did not produce a large surface to liquid angle as seen

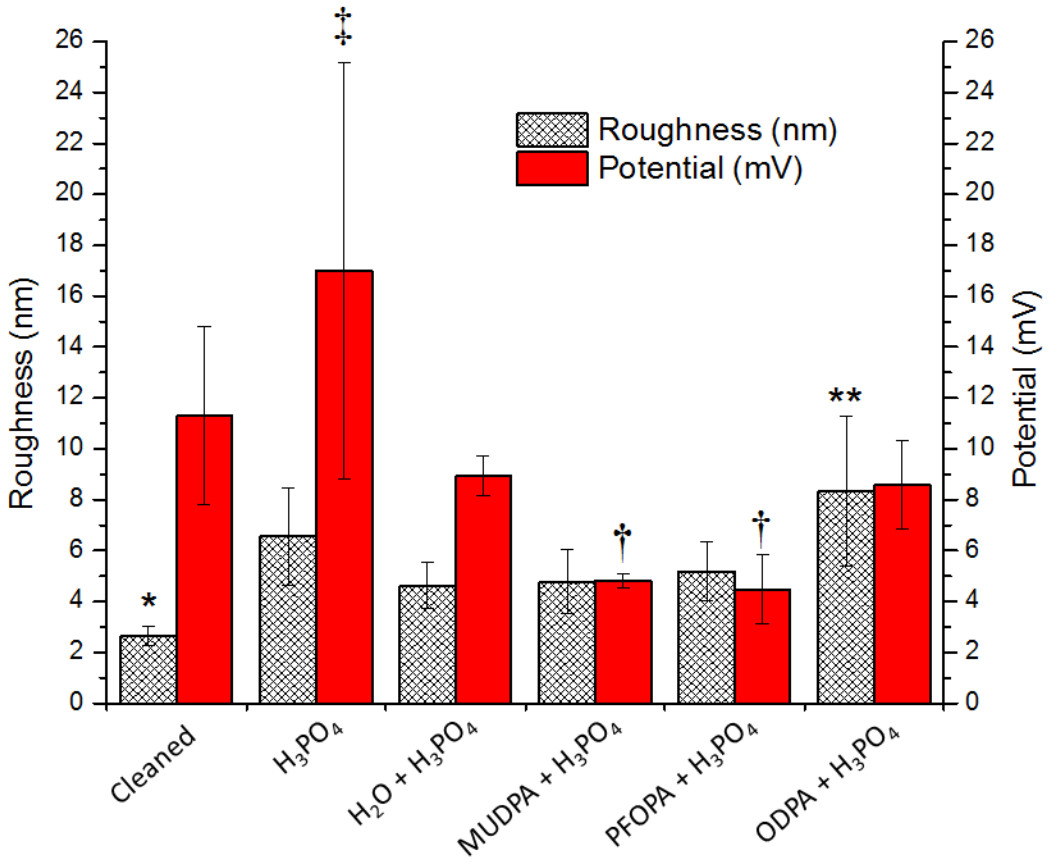

Figure 26 Compilation of RMS surface roughness (black thatch) with associated surface potential (red) of GaN following various acid treatments.

with other phosphonic acid treated GaN surfaces (Table A.2).[128, 133] Small contact angles for phosphonic acid treatments result from nonuniform coverage of the GaN surface, which has been seen previously.[265] While the concentration used here is similar to that in other studies,[125, 128, 132, 266] the use of phosphoric acid rather than a solvent in addition to a shorter dwell time and no post annealing may lead to incomplete coverage.

5.4.2 Surface Composition

The surface chemistry was investigated via XPS to identify phosphonic acid attachment onto GaN. The phosphonic acids are known to adhere to III-V semiconductors by utilizing dangling hydroxyl bonds [92, 128, 132] in either bidentate or tridentate configuration through condensation reactions.[256, 261] Due to the sensitivity of phosphonic groups to surface oxide, the $Ga2p_{3/2}$ spectra shown in Figure 27 reveal the effects of treatments on oxide formation. The $Ga2p_{3/2}$ peak was deconvoluted into four distinct peaks associated with Ga-Ga bonding, Ga-N bonding, gallium oxide formation (Ga_2O_3), and assorted gallium oxide formations (Ga_2O, GaO-termed sub oxides). The gallium oxide is reported to have a binding energy at 1119 eV,[204, 267] gallium sub oxides at 1118.5 eV,[201, 205] Ga-N bonding at 1118 eV,[248] and metallic Ga-Ga bonding at 1116.5 eV.[268] Ga_2O has been shown to dominate the sub oxide spectra,[201] but was unresolvable due to a sprectrometer resolution of 0.4-0.5 eV. Additionly, many of these sub oxides, given enough time, will form Ga_2O_3 due to its lower Gibbs free energy of formation.[208] The Ga_2O_3 is most likely amorphous in nature due to functionalization treatment conditions.[263] The FWHM of the $Ga2p_{3/2}$ deconvoluted peak was controlled by that of the Ga-N species, with an average FWHM value of 1.35 ± 0.03 eV. This was done in order to eliminate a questionable peak broadening seen from oxide formation,[137, 206, 207] which allowed for the distinction of the sub oxide species. Among all the treatments, MUDPA, PFOPA, and additive free phosphoric acid produced the greatest amount of gallium oxide and sub oxides (indicated in green and orange). The use of phosphoric acid enhanced the formation of

gallium oxide, in agreement with previous findings.[152, 265] The use of MUDPA and PFOPA stabilized what little surface oxide was produced as the dilution of phosphoric acid limits gallium oxide formation. The ODPA appears to not stabilize the produced surface oxide, most likely due to its multiple binding configurations.

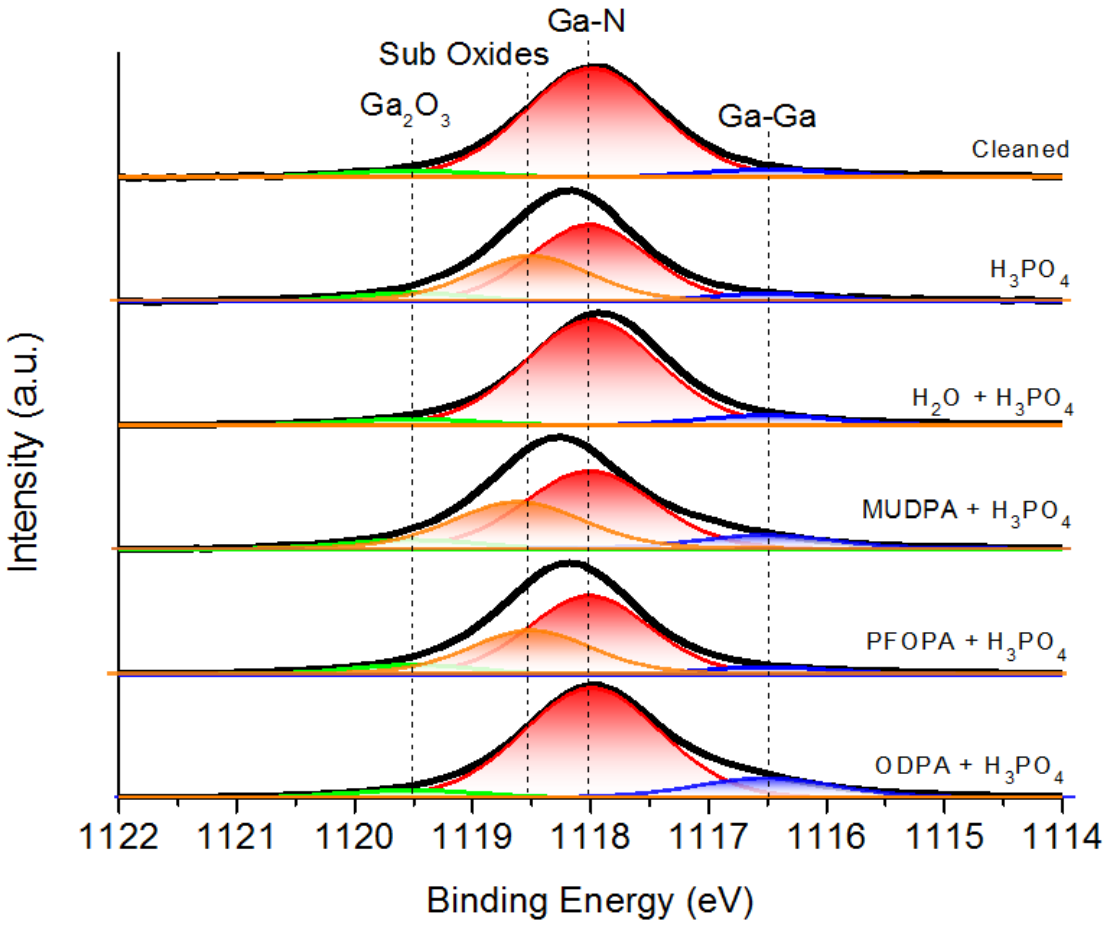

Figure 27 XPS Ga2$p_{3/2}$ spectra of free-standing bulk GaN following various treatments. The reported binding energies for Ga_2O_3, Ga-N, and Ga-Ga are indicated with dotted lines at 1119, 1118, and 1116.5 eV respectively. Gallium sub oxides (Ga_2O, GaO) binding energies are indicated at 1118.5 eV.

The attachment of phosphonic acids was confirmed by high resolution F1s (Figure A.3), C1s (Figure A.4), and S2p spectra (Figure 28). The fluorine spectrum identifies only fluorine content when PFOPA is utilized. The spectrum was not normalized, aiming to show the relative intensity difference of the pure PFOPA (powder form) signal versus the expected signal from PFOPA attached to GaN. HCl etching was performed to remove oxide from the surface so that the phosphoric acid could control the oxide formation (increased carbon contributions for cleaned GaN reflected decreased oxygen content post cleaning). Usually HF etching is performed post HCl etching to assist the oxide removal, however, in an effort to avoid fluorine contamination, the HF etching was not performed (hence no fluorine signal was seen for a cleaned sample). The attachment of PFOPA was confirmed by the C1s spectra (normalized intensities) with CF_3 and CF_2 binding at 293.5 eV and 291.1 eV from fluorine attachment along the phosphonic acid chain. The peak area ratio of 1:5 CF_3:CF_2 matched the chain configuration reported in the literature.[125] Significant primary peak broadening was observed with a shoulder near 286.8 eV associated with P-C and O-C bonding. The MUDPA adhesion was identified through the S2p spectra shown in Fig. 28 (normalized peaks). The MUDPA powder (black line) formed an S-H doublet at 163.5 eV ($S2p_{3/2}$) and 164.7 eV ($S2p_{1/2}$).[269, 270] The addition of MUDPA resulted in a broadening of the Ga3s peak, which is in close proximity of the S2p peak. The Ga3s spectra of a cleaned sample displayed some broadening, which accounted for no more than 7% of the total area from sulfur impurities/contamination bound to gallium.[271] By adding MUDPA, this shoulder increased

to almost 15% of the area, supporting a thiol contribution. The FWHM of the S2p peaks hovered near 0.98 eV, while the Ga3s demonstrated significantly larger FWHM of 2.32 eV.

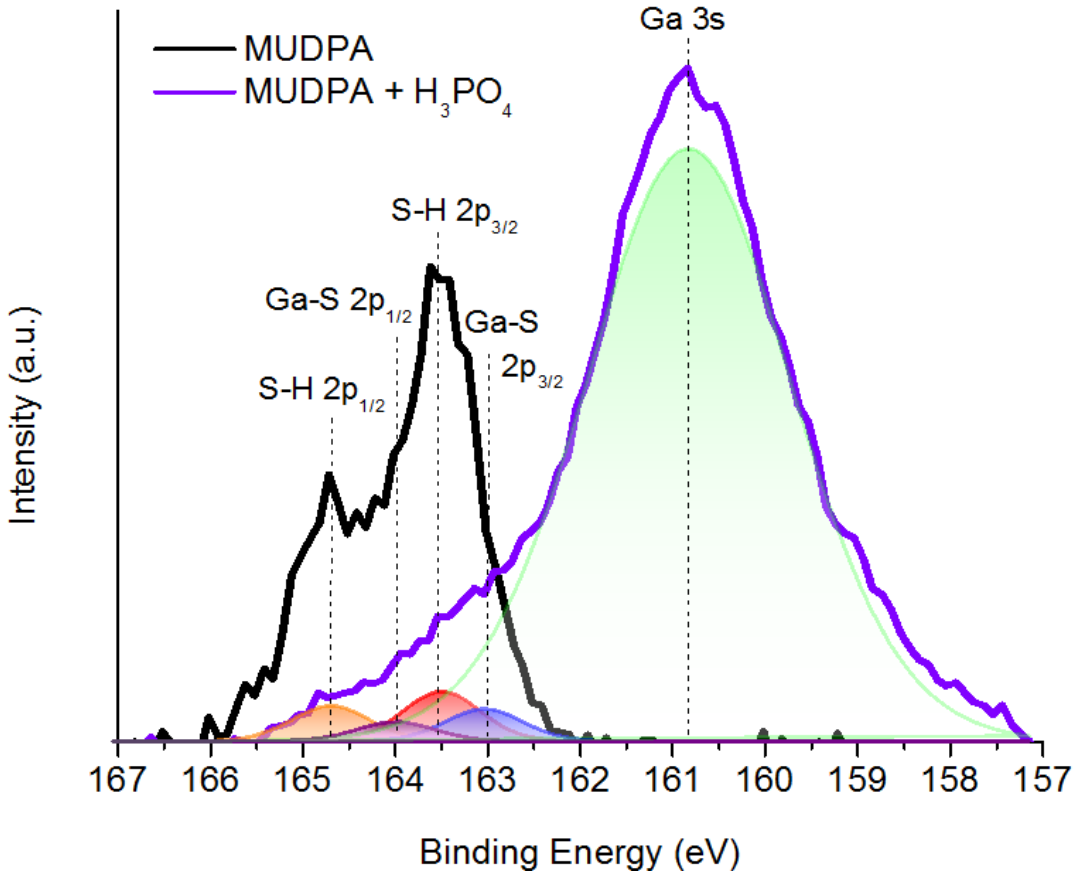

Figure 28 XPS S2p/Ga3s spectra for MUDPA (chemical only showing in black) and MUDPA with phosphoric acid treated GaN (shown in purple). Carbon-sulfur and gallium-sulfur bonding is shown with associated doublets.

Atomic percentages were calculated utilizing Ga3d (Tables A.3-9) and $Ga2p_{3/2}$ (Tables A.10-15) for gallium content. $Ga2p_{3/2}$ provides an excellent surface qualification (attenuation length of 0.7 nm); however, the shorter attenuation length is limited to thin

layers.[137] The atomic percentages were calculated using non-normalized data from C1s, O1s, S2p, P2p, Ga3d/Ga2p$_{3/2}$, F1s, and N1s peaks. Gallium auger peaks seen within the N1s spectra (not shown) were excluded as well as Ga3s overlap with S2p for atomic % calculations and subsequently the Ga/P, Ga/C, Ga/O, Ga/N, and O/P ratios (Tables A.16-21 via Ga3d and Tables A.22-27 via Ga2p$_{3/2}$). The angle resolved XPS indicates greater carbonaceous and oxide species closer to the surface. It is observed that the phosphorous was absent from a cleaned substrate (as well as sulfur and fluorine) but appears as soon as a phosphoric acid solution is used. The nitrogen and gallium content decreases with increasing photoemission angle, but the gallium to nitrogen ratio remains in the range of 1.5 to 2.0 throughout all of the treatments. Summarized in Table 10 are the Ga/P, Ga/O, and O/P ratios for the various treatments at a 0° photoemission angle using Ga3d for gallium content. While the phosphoric acid and diluted phosphoric acid treatments added some phosphorous to the surface, MUDPA and PFOPA treated samples showed increased phosphorous content as seen by lowered Ga/P ratios from terminal phosphonic groups. Due to complex adsorption mechanisms, the addition of ODPA increased the amount of phosphorous marginally compared to dilute phosphoric acid solutions. The binding of phosphonic acids to GaN require an oxide layer, which was seen with low Ga/O ratios for MUDPA and PFOPA functionalized surfaces. The combination of both increased phosphorous and oxygen contributions for both MUDPA and PFOPA treated samples in addition to individual identifier spectras (S2p and F1s respectively) indicate surface coverage via phosphonic acids. The similar O/P ratios for MUDPA and PFOPA infer similar adsorption mechanisms versus

the ODPA treated sample, which has a O/P ratio between phosphonic acid solutions and phosphoric acid only treatments.

Table 10 Averaged Ga/P, Ga/O, and O/P ratios of various treatments at a 0° photoemission angle.

Treatment	Ga/P	Ga/O	O/P
Cleaned	-	4.4	-
H_3PO_4	29.3	2.6	11.5
$H_2O + H_3PO_4$	39.6	3.6	11.1
MUDPA + H_3PO_4	7.2	2.1	3.2
PFOPA + H_3PO_4	4.0	1.3	3.0
ODPA + H_3PO_4	28.3	4.3	6.6

5.4.3 Photoluminescence Properties

Room temperature photoluminescence of treated substrates in the near band-edge (NBE) region are shown in Figure 29. The NBE appears centered near 363 nm and does not shift with the treatments or additives used. Usually, high-quality free-standing bulk GaN demonstrates a shoulder formation at longer wavelengths due to contribution of longitudinal-optical phonon replicas to the PL spectra [211] Though a shoulder exists (~368 nm), the decreased intensity of the NBE indicates a nonradiative recombination through increased defect density compared to previously studied substrates.[59, 233, 265]

The treatment with phosphoric acid and additive assisted phosphoric acid etches appear to reduce the overall photoluminescence intensity of the treated gallium nitride samples. A decrease in the luminescence of samples treated with phosphoric acid alone has

been observed previously;[265] however, the use of longer chained phosphonic groups appear to have a negative effect on the emission intensity as compared to their shorter chained counterparts.[265] Optical images (Figure A.5) does not reveal surface deterioration upon etching (such as formation of pits)[86] to be the reason for this reduction. The addition of MUDPA led to a similar photoluminescence intensity decrease as compared to the unmodified phosphoric acid, which is the greatest reduction in the overall signal. The addition of ODPA to a phosphoric acid solution does not result in any increased luminescence relative to that of the phosphoric acid solution alone. Only by adding PFOPA does the photoluminescence intensity approach the intensities seen from a cleaned substrate. The addition of PFOPA increases the photoluminescence intensity by 184% versus a stand-alone phosphoric acid solution. An increase in photoluminescence has previously been observed for ITO treated surfaces, where a fluorine terminated phosphonic acid resulted in greater luminescence versus carbon backbone only phosphonic acid.[257] The improved quantum efficiency derived from surface modifications is a direct result of induced band bending on the surface. Though only the surface potential was analyzed, there is an indication that organic groups on the surface substantially affect the optical properties of polar GaN.

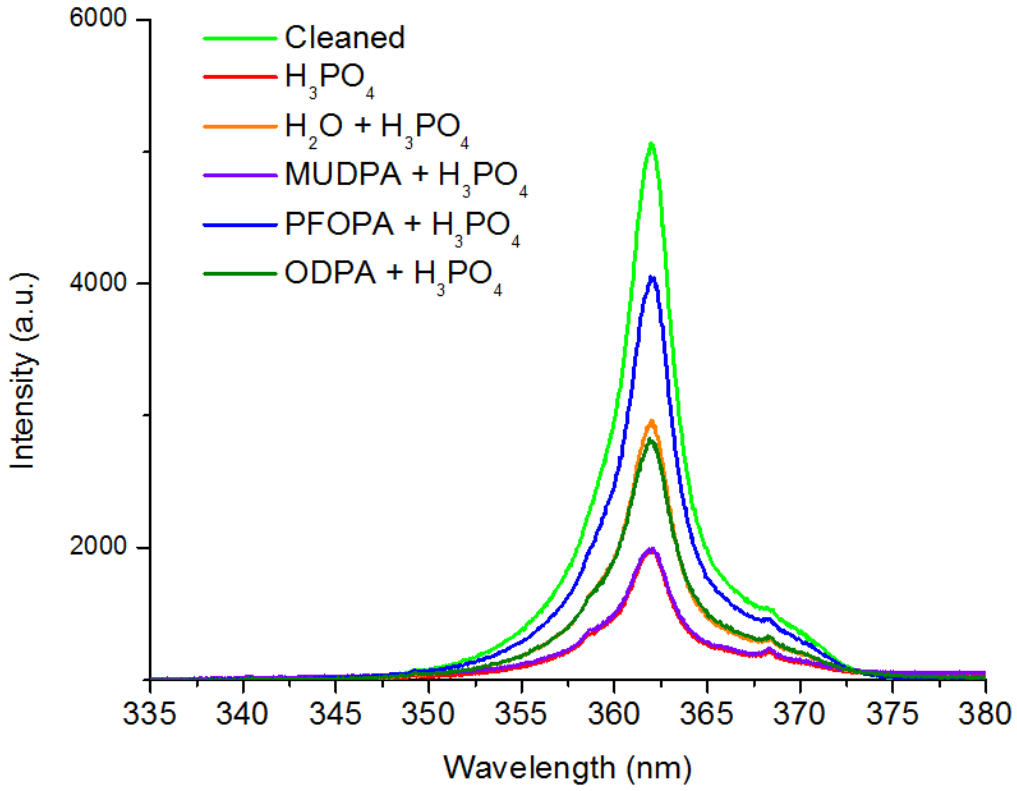

Figure 29 PL spectra of treated GaN utilizing maximum intensities for each treatment.

A quantitative comparison of PL intensities can be seen in Figure 30. The star indicates a statistical significance between the PFOPA treatment and other additive and additive-free solutions. While the MUDPA produced a similar surface potential to the PFOPA solution (Fig. 26), the PFOPA exhibited significantly (281%) improved emission. It is thought that while the sulfur terminated chain can produce a locally similar surface potential, the incomplete coverage (seen by a diminished oxygen content required for surface adhesion and phosphorous content relative to PFOPA treatments) combined with minimal side groups does not impart enough of a change on the bulk material to promote improved

emission characteristics. By having a diminished surface coverage and oxide layer, not enough of a bulk modification is reached to distinguish unique optical properties from phosphoric acid alone via band bending.[257, 272]

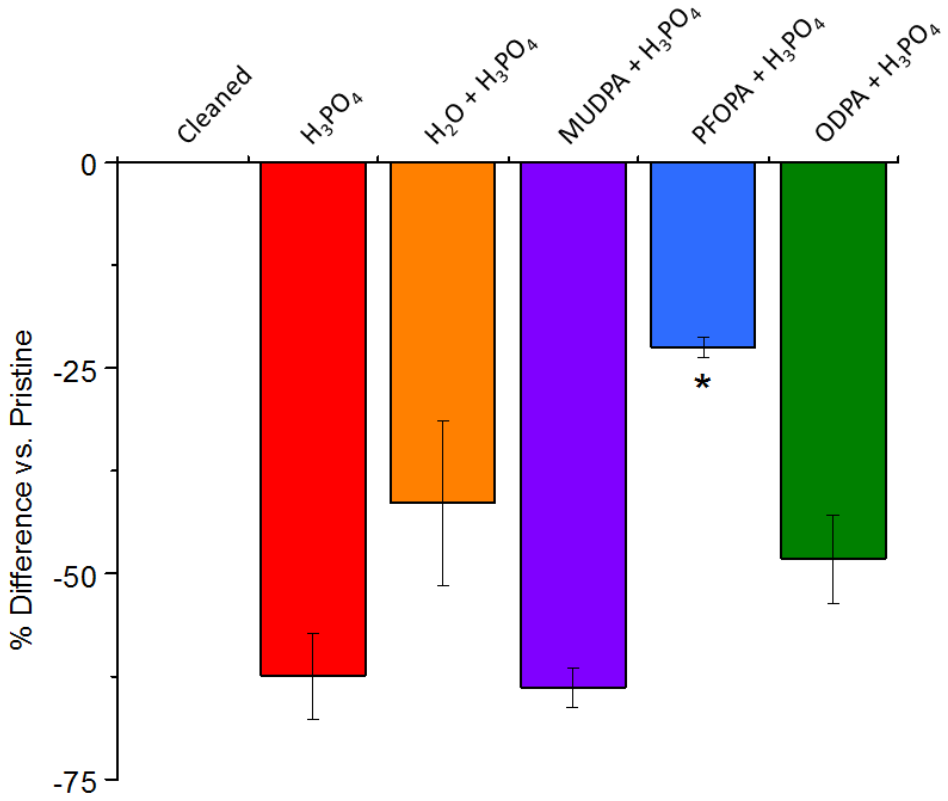

Figure 30. Calculated % difference from maximum PL intensities in Fig. 4 versus pristine substrates.

5.5 Conclusions

In this study three distinct phosphonic acids were used to alter the etching characteristics of phosphoric acid and subsequently, the surface properties of polar free-standing GaN. Among the three phosphonic acids utilized, the MUDPA and PFOPA attached more readily than the ODPA. This was seen from increased phosphorous intensity from XPS, as well as increased surface oxide that was necessary for the attachment and surface stability. Both phosphonic acids resulted in a lowered surface potential and similar surface roughness; however, only the PFOPA led to a decreased luminescence upon treatment. The ODPA treatment led to a similar oxide level compared to the treatment with unadulterated phosphoric acid, as well as a similar surface roughness and photoluminescence properties; however, ODPA closely matched a mixed water/phosphoric acid etch for modifications of the surface potential. Due to the potential for multiple binding sites, the ODPA is likely to form many configurations on the surface that may not cover the surface enough at moderate concentrations.

6 Modulated Optical Sensitivity with Nanostructured Gallium Nitride

S. J. Wilkins,[1] M. J. Slomski,[1] T. Paskova,[2] J. L. Weyher,[3] A. Ivanisevic[1]

[1]Department of Materials Science and Engineering, North Carolina State University, Raleigh, North Carolina 27695, USA

[2]Department of Electrical and Computer Engineering, North Carolina State University, Raleigh, North Carolina 27695, USA

[3]Institute of High Pressure Physics, Polish Academy of Sciences, ul. Sokolowska 29/37, 01-142 Warsaw, Poland

6.1 Abstract

Surface functionalization via etching of high aspect ratio GaN nanostructures provides a way to modulate the optical properties in addition to properties gained from unique topographical formations. In this study, planar layered (heteroepitaxy) and bulk free-standing gallium nitride were modified via a phosphonic acid (1H,1H,2H,2H-Perfluorooctanephosphonic acid) assisted phosphoric acid etch in conjunction with an aqueous KOH + $K_2S_2O_8$ formed gallium nitride nanostructured surface. Despite the high defect concentrations in the thin planar and nanostructured GaN layer, the nanostructured GaN sample produced improved photoluminescence intensities versus the high quality bulk free-standing gallium nitride. Subsequent treatments with additive and additive-free phosphoric etches provided a means of additional optical manipulation in the form of red-

shifting the near-band-edge (NBE) emission of the nanostructured GaN sample and increasing the maximum NBE photoluminescence intensity.

6.2 Introduction

Deposition, growth, and processing of planar gallium nitride (GaN) provides many quality challenges resulting from numerous stacking faults and threading dislocations from lattice mismatches between growth substrates and subsequent epilayers. Techniques such as lattice mismatches between growth substrates and subsequent epilayers. Techniques such as epitaxial lateral overgrowth,[273] laser-induced lift-off,[274] and native epi-deposition[275] have sought to reduce defect densities, currently on order of $5x10^5$ - $1x10^6$ cm^{-2},[274] but work continues in the drive towards higher quality GaN. Planar GaN already sees uses as light emitting diode stacks[276] and high-electron mobility transistors,[277] which require high quality defect free substrates. In a push to improve device performance, particularly in the realm of light emitting diodes, multi-dimensional GaN morphologies are being explored.[278-280] 3D GaN morphologies such as wires,[279] rods,[281] and pyramids[282, 283] have been introduced in an effort to modulate optical properties of GaN that are nominally limited in a purely planar format due to the critical angle of escape for photons.[284] By increasing the number of facets and subsequent area of escape, internal reflection is reduced and subsequent devices provide enhanced output.[88, 284]

Like planar GaN, nanostructured GaN fabrication is ultimately controlled by defects within the starting material. Nanostructured surface fabrication primarily utilizes techniques

such as reactive ion etching (RIE),[285] catalyst deposition,[286] and chemical etching[282] as methodologies of choice. Reactive ion etching requires the use of pristine GaN to form the final structure by physically ablating material with reactive ions. Though RIE provides direct control universally throughout GaN regardless of orientation via top-down fabrication, physical damage and subsequent thermal zones are induced via RIE.[287] The thermal damage increases the degree of dangling bonds and physical damage, which in addition to being low throughput in nature result in poor performing devices.[288] By utilizing chemically assisted etching, benefits such as high throughput and rapid fabrication can be achieved by using chemicals such as molten KOH, phosphoric acid, sulfuric acid, or dilute aqueous KOH solutions.[281] In addition to open cell etching, chemical etching can be assisted by UV sources and placed in a galvanic cell to improve etching characteristics.[281] Owing to its natural chemical resistance, GaN offers unique etching rates based upon crystallographic orientation. This stems from the preferential removal of nitrogen versus gallium.[289] In this way, the final structure can be defined along different crystallographic orientations from a given starting material.

In this study, chemical functionalization is used to modulate the optical response across planar and high aspect ratio GaN topographies. The GaN nanostructure utilized dislocations as site specific etching centers, termed defect-assisted etching, that are indicative of the starting crystalline quality. Defect-assisted etching has already been seen with dilute aqueous KOH solutions[281, 282] and provides a repeatable and scalable fabrication technique. The benefit of defect-assisted etching is that defects, normally unwanted, are

required to form uniform structures. To compare the properties of nanostructured GaN, photoluminesce (PL) is used to identify changes to the critical photon escape angle as a result of faceting and formation of high aspect structures. In the case of nanorods or nanopyramids, the high aspect ratio provides unique opportunities for tailorable luminescence and binding sites from increased surface area,[290] which is compared to both thin layer GaN and bulk free-standing GaN. The thin layer GaN was residing on a sapphire substrate[282] whereas the bulk free-standing GaN is a self-separated free of foreign substrate that has been subsequently chemically-mechanically polished.[274] Chemical functionalization of GaN has shown unique properties such as modified optical,[291] electrical,[182] and unique surface hydrophobicity[290, 292] by chemical termination. With recent interest in interfaces for applications such as organic light emitting diodes[293] and sensors,[294, 295] chemical functionalization with desired adsorbates can provide tailored electrical, chemical, topological and optical properties. In this investigation, the use of in-situ functionalization with 1H,1H,2H,2H-perfluorooctanephosphonic acid (PFOPA), which has been previously used on ZnO[103] and ITO,[296] is used to modulate the optical responses of the three types of GaN structures in addition to identifying the resulting optical output following a lengthy environmental soak that potential devices might encounter.

6.3 Experimental Methods

6.3.1 Sample Preparation

The GaN samples are separated into three categories: planar layer GaN residing on sapphire, nanostructured GaN also residing on sapphire, and bulk free-standing GaN. The nanostructured GaN formations were produced from the planar thin layer GaN deposited on sapphire with n-type conductivity (Si doped) via metalorganic chemical vapor deposition (MOCVD The samples were placed in an illuminated-galvanic cell utilizing a KSO-D (0.02M KOH + 0.02 M $K_2S_2O_8$)[282] aqueous solution and platinum counter electrode while being exposed to a 300 watt xenon lamp for 60 minutes. The Ti contact protected about ¼ of the sample surface against etching and this area was used as a comparison versus the etched nanostructure.

The bulk free-standing GaN was grown via hydride vapor phase epitaxy (HVPE) on sapphire until the GaN boule was 1.2 mm thick.[274] They were then self-separated from the substrate during cooling down and subsequently chemically-mechanically polished and diced. The thin layer GaN material was characterized with high dislocation density in the range of 10^9 cm^{-2}, while the bulk GaN material possessed a low dislocation density in the range of 10^5-10^6 cm^{-2}. The nanostructured material produced from the same thin layer GaN possessed a slightly lower dislocation density as significant portions of the layer were etched away. The remaining nanostructures still exhibits high dislocation density due to the fact that the photo-etching process tends to take place around dislocations.[297]

6.2.2 Surface Treatment

Prior to the secondary etching, all samples were placed in acetone, methanol, and dilute HCl baths. The samples (nanostructure, layered, and bulk) were separated into three groups: cleaned (no treatment) and etched with either a 50 vol. % H_3PO_4 or a 50/50 vol. % H_3PO_4/3mM PFOPA solution. Samples were rinsed with deionized water, dried with nitrogen and characterized. To replicate environmental conditions, samples were soaked in deionized water for 7 days and characterized again.

6.3.3 Characterization

Surface morphology of the three types of samples was evaluated by Atomic force miscroscopy (AFM) using Digital Instrument Nanoscope IIIa in tapping mode and by scanning electron microscopy (SEM). The SEM images of the nanorod structure were recorded with a Verios 460L SEM. Images were taken at a 4.4 mm working distance, 13 pA filament current, 2.0 kV accelerating voltage at a 30˚ tilt without a stage bias. Photoluminescence at room temperature was done with a Horiba Jobin Yvon LabRam ARAMIS Raman/PL setup employing a 325 nm HeCd laser. Calibration was done using a Raman peak of 1295 cm^{-1} from Teflon with a 40x UV objective at a 2400 grating/minute resolution. The real-time display (RTD) exposure time, accumulated exposure time, and number of acquisitions for averaged signal were 0.5 second, 0.5 second, and 5 respectively, with a 90% signal filter. To ensure equal exposure, laser spot size was maintained at 10 um (crossover) due to the different sample thicknesses. Each sample was evaluated at five

random locations to account for surface variances with spectra capturing from 340 to 390 nm.

6.4 Results and Discussion

6.4.1 Surface Morphology

Figures 26(a) and 1(b) reveal smooth planar surface for both planar thin layer and bulk GaN materials, with root mean square values were 0.7 and 0.2 nm, respectively. The lower value for the bulk GaN surface is consistent with lower dislocation density, reflected in lower number of surface depressions related to dislocations intersecting the surface. From Figure 30(c), nanostructures with pyramidal shape, approximately 700 nm in length can be seen. Their uniform shape and cone-like tip structure (Figure 30(c) inset) reveal gallium enriched facets frequently associated with semipolar planes.[298] The KSO-D formula is known to produce nanostructured surfaces of different shape, e.g. nanorods, nanowires, nanopyramids. The nanotextured surface can be controlled by the etching time,[282] etching solution[281] and UV source power. In addition, the properties (dislocation density and carrier concentration/doping) of the initial GaN layer[299] were found to enable different etching rates and nanostructures of various shape, density and aspect ratios. The moderate doping, i.e. carrier concentration of about $1x10^{17}$ cm^{-3} and high dislocation density in our GaN template, allowed pyramidal topography with semipolar facets, as opposed to the nanorod structure (with more uniform diameter and no semipolar surfaces) typically produced from highly doped GaN layer.

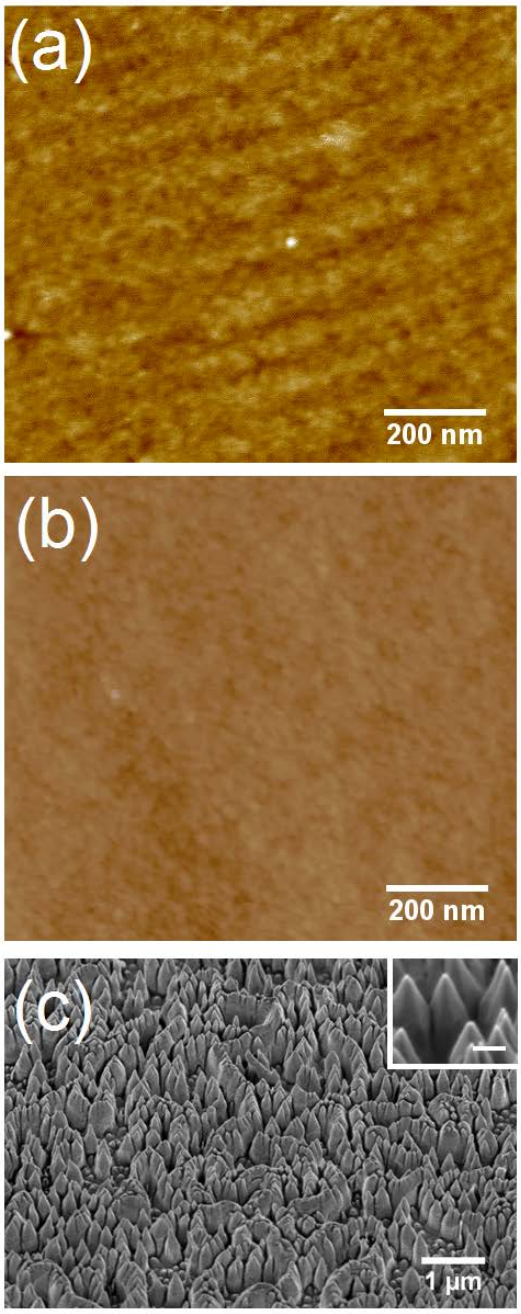

Figure 31 Surface morphology of the three representative pristine samples: (a) AFM image of 1 □m x 1□m a
from bulk GaN sample; (c) SEM image of nanorods surface of etched thin GaN film tilted at 30˚. The inset shows a magnified image of the tip of the nanostructures with a scale bar of 200 nm.

6.4.2 Optical Response

The PL responses to the different treatments shown in Figure 32 reveal that the near band-edge (NBE) for the layered GaN resides at 361 nm, while the NBE for nanostructured and bulk-freestanding GaN reside near 362 nm. The blue shift of the NBE emission from the thin GaN layer on sapphire is a typical feature related to the biaxial substrate induced strain. The similar spectral position of PL spectra from the nanostructure and the bulk free-standing GaN can be explained by the reduced strain in both samples due to removed or reduced substrate effect, respectively. For the planar layered GaN and the bulk free-standing GaN, the NBE does not change with different treatments both pre and post water soak. In contrast, the nanostructured samples allow for a greater response due to larger surface alterations as a result of increased surface area and improved light extraction. In addition, one could also expect a better surface sensitivity of the semipolar surfaces to the chemical treatments as compared to the well-known chemical stability/resistivity of the Ga-face polar surface. By utilizing a dilute phosphoric acid, a noticeable NBE shifting versus PFOPA added phosphoric acid could be seen. In comparison to the PL spectrum from a cleaned nanostructured sample, the NBE wavelength red-shifted by 0.4 nm in the spectrum from the sample treated with the addition of phosphoric acid and an additional 0.2 nm with PFOPA modified phosphoric acid. Concentrations below 43 vol. % were used to ensure that the nanostructured surface would not undergo additional etching as well as to prevent phosphonic acid agglomeration. Phosphonic acids, particularly those with unique electrical signatures, provide another avenue to modulate optical properties by utilizing native

oxides.[300] The PFOPA enables simplified characterization and is known to spontaneously form on oxides.[301] Silanes, which offer a similar binding mechanism, have already been demonstrated as potential nucleic acid detectors by means of nanorod platforms.[302] By utilizing phosphonic acids, issues with increased toxicity are alleviated. In addition to the shifting of the NBE, a shoulder can be seen on the PL spectra from nanostructured and layered GaN samples at approximately 369 nm, which is associated with longitudinal-optical phonon replicas being expressed.[303] This shoulder is also present in the PL spectra of the bulk-free standing GaN, but was not visualized due to size of scale used.

In addition to shifting the spectra due to the chemical treatments, by exposing the samples to water for 7 days resulted in an overall decrease in PL intensity (Figure 32 (a) vs. Figure 32 (b)). Decreased PL signal, particularly of the NBE, is usually associated with increased nonradiative recombination events verses radiative recombination events.[59, 304] In this case, increased hydroxide and oxide species from soaking increased the amount of nonradiative recombination sites at the surface, and thus lowering the overall emission intensity between samples. This was particularly evident in the PL spectra of the thin GaN layer treated with phosphoric acid, which saw a 41% decrease pre vs. post soak. Unlike the PFOPA treated samples, phosphoric acid provides no passivation via oxide stabilization as phosphonic acids have already shown decreased leaching characteristics for GaN not available with unfunctionalized surfaces.[265] The degree of emission intensity decrease between pre and post soaking provides relevant information for environmentally active optical devices.

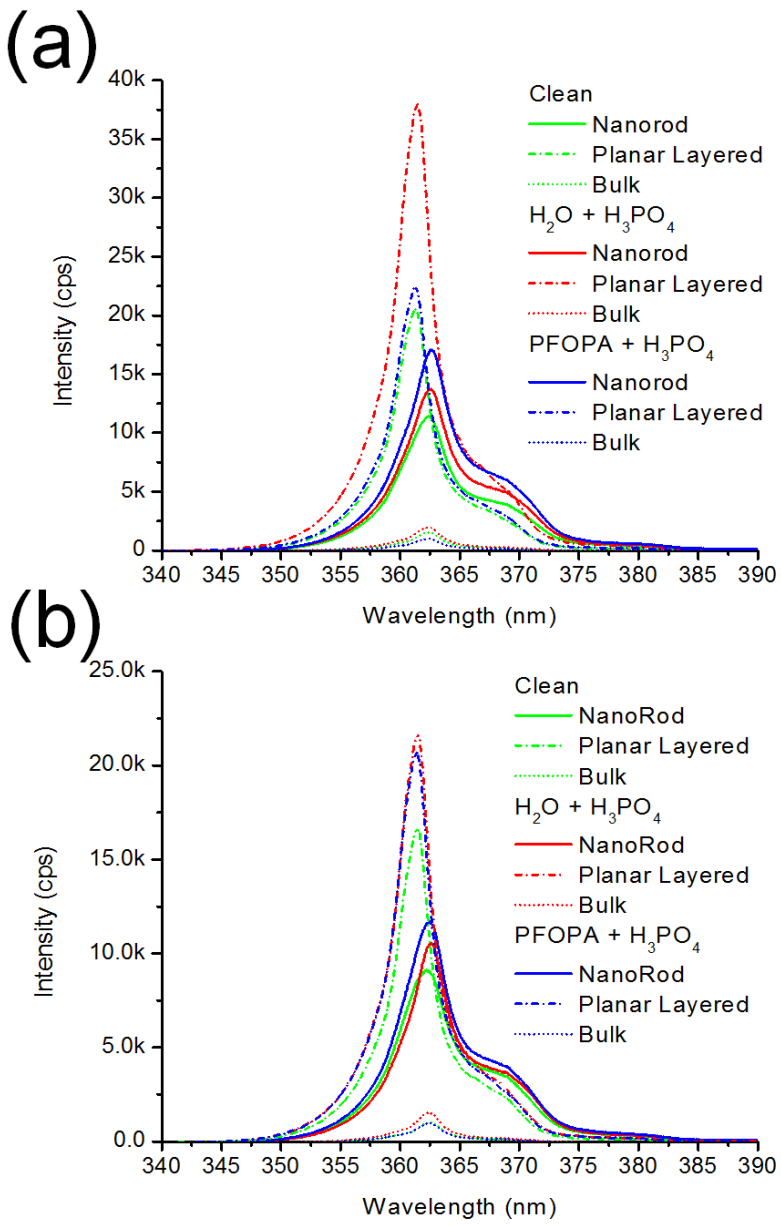

Figure 32 PL responses pre-DI water soak (a) and post (b).

For a more detailed look at the effect of treatments on the optical properties, Figure 33 compares alterations in maximum PL intensities versus individual treatments. In the pre-soaked samples, the use of both treatments results in an increase in total photoluminescence for nanostructured and layered GaN, which was not the case for bulk free-standing GaN. As the nanorod and layered GaN had already experienced both a polishing and etching process (with a protective wax layer for layered GaN), it is likely that the surface of bulk free-standing GaN retained a greater number of nonradiative recombination centers as a result of etching. It is not until the samples are soaked that all samples' PL intensities are greater than the cleaned versions. In the case of the nanostructured GaN, the PFOPA treatment demonstrated the ability to increase the PL signal versus an additive free treatment, while this was the reverse case for layered GaN. Based on these results, we conclude that the use of PFOPA provides a way for optical modulation in of 3D GaN nanostructures with a stronger sensitivity as compared to the planar GaN surfaces.

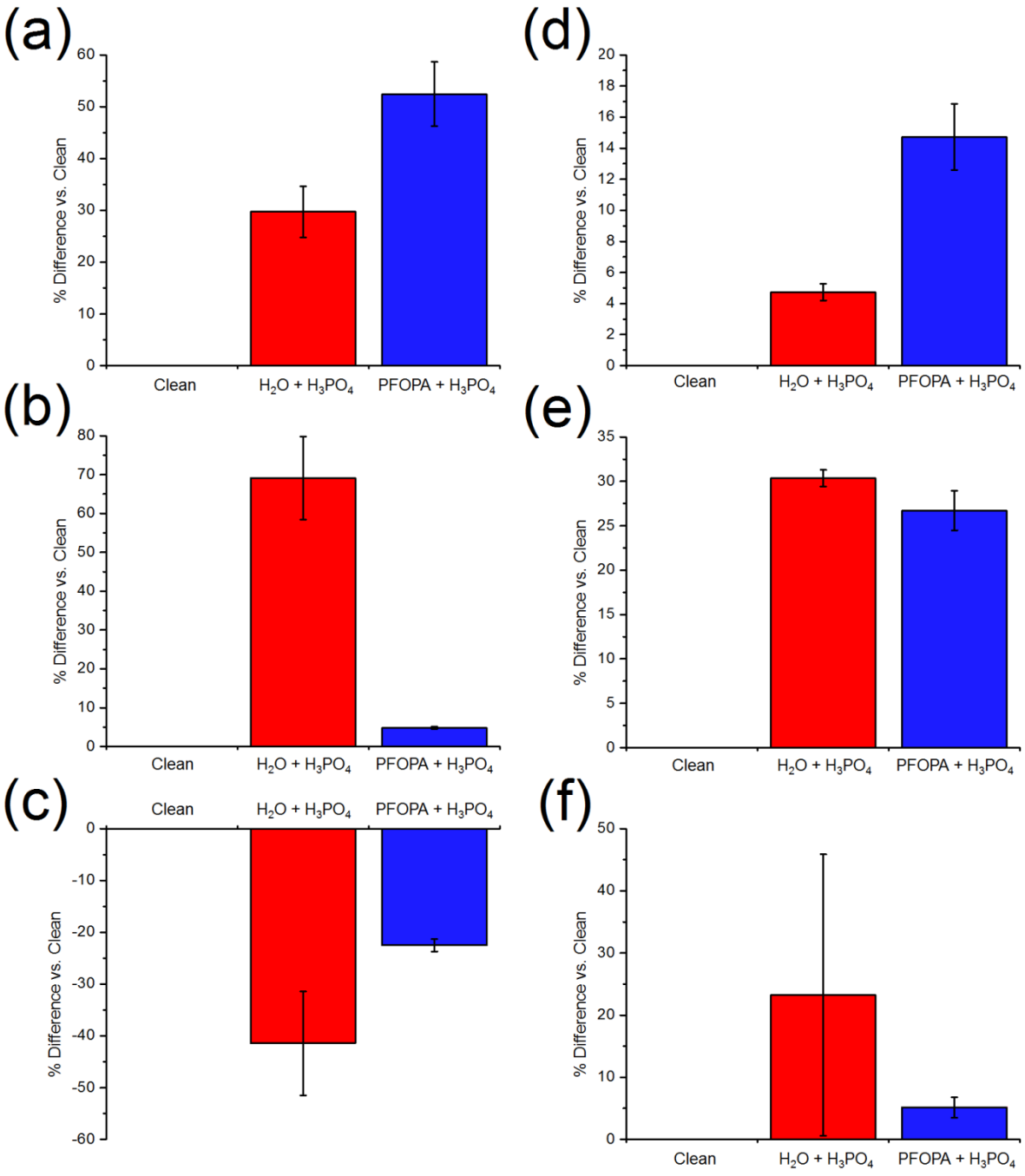

Figure 33 PL response versus cleaned samples for (a, d) nanorods, (b, e) planar layered, and (c, f) bulk free-standing GaN prior to DI water soak and post water soak respectively.

6.5 Conclusion

In conclusion, additive assisted etching provides a unique way to modulate the optical properties of both planar and 3D GaN nanostructures. This was seen particularly in the increased PL intensity for nanostructured GaN treated with PFOPA as a result of the increased surface area, improved light extraction and possible higher semipolar sensitivity contribution versus polished polar GaN surface. All materials showed significant optical sensitivity to surface functionalization, even following lengthy soaking. It is beneficial to note that general trends, particularly for the defect rich layered GaN, remained consistent with treatments and subsequent soaking. Acid treatments provided NBE wavelength manipulation that was only seen with the high aspect ratio nanostructured GaN.

7 Comparison of the Stability of Functionalized GaN and GaP

S. J. Wilkins,[1]T. Paskova,[1,2] C. L. Reynolds Jr.,[1] A. Ivanisevic[1]

[1]Department of Materials Science and Engineering, North Carolina State University, Raleigh, North Carolina 27695, USA

[2]Department of Electrical and Computer Engineering, North Carolina State University, Raleigh, North Carolina 27695, USA

The following manuscript is reprinted with permission from S.J. Wilkins, T. Paskova, C.L. Reynolds, Jr., A. Ivanisevic, "Comparision of the Stability of Functionalized GaN and GaP," *ChemPhysChem*, **2015**, (Accepted).

7.1 Abstract

Surface functionalization via 1H,1H,2H,2H-perfluoro octanephosphonic acid was done in the presence of phosphoric acid to provide a simplified surface passivation technique for gallium nitride (GaN) and gallium phosphide (GaP). In an effort to identify leading causes of surface instabilities, hydrogen peroxide was utilized as an additional chemical modification to cap unsatisfied bonds. The stability of the surfaces were studied in an aqueous environment and subsequently characterized. Physical characterization sought to distinguish surface roughness and water hydrophobicity pre and post stability testing via atomic force microscopy and water goniometry. Surface chemistry changes and solution leaching were quantified via X-ray photoelectron spectroscopy and inductively-coupled

plasma-mass spectrometry. Results indicate sensitivity to hydroxyl terminated species for both GaN and GaP under aqueous environments as the increase of the degree of leaching was more significant for hydrogen peroxide treated samples. The results support the notion that hydroxyl species act as precursors to gallium oxide formation and lead to subsequent instability in aqueous solutions.

7.2 Introduction

Organic surface functionalization of semiconductors provides a convenient way to modify surface properties without using expensive materials or processing equipment.[96] Surface functionalization seeks to control surface chemistry that frequently lead to undesirable characteristics[100] as a result of nonradiative recombination centers[99] and higher carrier recombination velocities from incomplete surface termination.[101] Although the bulk properties are controlled by the overall quality of the crystal by dopants used and/or defects present, the surface interface ultimately controls properties such as electrical conductivity,[131, 250] chemical selectivity,[17] optical recombination events,[182] and environmental stability.[265] The inherent need to reduce the total surface energy drives the natural reduction of dangling bonds[305, 306] which, in the presence of organic functional groups, form chemically adsorbed layers.[97] Many groups have explored surface adsorbates such as thiols,[109] silanes,[92] phosphonic acids,[129] and carboxylic acids[235] as ways to modulate the surface properties. Thiols, perhaps the most widely reported, bind directly to metallic or low valence atoms centers.[239] Because of this, natural oxides must be removed

prior to thiol functionalization. In the drive to improve environmental sustainability, ways to produce similar qualities without expensive processing facilities or hazardous solvents has led to interest in phosphonic and carboxylic acids. Both carboxylic and phosphonic acids are known to utilize protonated surfaces, native oxide, and hydroxyl groups as potential adsorption sites, which provides flexibility for binding not available with other adsorbates.[18, 125, 307] In the case of phosphonic acids, up to three binding sites are available, although only the two hydroxyl groups are expected to provide binding due to lower dissociation energy.[125, 256] By utilizing the native oxide layer, not only are the surface properties altered by adsorbate functionality, but the underlying material and oxide layer is capped.[247] Normally oxides of monoatomic semiconductor species (such as Si) form uniform, thick oxide layers that prevent subsequent attack of the underlying material. Due to the diatomic nature of III-V semiconductors, a thick protective layer of oxide is not available, which is problematic in both stability and in situations requiring high K dielectric properties.[237, 308] In this way organic functionalization provides additional benefits needed for materials with challenging chemistry in dynamic environments.

Of the semiconducting materials available, gallium nitride (GaN) and gallium phosphide (GaP) are frequently cited as inherently resistant to chemical attack and corrosion.[78, 84, 265] Their natural stability provides a platform for chemical sensors,[309] solar technology,[310] and biological sensors.[294, 311] Fabrication for GaN and GaP applications is limited to extreme acidic and basic conditions[312] as well as energetically driven environments[227, 313] via etching solutions of molten KOH,[85] NaOH,[227]

phosphoric acid,[314] sulfuric acid,[78] or nitric acid.[191, 315] Increased complexity is added due to the different stabilities between group III and group V atoms, which leads to preferential removal of group V atoms to form group III-rich crystallographic features.[249, 314] Within an acidic environment, the simplified etching mechanism for GaN can be seen in Eq. (1).[85] The formation of ammonia provides the primary mechanism of crystal attack

$$2GaN\ (s) + 3H_2O\ (l) \rightarrow Ga_2O_3\ (s) + 2NH_3\ (aq) \quad (1)$$

and subsequent isolation of insoluble gallium oxide (Ga_2O_3). Ga_2O_3 is the primary oxide formed for gallium in neutral solutions, whereas ionic species of Ga^{3+}, $HGaO_2^{2-}$, and $GaPO_4$ provide paths for gallium solubility in acidic environments.[139, 314, 316] Ionic species are available only for pH < 3.0 as Ga_2O_3 dominates and limits subsequent gallium solubility. Nitrogen does form oxides of its own but require oxygen rich environments in order to form insoluble N_2O_5 (as all other oxide formations are soluble or reactive in water).[136] Unlike GaN where the group V atoms do not readily form insoluble oxides of their own, GaP possesses a unique metastable group V oxide. To date, etching GaP with phosphoric acid (H_3PO_4) remains sparsely explored and not well understood.[317] GaP etching does not follow Eq. (1) in aqueous solutions due to the insolubility of phosphine in water.[136] Some have theorized that GaP immersed in an acidic environment under illumination forms a phosphonic acid.[227] However, this does not account for the predominantly formed Ga_2O_3 seen from GaN as well as phosphorous oxides (P_xO_y) that have been reported in aqueous environments.[196, 318] It is expected that phosphorous forms a phosphoric derivative (depending on the degree of hydroxyl termination) to maximize solubility in low pH

environments.[136] In addition to preferential removal of group V species, defects play a crucial role as they present preferential etching locations due to increased energy at the crystal defects. Although much of this has been documented, actual device testing in non-extreme conditions for response and subsequent corrosion has not been systematically documented.

By utilizing an *in-situ* functionalization technique, the formation of oxide layers via etching is critical to the subsequent adsorption of functional groups. Through this route, simultaneous etching and functionalization can occur; however, there may remain regions free of both oxide and functional adsorbates. By utilizing incomplete regions, this study seeks to understand what role hydroxyl groups and other oxides play in the stability of GaN and GaP in aqueous environments. To accomplish this, the surface was initially stripped of the native oxide layer (Figure 35) via hydrochloric acid. Once protonated, subsequent etching at low temperature provides additional hydroxyl groups on the surface[319] without the concern of detrimental etching and pitting.[320] This in turn promotes adhesion of 1H,1H,2H,2H-Perfluorooctane phosphonic acid (PFOPA-Figure 34), which was chosen due to its ability to modify work functions[18] as well as provide a prominent fluorine signature.[320] Regions not capped with functional groups were used to test the leaching capacity of hydroxyl groups versus subsequent oxide formations such as gallium sub-oxides (GaO(OH), Ga_2O, GaO) and amorphous gallium oxide (Ga_2O_3).[313] In addition to analyzing patchy regions, use of hydrogen peroxide (H_2O_2) provides greater control of the

surface terminal groups, specifically hydroxyl groups from H_2O_2 degradation.[321, 322] This has already been shown to provide better control over surface termination[323] and subsequent surface coverage.[324] As etching techniques require the formation and subsequent dissolution of oxides, the degree of environmental degradation within an aqueous environment should provide insight onto the more reactive species on the surface.

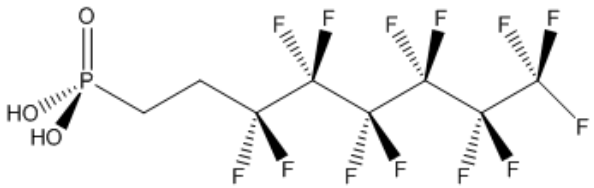

Figure 34 1H,1H,2H,2H-Perfluorooctane phosphonic acid

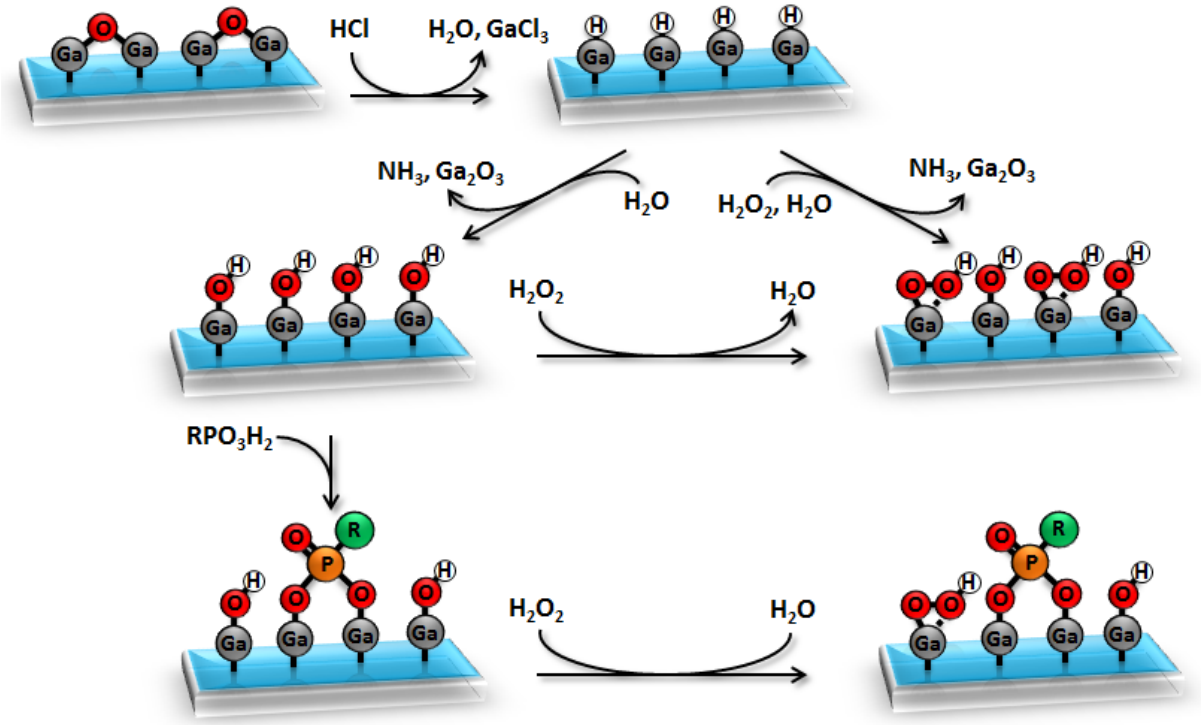

Figure 35 Surface stripping, etching, functionalization, and capping of GaN and GaP.

7.3Results and Discussion

7.3.1Topography and Hydrophobicity

Macroscopic changes to the surface were recorded by both atomic force microscopy (AFM) and contact angle goniometry. AFM images of GaN (Supprting Information, S1) indicate wavy structures consistent with other HVPE grown GaN.[264] The finger-like trenches on the surface are a combination of surface pits that do not present themselves as distinct polygonal pits consistently seen with hillock-type GaN from prominent screw dislocations.[179, 233] The GaP samples, which were heteroepitaxially grown on Si, do not show any defining surface features like the ones on GaN.[325] Optically, it appeared purple

with a mirror-like finish, whereas the GaN was transparent with a light tint. The surface roughness data (Figure 36) indicate a similar surface roughness for both samples. GaN experienced surface roughening with subsequent treatments, while GaP produced a mixed response. Soaking in water was expected to produce little change relative to pre-soaked samples, which can be seen in Figure S1. Although no statistical quantities can be derived, sensitivity of GaP to hydrogen peroxide is evident for post-soaked etched samples. Hydrogen peroxide has shown the ability to form smooth microstructures on AlGaN[321, 322] and ZnO[250] surfaces by forming secondary oxide structures, which seems to be the case for pre-soaked etched GaN samples. By soaking them, the change for GaN is diminished, whereas it becomes more evident for GaP.

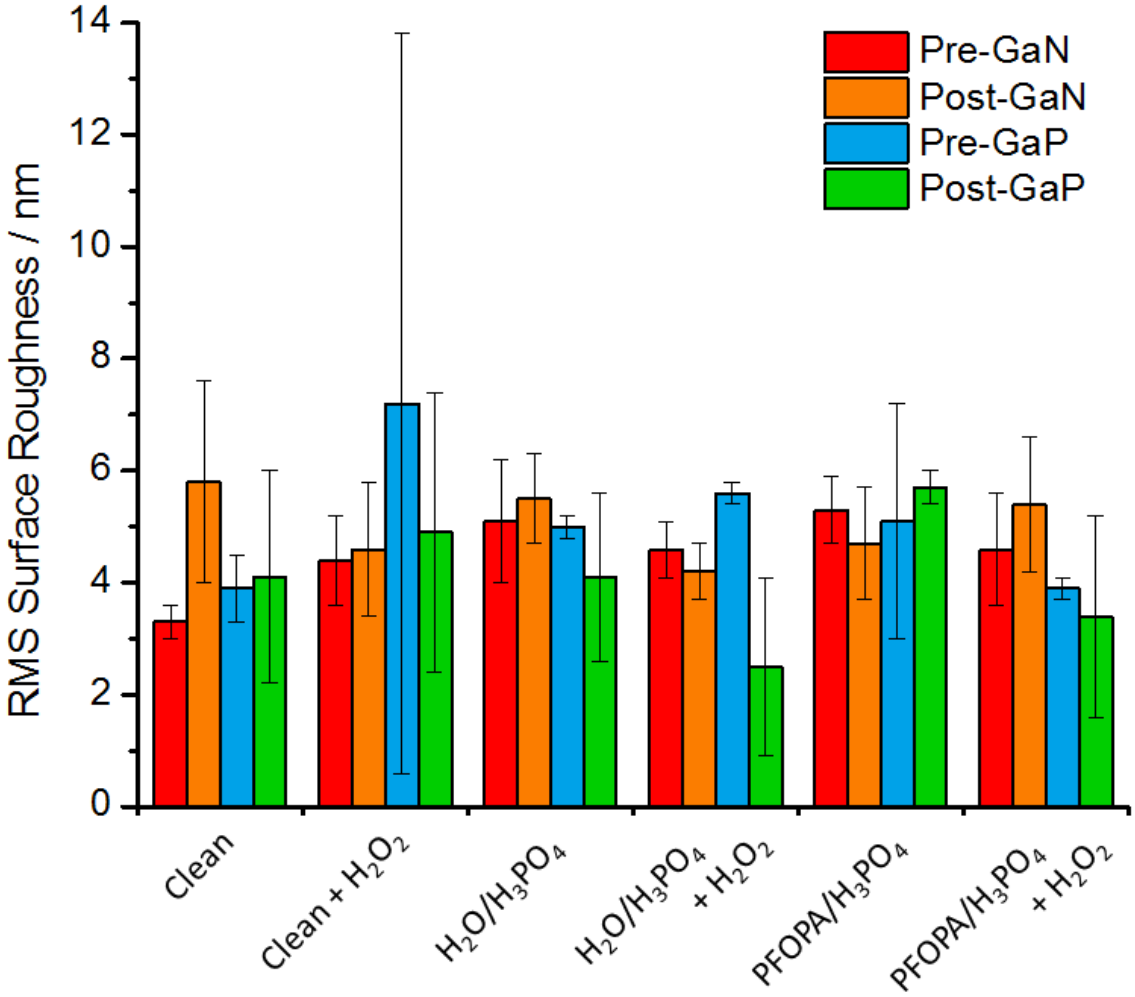

Figure 36 Surface RMS roughness captured via AFM both pre and post 7 day soak for GaN and GaP.

Water goniometry (Figure 37) shows a unique response relative to the various treatments and substrates being used. For GaN, the use of phosphoric acid without subsequent hydrogen peroxide capping provides increased surface roughness, which is matched with a decrease in the contact angle. By adding hydrogen peroxide, the roughness

hardly changes whereas the water contact angle increases, indicating a response due to surface chemistry rather than surface topography.[321, 322] For GaP, the contact angle is based solely upon treatments rather than topography, confirming interactions via surface chemistry. PFOPA is known to produce increased contact angles due to the repulsion from fluorine termination.[103] The contact angle data indicates better coverage of PFOPA for GaP than for GaN at a 3mM concentration.[125, 128] The low treatment temperatures as well as water instead of an organic solvent were expected to have this effect. The one trend consistent throughout the treatments is an increased water contact angle post soaking. Normally decreased contact angles are expected post hydration due to residual water; however, these effects are short lived and did not survive the time delay following XPS and AFM analysis. Additionally, lower pH values tend not to result in as great of a decrease in water contact angle post hydration as has been seen for neutral or basic conditions.[196]

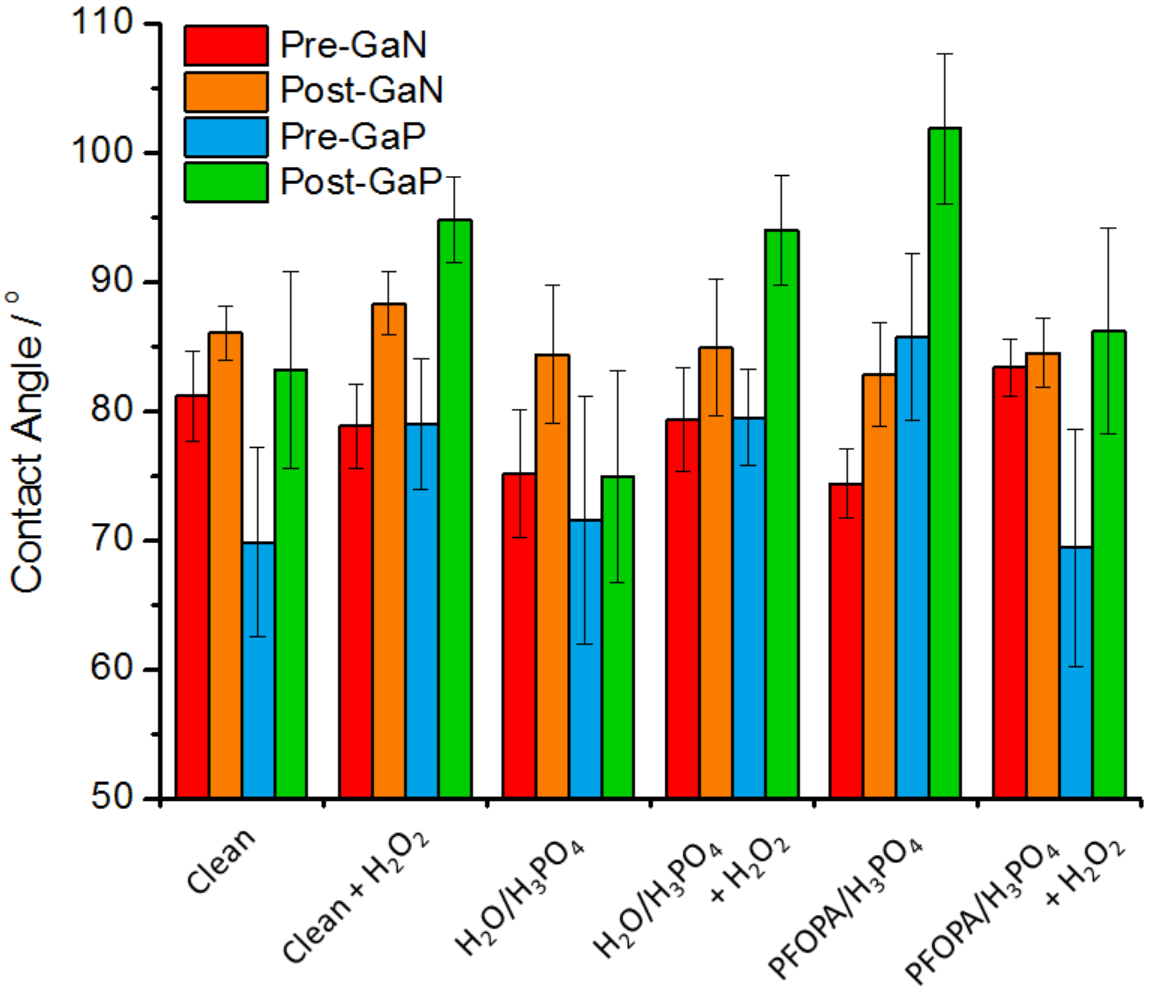

Figure 37 Water contact angle captured via water goniometry both pre- and post-7 day soaks for GaN and GaP.

7.3.2 Surface Composition and Stability

In order to understand the mechanism behind surface stability of GaN and GaP, XPS and ICP-MS were employed to investigate surface chemistry and leaching characteristics. Atomic ratios (Supporting Information, S2 and S3) captured from the area ratios of high

resolution C1s, F1s, Ga3d, N1s, O1s, and P2p spectra via XPS form a series of trends based upon the various treatments. From the F1s data, PFOPA appears to bind more concentrated to GaN than to GaP as the peak intensity is higher without any additional properties observed from water goniometry. Subsequent capping with hydrogen peroxide masks any fluorine signature from PFOPA for GaP, which was not seen for GaN. Regardless, PFOPA desorbs during soaking as a result of unstable oxides binding of the phosphonic acid to the surface. The degree of removal is a minimum of 77% fluorine contribution for GaP and 93% for GaN. The P2p spectra indicate residual phosphoric acid species from etching that were not removed post rinsing. The presence of fluorine and additional phosphorous from phosphonic acid functionalization indicate surface attachment on GaN,[320] but is only inferred for GaP due to the complex P2p spectra from oxide complexes. The oxygen content, which is employed in both functionalization and subsequent leaching, increased by 2.6% for GaN and 4.5% for GaP from pre- to post-soaking. In addition, hydrogen peroxide capped surfaces indicated greater oxygen content than uncapped surfaces, particularly for pre-soaked samples. When looking at the gallium content, there appeared to be no significant differences for GaN, but a decrease was seen for post-soaked GaP. Carbon and nitrogen content fluctuated due to environmental impurities induced from a more relaxed and sustainable functionalization process.

From the observed trends, it appears oxygen plays a crucial role in stability and functionalization. To elucidate the role gallium oxide plays, the $Ga2p_{3/2}$ spectra was deconvoluted into five primary binding species: Ga-Ga (1116.0 eV),[200, 201] Ga-N (1117.7

eV),[248, 249] Ga-P (1117.3 eV),[326] Ga-oxides (1118.5 eV),[201, 205] and Ga_2O_3 (1119.5 eV)[248] as seen in Figures 38 and 39. For pre-soaked GaN in Figure 38, hydrogen peroxide capped surfaces produced more gallium sub-oxides (which include Ga_2O, GaO, GaO(OH) species) than Ga_2O_3. This was seen by the shifting of the $Ga2p_{3/2}$ peak to higher binding energies associated with oxide formation. Despite preferring sub-oxide formation, H_2O_2 capping appears to promote the formation of insoluble Ga_2O_3 as well. Soaking from Figure 38 indicates that exposure to a water environment alters the oxide composition to a Ga_2O_3-centric makeup by either removing the sub-oxides into solution or converting them into insoluble Ga_2O_3. Quantitatively (Supporting Information, S4 and S5) the type of oxide as well as amount is highly dependent upon whether H_2O_2 treatment was performed, particularly for post soaked samples. Although H_2O_2 was expected to decompose and cap the surface with hydroxyl species prior to soaking,[250, 327] the data indicate a rapidly grown thin Ga_2O_3 layer relative to uncapped samples. This changes post soaking as the ratios from S4 confirm a difference in oxide composition (sub-oxide to Ga_2O_3), which is likely a result from the spontaneous dissociation of water onto the surface.[328, 329] Deconvolution of the O1s spectra (Supporting Information, S6) confirms the initial hydroxyl terminated oxide setup (represented in Scheme 1) in addition to the migration of sub-oxides to Ga_2O_3 formations following soaking. This was supported by the shifting of the O1s spectra from 533 eV (corresponding to –OH termination) to 531 eV (corresponding to -O- type bonding).[250, 327, 330] Subsequent soaking forms gallium rich oxide species for etchants

not capped with hydrogen peroxide, while those capped continue to form gallium deficient sub-oxides.

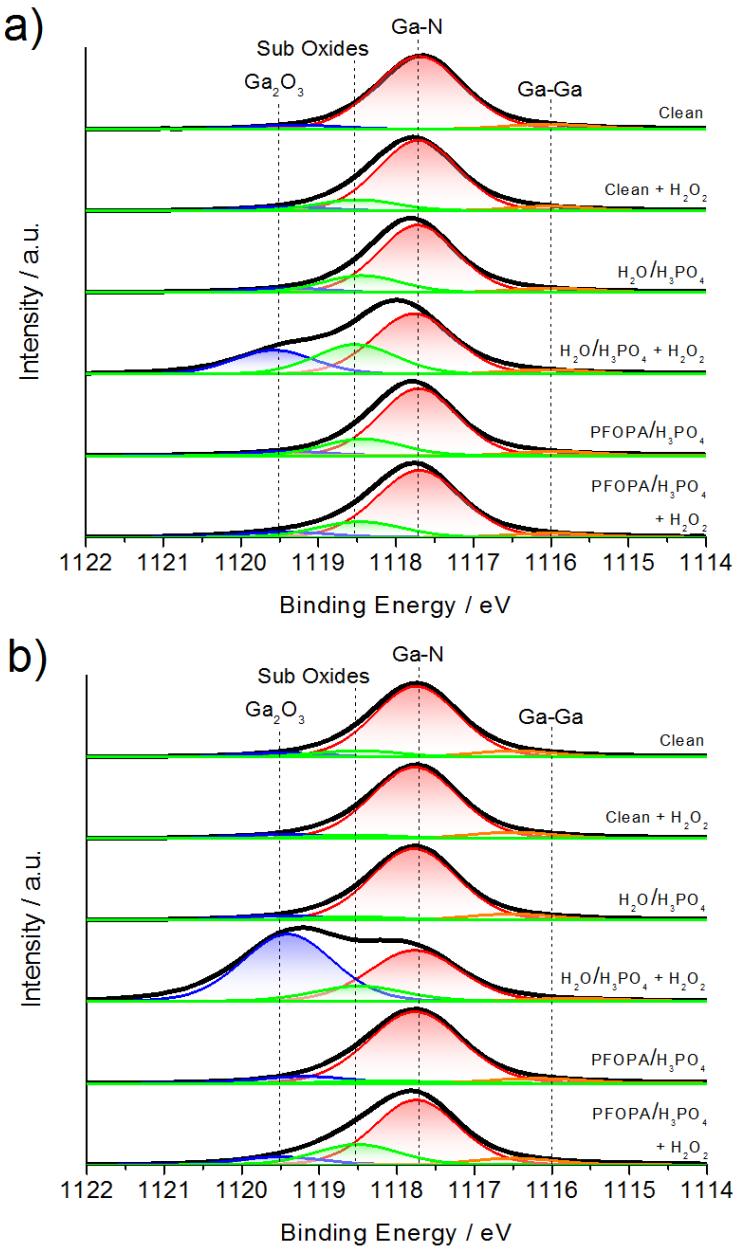

Figure 38 Deconvoluted $Ga2p_{3/2}$ spectrum for GaN pre (a) and post (b) 7 day soaking.

GaP behaves much the same to the treatments as GaN does prior to soaking. Capping with hydrogen peroxide results in rapid oxide growth (Figure 39), whereas uncapped treatments produce more sub-oxide species. The difference lies in the soaking process. Unlike GaN which devolves into insoluble gallium oxide species and ammonia (no N-O peak seen to indicate formation of nitrogen oxide-N_xO_y or hydroxyl termination), GaP forms gallium oxide as well as phosphorous oxide (P_xO_y).[196, 271, 310, 331] Whereas post soaking resulted in the formation of gallium rich species for primarily uncapped GaN, the soaking produced gallium oxides of almost equal gallium content regardless of treatments. There is a slight variation, but when observing the degree of phosphorous oxide the difference is made up with increased phosphorous content (Supporting Information, S7). The terminal oxide species from O1s follow the trend seen for GaN with decreasing hydroxyl groups after soaking; despite the fact that the O= is now being divided between surface gallium and phosphorous atoms.

The degree of surface stability was tested by the amount of leached gallium within solution that was captured via ICP-MS. Other species (such as nitrogen or phosphorous) were not tested due to the natural instabilities of V-group atoms relative to gallium.[137, 196] Understanding that the surface areas contribute more to the stability than the bulk volume, a ratio taken between total gallium leached (ppb) versus the total area exposed (mm^2) provides a mechanism to compare the two material types, which has not yet been explored. The use of gallium terminated GaN and GaP morphologies (Supporting Information, S8) allows for a more direct comparison. Following 7 days of soaking, GaN on average released less gallium

into solution than GaP (27±11 ppb/mm^2 vs. 34±7 ppb/mm^2). It is expected that GaP is less stable than GaN due to less ionic behavior,[332] which equates to lower bond strength

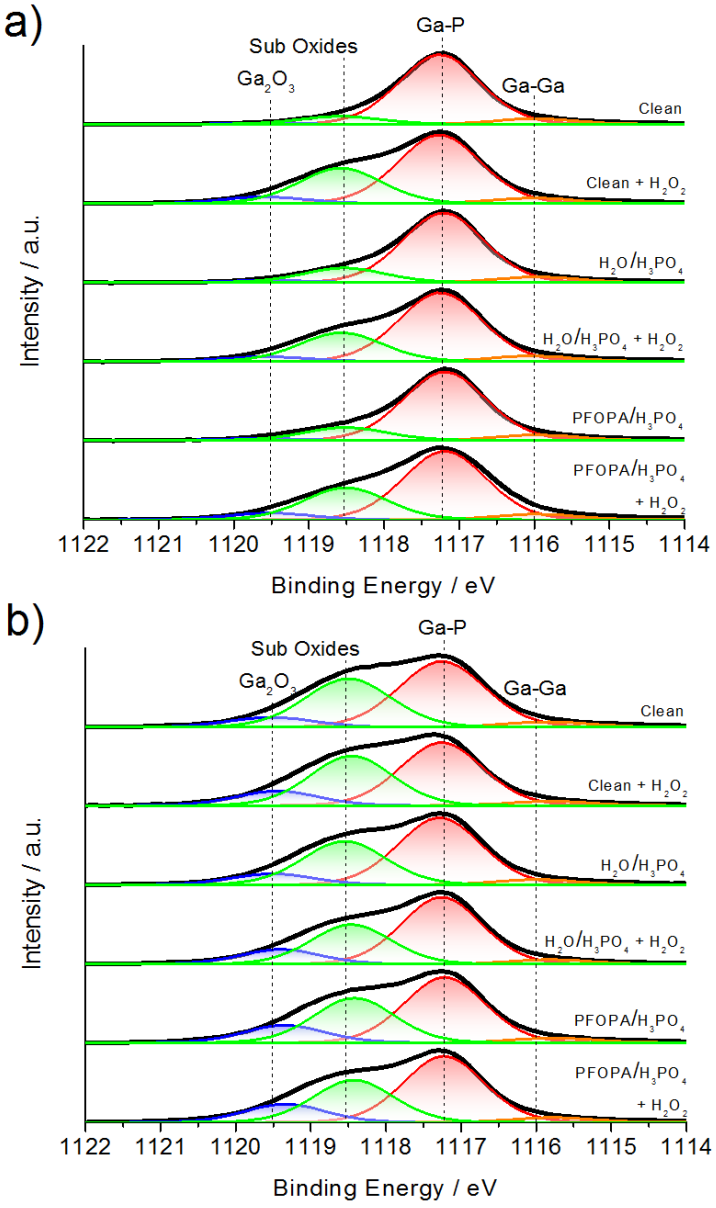

Figure 39 Deconvoluted Ga2p$_{3/2}$ spectrum for GaP pre (a) and post (b) 7 day soaking.

between III and V species.[186, 207, 333]. We note that for the free-standing high-quality GaN samples both polar faces and nonpolar sides were exposed to the chemical treatments. While we accounted for this by calculating the total exposed area, our experimental results were influenced by both the Ga-face polar surface known as the most chemically resistant, and by a contribution from the other surfaces, that are less chemically stable. Due to the greater ionic strength, GaN preferentially forms Ga_2O_3, which due to the structural conformation, limits access to nitrogen atoms. This subsequently slows leaching of gallium into solution by forcing water to attack Ga_2O_3. GaP responds much the same way but forms a secondary oxide via phosphorous. Comparing the oxide ratios of each species, the ratio of Ga_2O_3 vs. P_xO_y went from 8:1 for pre-soaked GaP to a ratio of 7:1. The decrease in Ga_2O_3 indicates a mechanism for increased leaching of Ga from GaP via the more soluble P_xO_y species.[4, 196, 239, 334] Given enough time, gallium oxides would have limited subsequent leaching as simply by soaking the surface became more gallium rich. Despite the reported insolubility of gallium oxide formations, the fact that water spontaneously dissociates when in contact with these materials[328, 330] ultimately controls the degree of stability that appears similar to one another.

By utilizing hydrogen peroxide to terminate uncoated regions, the amount of gallium collected following each treatment indicates that hydroxyl termination is a catalyst for gallium removal. In each case (Figure 40), the capping of hydrogen peroxide promotes leaching by as much as 145% (Supporting Information, S9) for each individual treatment. Correlation with XPS data confirms the increased reactivity caused by hydroxyl termination

versus gallium oxide (specifically Ga_2O_3) formation. In reference to the Pourbaix diagram for GaN,[335] the pH and potential utilized imply that Ga_2O_3 does provide some level of surface

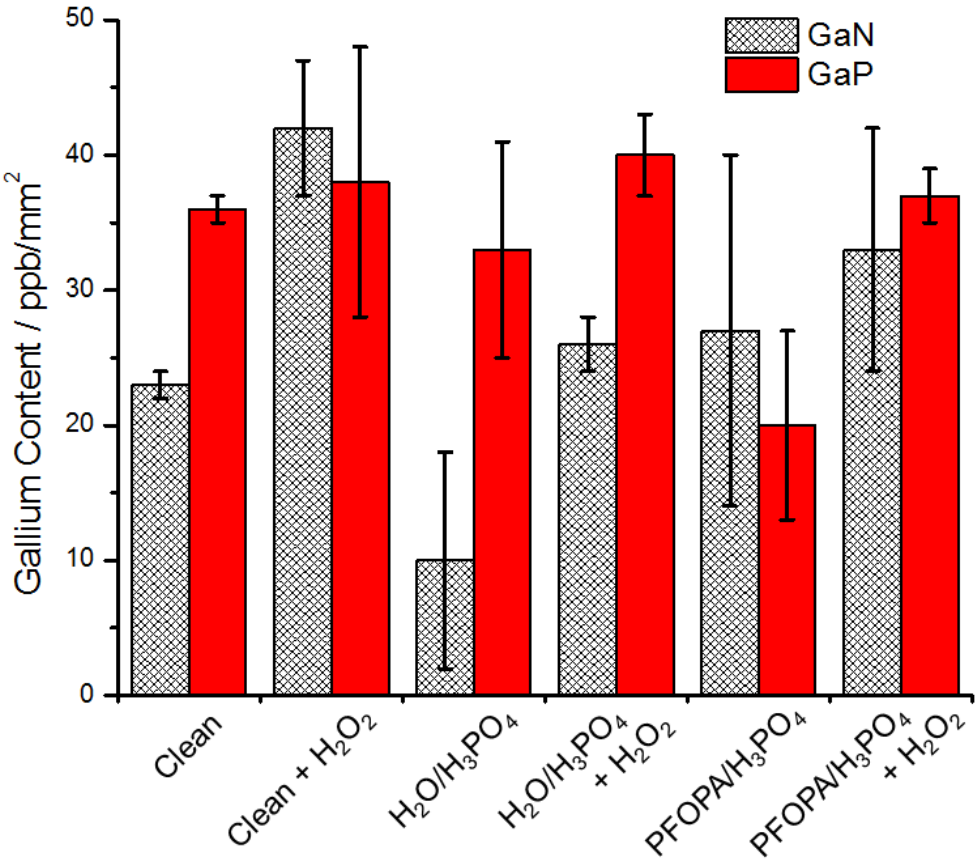

Figure 40 ICP-MS data corrected for exposed surface area for GaN and GaP following a 7 day soak in DI water.

protection as phorphoric acid and hydrogen peroxide treated GaN produced the largest amount of Ga_2O_3 and subsequently less leaching verses other treatments. Despite that, the same treatment without hydrogen peroxide capping provides gallium rich oxide formations, which indicates the degree of gallium content on the surface controls the ultimate stability.

GaP mimicked this with the PFOPA treatment due to increased uniform coverage of PFOPA and thus improved gallium oxide stability.

7.4 Conclusion

From this study, the surface stability of GaN and GaP was monitored following surface functionalization with 1H,1H,2H,2H-perfluorooctanephosphonic acid and a phosphoric acid etchant. Surface roughness data from AFM indicated no quantifiable changes after the surface chemistry was altered. Water contact angle confirmed the stability of bulk surface hydrophobicity with no significant differences between GaN and GaP. Although macroscopic properties remained the same, XPS confirmed alterations to the surface chemistry with significant signal contributions from hydroxyl groups, particularly following hydrogen peroxide capping. By pairing with ICP-MS, the degree of sensitivity of GaN and GaP to hydroxyl groups for subsequent gallium dissociation and oxide stability became evident. Although GaN and GaP demonstrated similar degrees of solution stability, GaP is more susceptible to gallium leaching than GaN.

7.5 Experimental Section

7.5.1 Sample Preparation

The two starting materials were polar (001) free-standing GaN and a polar (001) thin GaP film. The GaN samples were grown via hydride-vapor phase epitaxy on sapphire and were self-separated from the substrate during the cooling. These GaN samples typically

possess a dislocation density in the range $5x10^5$-$1x10^6$ cm^{-2}.[190] Following growth, the GaN was chemically-mechanically polished on the gallium rich side post substrate separation. The free-standing GaN was 0.78 mm thick after final processing. A thin (80 nm) film of GaP was grown on (100) silicon via metallorganic vapor phase epitaxy and exhibited a single crystal X-ray diffraction pattern. Both GaN and GaP wafers were diced into 3x3 mm^2 squares by American Precision Dicing. Following dicing, samples were cleaned via sonication baths of acetone and methanol seperately. Each sample was rinsed with deionized (DI) water (18.2 MΩ/cm) and exposed to a 100°C 50/50 vol.% hydrochloric acid (Fisher Scientific 35-38% vol.%)/water solution for 10 minutes. Following the HCl bath, samples were rinsed again with DI water for 2 seconds and immediately exposed to respective functionalization and capping regimens. Samples were characterized following cleaning without further modification.

7.5.2 Chemical Functionalization

Following cleaning samples were either exposed to a solution of 50/50 vol.% phosphoric acid (Fisher Scientific, 95%)/DI water or a 50/50 vol.% phosphoric acid/ 3mM 1H,1H,2H,2H-Perfluorooctanephosphonic acid solution at 40˚C. After 150 minutes, each sample was rinsed with DI water for 2 seconds and dried with nitrogen. One of each sample (GaN and GaP) from each treatment was then subsequently exposed to a 10 vol.% H_2O_2 solution (Fisher Scientific, 30%) for 7.5 minutes at room temperature. A cleaned sample of GaN and GaP was exposed to the H_2O_2 solution without undergoing functionalization.

Samples were dried with nitrogen following H_2O_2 capping. All samples were analyzed via XPS within 2 hours of post processing.

7.5.3 Physical Characterization

Structural configuration was confirmed with a Rigaku Geigerflex model D/Max IIA XRD utilizing a Cu Kα ($\lambda = 0.1542\ nm$) source excited by a 20 mA electron beam accelerated to 25 kV. 1˚ diffraction slits were used with 0.6 mm and 0.8 mm receiving and monochromator slits, respectively. The XRD was calibrated using the silicon (004) reflection that corresponds to a 2θ of 69.13˚. 2θ scans were taken from 25-75˚ and captured with MDI DataScan4 software. The XRD data (provided in supporting information) was to confirm both polarity and epi-layer location on diced samples. The GaP diffraction pattern revealed a (001) oriented film (see supporting information).

Surface roughness data was collected with an Asylum Research Cyper AFM following XPS measurements. Samples were mounted to steel chucks and randomly scanned at 5 locations over a 10 x 10 μm^2 area per location. Asylum Research AC240TM tips were used to raster at a scan rate of 1 Hz. Images were flattened within Igor Pro Ver.14 (for visual effects only, see supporting information) and averaged for root mean square (RMS) surface roughness quantification.

Surface hydrophobicity was tested after AFM with a Ramé-Hart Model 200-F4 goniometer. Water droplets were formed with DI water from a 28 ga. (AWG) needle. Each droplet was brought into contact with the surface before the needle was retracted. The half-

angles from each side were averaged to form the contact angle for each test. Half-angles were collected via DROPImage (Ver.2.4.07) software at a rate of 2 frames per second for 5 seconds. Once images and angles were collected, the sample was dried with nitrogen. A total of 5 random droplets were placed on each sample.

7.5.4 Chemical Characterization

Surface chemical characterization was performed with a Kratos Axis Ultra XPS. A monochromated Al Kα (*hν* = 1486.7 eV) source with a 2.0 A charge neutralized were used at 3 x 10^{-8} torr. Samples were mounted on an aluminium stage with copper tape and analysed at photoemission angles 0˚, 45˚, and 60˚. Three random spots were selected per sample with the three aforementioned photoemission angles performed per spot. A single survey scan with 160 eV pass was performed in addition to high resolution region spectras of C1s, Cl2p, F1s, Ga2p, Ga3d, O1s, N1s, P2p, and S2p composed of 5 averaged scans with 20 eV passes. The XPS was calibrated to Ag (368.21 eV) in accordance to ISO TC/201.[145] All processing and peak deconvolution was performed via Casa XPS (Ver. 2.3.16 PR) software. Spectra were charge corrected using C1s (284.8 eV)[144] prior to deconvolution. Primary peak full-width at half-maximum (FWHM) served as limiter for subsequent peaks in the spectra to prevent imaginary broadening. Each peak as fitted using the Lorentzian profile and the background spectra was subsequently removed. For atomic species calculations, the Kratos atomic sensitivity factors were loaded prior to quantification. Comparing atomic percentages, Ga3d region was used rather than $Ga2p_{3/2}$ due to greater depth profiling and decreased

energy disparity between species.[191] No auger peaks were included within quantification, such as gallium auger peaks within the N1s spectra.

Solution stability was tested following physical characterization. All samples were soaked in 1.5 mL of DI water (pH 5.22) for 7 days. The samples were then removed from solution and dried with nitrogen to undergo secondary characterization with XPS, AFM, and water goniometry. The solutions were analysed for gallium with a Perkin Elmer Sciex Elan DRCII ICP-MS after calibration with gallium 69 and solution dilution with water 5 times.

8 Future Work

The stability studies from the previous section shed light onto natural differences in reactivity between various III-V materials that would benefit from a more thorough treatment. There are many III-V materials currently seeing use in aqueous environments under various conditions.[336-338] Though it is accepted that specific pH ranges promote leaching or even etching,[139, 312] but there is no consistent studies citing repeatable loss rates or quantifiable stabilities. This is of concern, particularly for devices seeing action within biological environments. It is known that indium alloys are exceedingly hazardous to gallium derivatives,[339, 340] but the use of specific V-group species such as arsenic and antimony are known by health organizations to produce toxic byproducts within the body.[339, 341] Many of these species are limited to 10 ppb for arsenic[342] and 20 ppb for antimony[343] by governing bodies. By focusing efforts on more benign V-species such as nitrogen and phosphorous (which already account for 3.0% and 1.1% of the human body respectively)[344] the hazards of leached material can be mitigated. Though the previous section touched on the differences between GaN and GaP, a direct quantitative analysis independent of exposed surface area would provide improved quantitative analysis. This can be achieved by isolating equal surface areas to duplicate environments. With recent advances in microfluidics, the ability to control flow rates, exposed surfaces, volumes, and fluid compositions promises a unique ability to identify elemental species not available in larger volumes.[345, 346] This enables the direct comparison of the surfaces explored here, but also other crystallographic orientations that remain unexplored to date.

The identification of specific adsorbate binding remains a challenge with the characterization techniques previously utilized. XPS provides high resolution chemical characterization, but is limited to small areas due to the time requirements to perform elemental mapping. PL provides a higher throughput method than XPS but is ultimately limited to the source and subsequent predetermined excitation paths.[347] It is not yet been confirmed if adsorbates bind on high energy regions such as defects or prefer pristine surfaces for agglomeration. Cathodoluminescence (CL) offers a novel approach to addressing this concern, but also to identifying alloy composition for mixed III-V materials as well as band structures of surface species.[348-351] CL is available in both hybid-optical microscopy setups[347] in addition to SEM add-on detectors.[352] It is recommended that SEM based CL provides high resolution-small area identification of the initial binding sites and surface band structures. Once properly correlated, CL-optical microscopy offers a high throughput option for systematic identification of surface adsorbates on the surface at both a fraction of the equipment and operational costs. In this way the bulk properties, defects, and surface species can be quantified.

9 Conclusions and Outlook

9.1 Conclusion

III-V semiconductors have seen a recent surge in interest due to properties such as faster charge mobility, customizable wide band gaps, chemical stability, and biocompatibilities that silicon cannot offer. Because the surface controls most of the aforementioned properties, this dissertation seeks to investigate how surface properties of GaN can be modified through surface passivation with organic adsorbates, which has been little studied to date. Adsorbate binding was controlled by an in-situ etch in an effort to understand the role crystallographic orientation, crystal quality, and adsorbate has on the surface chemical, optical, and electrical properties of GaN. This work seeks to provide future researchers with a greater understanding, of GaN surface interface interactions for potential applications.

The first part of this dissertation discussed the adhesion of a short chained thiol (cysteamine) onto polar GaN in both thin and thick layered configurations. Two temperatures of phosphoric acid were utilized to understand the degree of cysteamine binding and oxide formation that was captured through surface sensitive techniques (AFM, water contact angle, XPS, PL). Surface passivation with cysteamine was observed at both temperatures; however, bulk free-standing GaN appeared to be more sensitive to oxide formation due to sizable surface pits. These pits rendered the surface hydrophilic with high temperature etching. The

effects of cysteamine on topography, particularly for the defect rich thin layered GaN, was seen in the control of surface roughness that promoted the greatest photoluminescence.

The second part continued the study but utilized nonpolar GaN in order to understand the role of crystallographic orientation and cysteamine adsorption. Binding was again confirmed via XPS; however, the difference in atomic compositions for etchants with and without cysteamine was not as significant. This confirmed the role gallium stoichiometry has on thiol binding as the increased nitrogen content for nonpolar GaN did not demonstrate the same response as polar GaN. Free-standing nonpolar GaN showed increased sensitivity to etching than the bulk polar GaN due to increased defect sites. Cysteamine was able to limit oxide formation and subsequent etching for bulk GaN, but showed little effect for thin layered GaN. This was identified with photoluminescence, which demonstrated decreased intensities from solutions with cysteamine, primarily for thin layered GaN. Etchant temperature had little effect on etching for nonpolar GaN, but was sensitive in the case of polar GaN.

The third part expanded the study with the use of short chained phosphonic acids. Again, the role of etchant composition and temperature were investigated on various GaN configurations (polar and nonpolar as well as thin and thick layered samples). Though the binding mechanism differs from thiols, the phosphonic acids added to the etchant provided oxide stabilization which subsequently controlled topography and hydrophobicity. This in turn controlled the photoluminescence, particularly for nonpolar GaN samples. The mechanism of etching was confirmed as gallium oxide dependent (seen via gallium to

nitrogen content across all samples), in addition to the higher sensitivity of thick GaN layered samples to oxide formation. Polar bulk GaN demonstrated not only decreased oxide formation with the use of phosphonic acids (as a result of passivation), but a significant reduction of gallium oxide content for bromine terminated phosphonic acid. This indicates not only good coverage but also a direct correlation between terminal groups and functionalization characteristics. An environmental study was added via ICP-MS, which confirmed passivation properties of adsorbates within etchants versus adsorbate free etchants.

Due to the unique behavior of the bromine terminated phosphonic acid, the fourth section explores the role terminal groups have on passivation and other properties on polar bulk GaN. The use of long chained phosphonic acids enabled retention of oxide formation that was limited by both concentration and temperature, as well as reduced the surface potential of GaN for adsorbates with electronegative species. Unlike the previous studies that showed improved photoluminescence output with short chained phosphonic acids, the use of long chained phosphonic acids inhibited photoluminescence intensities, but were able to again control the surface chemical makeup and surface topography.

Utilizing the long-chained fluorine terminated phosphonic acid from the previous section, the effects of functionalization of high aspect ratio GaN nanostructures was compared to planar free-standing and epitaxial layered GaN in the sixth section. Nanostructured GaN and layered planar GaN demonstrated significant changes to PL response as a result of etching and functionalization. Free-standing bulk GaN, known for its high crystalline quality, replicated the weak response from the previous section; whereas

defect rich planar GaN reacted in an opposite manner. The mechanism of PL response is oxide sensitive as by soaking the samples the ratio of etch to functionalization PL intensity decreased for layered GaN. Nanostructured GaN, dominated by semipolar facets, did not vary significantly over the course of soak. This indicates the importance of oxides to functionalization and surface termination, as well as to the optical response.

The seventh section expanded the stability study from the fourth section by utilizing hydrogen peroxide as a way to initiate hydroxyl termination to better understand the role oxides play in III-V environmental stabilities. The degree of surface stability is controlled not only by adsorbed molecules as seen previously, but also by the constituents available to form insoluble passivating species. The complex nature of oxide formation for GaP lead to increased leaching per area relative to GaN. The hydrogen peroxide formed gallium rich oxides that when exposed to aqueous environments, lead to increased leaching and sub-oxide rich termination. In this way, oxygen rich surface termination is required for surface passivation in moderate pH environments.

9.2 Outlook

Due to the size of scale within the manufacturing world, the ability to remove a single step from a process flow has the potential to vastly reduce production time and material costs. Some applications, such as dye-sensitized solar cells, are already seeing interfacial functionalization as a way to realize more efficient solar technology.[353] It is accepted that III-V materials are unlikely to reach such magnitudes of production in terms of shear material

mass; however, their uses in focused applications such as transistors, LEDs, and sensors is rapidly growing. In the case of LEDs, the methods described in this dissertation shed light on a convenient way to modulate surface chemistry and topography to alter optical and electrical properties. With the advent of organic LEDs, the importance of electrical interfaces and pairing between the inorganic and organic is magnified. GaN and similar III-nitride based semiconductors have already breached the 100 lumens/watt threshold and are expected to become the world's most efficient light source according to Haitz's law (an LED derivative to Moore's law).[354] White LEDs are typically blue LEDs with a yellow phosphor coating that emits white light. This method suffers from inefficiencies due to the phosphorescent process. By utilizing organic phosphors, direct grafting to specific regions could allow for increased efficiency as well as higher pixel densities due to selective color segregation.[355]

In the realm of chemical and biological sensors, the proposed materials and methodology could almost certainly be applied as a primary or additional processing technique.[255, 356] Without additional surface treatments, GaN has already demonstrated pH sensitivity simply from oxide formation.[357] By adding functional adsorbates, the sensitivity and selectivity could be magnified significantly by increasing the surface area to allow for more binding sites. This could be extended into high aspect ratio formations such as quantum dots or nanowires that are difficult to functionalize. The focus of this dissertation was primarily on GaN, a limited number of adsorbates, and one of five widely used III-V semiconductor etchants, which leaves a lot of open possibilities.

REFERENCES

[1] A. Ulman, "Formation and structure of self-assembled monolayers," *Chemical Reviews,* vol. 96, pp. 1533-1554, 1996.

[2] Y. Liu, J. H. E. Chen, and A. V. Teplyakov, "Chemical passivation processes for biofunctionalization schemes on semiconductor surfaces," *Langmuir,* vol. 28, pp. 15521-15528, 2012.

[3] V. Duplan, E. Frost, and J. J. Dubowski, "A photoluminescence-based quantum semiconductor biosensor for rapid in situ detection of Escherichia coli," *Sensors and Actuators B-Chemical,* vol. 160, pp. 46-51, 2011.

[4] F. Seker, K. Meeker, T. F. Kuech, and A. B. Ellis, "Surface chemistry of prototypical bulk II-VI and III-V semiconductors and implications for chemical sensing," *Chemical Reviews,* vol. 100, pp. 2505-2536, 2000.

[5] M. Losurdo, P. C. Wu, T. H. Kim, G. Bruno, and A. S. Brown, "Cysteamine-based functionalization of InAs surfaces: revealing the critical role of oxide interactions in biasing attachment," *Langmuir,* vol. 28, pp. 1235-1245, 2012.

[6] M. A. Garcia, M. Losurdo, S. D. Wolter, W. V. Lampert, J. Bonaventura, G. Bruno, C. Yi, and A. S. Brown, "Comparison of functionalized III-V semiconductor response for nitric oxide," *Sensor Letters,* vol. 6, pp. 627-634, 2008.

[7] S. K. Sahoo and V. Labhasetwar, "Nanotech approaches to delivery and imaging drug," *Drug Discovery Today,* vol. 8, pp. 1112-1120, 2003.

[8] S. Parveen, R. Misra, and S. K. Sahoo, "Nanoparticles: a boon to drug delivery, therapeutics, diagnostics and imaging," *Nanomedicine-Nanotechnology Biology and Medicine,* vol. 8, pp. 147-166, 2012.

[9] H. Onyuksel, O. M. Koo, V. Sethi, and I. Rubinstein, "Sterically stabilized phospholipid micellar human vasoactive intestinal peptide: A novel disease-modifying drug for rheumatoid arthritis.," *Arthritis and Rheumatism,* vol. 52, pp. S262-S262, 2005.

[10] A. Hagfeldt, G. Boschloo, L. C. Sun, L. Kloo, and H. Pettersson, "Dye-sensitized solar cells," *Chemical Reviews,* vol. 110, pp. 6595-6663, 2010.

[11] B. E. Hardin, H. J. Snaith, and M. D. McGehee, "The renaissance of dye-sensitized solar cells," *Nature Photonics,* vol. 6, pp. 162-169, 2012.

[12] A. L. Briseno, T. W. Holcombe, A. I. Boukai, E. C. Garnett, S. W. Shelton, J. J. M. Frechet, and P. D. Yang, "Oligo- and polythiophene/ZnO hybrid nanowire solar cells," *Nano Letters,* vol. 10, pp. 334-340, 2010.

[13] J. Lopez-Gejo, A. Arranz, A. Navarro, C. Palacio, E. Munoz, and G. Orellana, "Microsensors based on GaN semiconductors covalently functionalized with luminescent Ru(II) complexes," *Journal of the American Chemical Society,* vol. 132, pp. 1746-1747, 2010.

[14] C. W. Hsu, A. Ganguly, C. P. Chen, C. C. Kuo, P. P. Paskov, P. O. Holtz, L. C. Chen, and K. H. Chen, "Optical properties of functionalized GaN nanowires," *Journal of Applied Physics,* vol. 109, p. 053523, 2011.

[15] R. M. Petoral, G. R. Yazdi, A. L. Spetz, R. Yakimova, and K. Uvdal, "Organosilane-functionalized wide band gap semiconductor surfaces," *Applied Physics Letters,* vol. 90, p. 223904, 2007.

[16] K. H. Chen, B. S. Kang, H. T. Wang, T. P. Lele, F. Ren, Y. L. Wang, C. Y. Chang, S. J. Pearton, D. M. Dennis, J. W. Johnson, P. Rajagopal, J. C. Roberts, E. L. Piner, and K. J. Linthicum, "C-erbB-2 sensing using AlGaN/GaN high electron mobility transistors for breast cancer detection," *Applied Physics Letters,* vol. 92, pp. 57-63, 2008.

[17] D. N. Richards, D. Y. Zemlyanov, R. M. Asrar, Y. Y. Chokshi, E. M. Cook, T. J. Hinton, X. R. Lu, V. Q. Nguyen, N. K. Patel, J. R. Usher, S. Vaidyanathan, D. A. Yeung, and A. Ivanisevic, "DNA immobilization on GaP(100) investigated by kelvin probe Force Microscopy," *Journal of Physical Chemistry C,* vol. 114, pp. 15486-15490, 2010.

[18] P. J. Hotchkiss, H. Li, P. B. Paramonov, S. A. Paniagua, S. C. Jones, N. R. Armstrong, J. L. Bredas, and S. R. Marder, "Modification of the surface properties of indiumt tin oxide with benzylphosphonic acids: a joint experimental and theoretical study," *Advanced Materials,* vol. 21, pp. 4496-4501, 2009.

[19] B. Gupta, Y. Zhu, B. Guan, P. J. Reece, and J. J. Gooding, "Functionalised porous silicon as a biosensor: emphasis on monitoring cells in vivo and in vitro," *Analyst,* vol. 138, pp. 3593-3615, 2013.

[20] X. Song, J. Zhai, Y. Wang, and L. Jiang, "Self-assembly of amino-functionalized monolayers on silicon surfaces and preparation of superhydrophobic surfaces based on alkanoic acid dual layers and surface roughening," *Journal of Colloid and Interface Science,* vol. 298, pp. 267-273, 2006.

[21] S. E. Letant, B. R. Hart, A. W. Van Buuren, and L. J. Terminello, "Functionalized silicon membranes for selective bio-organism capture," *Nature Materials,* vol. 2, pp. 391-395, 2003.

[22] A. M. P. Dupraz, S. A. T. v. d. Meer, J. R. De Wijn, and J. H. Goedemoed, "Biocompatibility screening of silane treated hydroxyapatite powders, for use as filler in resorbable composites," *Journal of Materials Science: Materials in Medicine,* vol. 7, pp. 731-738, 1996.

[23] S. Bhattacharjee, I. M. C. M. Rietjens, M. P. Singh, T. M. Atkins, T. K. Purkait, Z. Xu, S. Regli, A. Shukaliak, R. J. Clark, B. S. Mitchell, G. M. Alink, A. T. M. Marcelis, M. J. Fink, J. G. C. Veinot, S. M. Kauzlarich, and H. Zuilhof, "Cytotoxicity of surface-functionalized silicon and germanium nanoparticles: the dominant role of surface charges," *Nanoscale,* vol. 5, pp. 4870-4883, 2013.

[24] H. Morkoc, S. Strite, G. B. Gao, M. E. Lin, B. Sverdlov, and M. Burns, "Large band gap SiC, III-V Nitride, and II-VI ZnSe based semiconductor device technologies," *Journal of Applied Physics,* vol. 76, pp. 1363-1398, 1994.

[25] W. Bludau, A. Onton, and W. Heinke, "Temperature dependence of the band gap of silicon," *Journal of Applied Physics,* vol. 45, pp. 1846-1848, 1974.

[26] T. Matsuoka, H. Okamoto, M. Nakao, H. Harima, and E. Kurimoto, "Optical bandgap energy of wurtzite InN," *Applied Physics Letters,* vol. 81, pp. 1246-1248, 2002.

[27] H. Kroemer, "The 6.1 angstrom family (InAs, GaSb, AlSb) and its heterostructures: a selective review," *Physica E-Low-Dimensional Systems & Nanostructures,* vol. 20, pp. 196-203, 2004.

[28] Y. S. Kim, K. Hummer, and G. Kresse, "Accurate band structures and effective masses for InP, InAs, and InSb using hybrid functionals," *Physical Review B,* vol. 80, p. 035203, 2009.

[29] N. Chestnoy, R. Hull, and L. E. Brus, "Higher excited electronic states in clusters of ZnSe, CdSe, and ZnS spin-orbit, vibronic, and relaxation phenomena," *Journal of Chemical Physics,* vol. 85, pp. 2237-2242, 1986.

[30] W. H. Strehlow and E. L. Cook, "Compilation of energy band gaps in elemental and binary compound semiconductors and insulators," *Journal of Physical and Chemical Reference Data,* vol. 2, pp. 163-200, 1973.

[31] R. L. Rudnick, S. M. Mclennan, and S. R. Taylor, "Large ion lithophile elements in rocks from high-pressure granulite facies terrains," *Geochimica Et Cosmochimica Acta,* vol. 49, pp. 1645-1655, 1985.

[32] J. D. Burton, F. Culkin, and J. P. Riley, "The abundances of gallium and germanium in terrestrial materials," *Geochimica Et Cosmochimica Acta,* vol. 16, pp. 151-180, 1959.

[33] D. C. Look, H. Lu, W. J. Schaff, J. Jasinski, and Z. Liliental-Weber, "Donor and acceptor concentrations in degenerate InN," *Applied Physics Letters,* vol. 80, pp. 258-260, 2002.

[34] S. Strite and H. Morkoc, "GaN, AlN, and InN-a review," *Journal of Vacuum Science & Technology B,* vol. 10, pp. 1237-1266, 1992.

[35] P. M. Smith, D. Dugas, K. Chu, K. Nichols, K. G. Duh, J. Fisher, L. MtPleasant, D. Xu, L. Gunter, A. Vera, R. Lender, and D. Meharry, "Progress in GaAs metamorphic HEMT technology for microwave applications," *GaAs Ic Symposium - 25th Annual Technical Digest 2003,* pp. 21-24, 2003.

[36] C. R. Chitambar, "Medical applications and toxicities of gallium compounds," *International Journal of Environmental Research and Public Health,* vol. 7, pp. 2337-2361, 2010.

[37] D. R. Webb, S. E. Wilson, and D. E. Carter, "Comparative pulmonary toxicity of gallium arsenide, gallium(III) oxide, or arsenic(III) oxide intratracheally instilled into rats," *Toxicology and Applied Pharmacology,* vol. 82, pp. 405-416, 1986.

[38] M. M. Hart and R. H. Adamson, "Antitumor activity and toxicity of salts of inorganic group IIIa metals: aluminum, gallium, indium, and thallium," *Proceedings of the National Academy of Sciences,* vol. 68, pp. 1623-1626, 1971.

[39] H. P. Maruska and J. J. Tietjen, "Preparation and properties of vapor-deposited single-crystalline GaN," *Applied Physics Letters,* vol. 15, pp. 327-329, 1969.

[40] S. Nakamura and M. R. Krames, "History of gallium-nitride based light-emitting diodes for illumination," *Proceedings of the IEEE,* vol. 101, pp. 2211-2220, 2013.

[41] S. Yoshida, S. Misawa, and S. Gonda, "Improvements on the electrical and luminescent properties of reactive molecular-beam epitaxially grown GaN films by using AlN coated sapphire substrates," *Applied Physics Letters,* vol. 42, pp. 427-429, 1983.

[42] T. Detchprohm, K. Hiramatsu, H. Amano, and I. Akasaki, "Hydride vapor phase epitaxial growth of a high quality GaN film using a ZnO buffer layer," *Applied Physics Letters,* vol. 61, pp. 2688-2690, 1992.

[43] A. Able, W. Wegscheider, K. Engl, and J. Zweck, "Growth of crack-free GaN on Si(111) with graded AlGaN buffer layers," *Journal of Crystal Growth,* vol. 276, pp. 415-418, 2005.

[44] J. H. Boo, C. Rohr, and W. Ho, "MOCVD of BN and GaN thin films on silicon: new attempt of GaN growth with BN buffer layer," *Journal of Crystal Growth,* vol. 189, pp. 439-444, 1998.

[45] S. Nakamura, "GaN growth using GaN buffer layer," *Japanese Journal of Applied Physics Part 2-Letters,* vol. 30, pp. L1705-L1707, 1991.

[46] S. J. Pearton, *GaN and Related Materials,* vol. 1, CRC Press, 1997.

[47] H. Morkoc, *Handbook of Nitride Semiconductors and Devices, Material Properties, Physics and Growth* vol. 1. Weinheim: John Wiley & Sons, 2009.

[48] G. Mula, C. Adelmann, S. Moehl, J. Oullier, and B. Daudin, "Surfactant effect of gallium during molecular-beam epitaxy of GaN on AlN (0001)," *Physical Review B,* vol. 64, 2001.

[49] T. Sasaki and T. Matsuoka, "Substrate polarity dependence of metal-organic vapor-phase epitaxy-grown GaN on SiC," *Journal of Applied Physics,* vol. 64, pp. 4531-4535, 1988.

[50] X. Gu, M. A. Reshchikov, A. Teke, D. Johnstone, H. Morkoc, B. Nemeth, and J. Nause, "GaN epitaxy on thermally treated c-plane bulk ZnO substrates with O and Zn faces," *Applied Physics Letters,* vol. 84, pp. 2268-2270, 2004.

[51] T. Katase, K. Nomura, H. Ohta, H. Yanagi, T. Kamiya, M. Hirano, and H. Hosono, "Large domain growth of GaN epitaxial films on lattice-matched buffer layer $ScAlMgO_4$," *Materials Science and Engineering B-Advanced Functional Solid-State Materials,* vol. 161, pp. 66-70, 2009.

[52] K. Xu, J. Xu, P. Z. Deng, R. S. Qiu, and Z. J. Fang, "MOCVD growth of GaN on $LiAlO_2$(100) substrates," *Physica Status Solidi a-Applied Research,* vol. 176, pp. 589-593, 1999.

[53] W. A. Doolittle, S. Kang, T. J. Kropewnicki, S. Stock, P. A. Kohl, and A. S. Brown, "MBE growth of high quality GaN on $LiGaO_2$," *Journal of Electronic Materials,* vol. 27, pp. L58-L60, 1998.

[54] A. Dadgar, J. Blasing, A. Diez, A. Alam, M. Heuken, and A. Krost, "Metalorganic chemical vapor phase epitaxy of crack-free GaN on Si (111) exceeding 1 um in thickness," *Japanese Journal of Applied Physics Part 2-Letters,* vol. 39, pp. L1183-L1185, 2000.

[55] H. Okumura, S. Misawa, and S. Yoshida, "Epitaxial growth of cubic and hexagonal GaN on GaAs by gas-source molecular-beam epitaxy," *Applied Physics Letters,* vol. 59, pp. 1058-1060, 1991.

[56] R. Suzuki, A. Kawaharazuka, and Y. Horikoshi, "MBE growth of GaN on MgO substrate," *Journal of Crystal Growth,* vol. 301, pp. 478-481, 2007.

[57] R. S. Pengelly, S. M. Wood, J. W. Milligan, S. T. Sheppard, and W. L. Pribble, "A review of GaN on SiC high electron-mobility power transistors and MMICs," *IEEE Transactions on Microwave Theory and Techniques,* vol. 60, pp. 1764-1783, 2012.

[58] A. Usui, H. Sunakawa, A. Sakai, and A. A. Yamaguchi, "Thick GaN epitaxial growth with low dislocation density by hydride vapor phase epitaxy," *Japanese Journal of Applied Physics Part 2-Letters,* vol. 36, pp. L899-L902, 1997.

[59] T. Paskova, D. A. Hanser, and K. R. Evans, "GaN substrates for III-Nitride devices," *Proceedings of the IEEE,* vol. 98, pp. 1324-1338, 2010.

[60] S. Zembutsu and T. Sasaki, "Growth of GaN single crystal films using electron-cyclotron resonance plasma excited metalorganic vapor-phase epitaxy," *Applied Physics Letters,* vol. 48, pp. 870-872, 1986.

[61] E. J. Tarsa, B. Heying, X. H. Wu, P. Fini, S. P. DenBaars, and J. S. Speck, "Homoepitaxial growth of GaN under Ga-stable and N-stable conditions by plasma-assisted molecular beam epitaxy," *Journal of Applied Physics,* vol. 82, pp. 5472-5479, 1997.

[62] T. Hashimoto, F. Wu, J. S. Speck, and S. Nakamura, "A GaN bulk crystal with improved structural quality grown by the ammonothermal method," *Nature Materials,* vol. 6, pp. 568-571, 2007.

[63] T. Paskova and K. R. Evans, "GaN Substrates: Progress, Status, and Prospects," *Selected Topics in Quantum Electronics, IEEE Journal of,* vol. 15, pp. 1041-1052, 2009.

[64] O. H. Nam, M. D. Bremser, B. L. Ward, R. J. Nemanich, and R. F. Davis, "Growth of GaN and $Al_{0.2}Ga_{0.8}N$ on patterened substrates via organometallic vapor phase epitaxy," *Japanese Journal of Applied Physics Part 2-Letters & Express Letters,* vol. 36, pp. L532-L535, 1997.

[65] L. Jastrzebski, "SOI by CVD - epitaxial lateral overgrowth (ELO) process - review," *Journal of Crystal Growth,* vol. 63, pp. 493-526, 1983.

[66] R. P. Gale, R. W. Mcclelland, J. C. C. Fan, and C. O. Bozler, "Lateral epitaxial overgrowth of GaAs by organo-metallic chemical vapor-deposition," *Applied Physics Letters,* vol. 41, pp. 545-547, 1982.

[67] P. Vohl, C. O. Bozler, R. W. Mcclelland, A. Chu, and A. J. Strauss, "Lateral growth of single-crystal InP over dielectric films by orientation-dependent VPE," *Journal of Crystal Growth,* vol. 56, pp. 410-422, 1982.

[68] P. Gibart, "Metal organic vapour phase epitaxy of GaN and lateral overgrowth," *Reports on Progress in Physics,* vol. 67, pp. 667-715, 2004.

[69] O. H. Nam, M. D. Bremser, T. S. Zheleva, and R. F. Davis, "Lateral epitaxy of low defect density GaN layers via organometallic vapor phase epitaxy," *Applied Physics Letters,* vol. 71, pp. 2638-2640, 1997.

[70] K. Hiramatsu, K. Nishiyama, M. Onishi, H. Mizutani, M. Narukawa, A. Motogaito, H. Miyake, Y. Iyechika, and T. Maeda, "Fabrication and characterization of low defect density GaN using facet-controlled epitaxial lateral overgrowth (FACELO)," *Journal of Crystal Growth,* vol. 221, pp. 316-326, 2000.

[71] M. K. Kelly, R. P. Vaudo, V. M. Phanse, L. Gorgens, O. Ambacher, and M. Stutzmann, "Large free-standing GaN substrates by hydride vapor phase epitaxy and laser-induced liftoff," *Japanese Journal of Applied Physics Part 2-Letters,* vol. 38, pp. L217-L219, 1999.

[72] M. K. Kelly, O. Ambacher, B. Dahlheimer, G. Groos, R. Dimitrov, H. Angerer, and M. Stutzmann, "Optical patterning of GaN films," *Applied Physics Letters,* vol. 69, pp. 1749-1751, 1996.

[73] L. Liu and J. H. Edgar, "Substrates for gallium nitride epitaxy," *Materials Science & Engineering R-Reports,* vol. 37, pp. 61-127, 2002.

[74] S. Kang, B. K. Kang, S. W. Kim, and D. H. Yoon, "Growth and characteristics of zinc-blende and wurtzite GaN junctioned branch nanostructures," *Crystal Growth & Design,* vol. 10, pp. 2581-2584, 2010.

[75] S. Nakamura, "Current status of GaN-based solid-state lighting," *MRS bulletin,* vol. 34, p. 101, 2009.

[76] H. Amano, M. Kito, K. Hiramatsu, and I. Akasaki, "P-Type conduction in Mg-doped GaN treated with low-energy electron-beam irradiation (LEEBI)," *Japanese Journal of Applied Physics Part 2-Letters,* vol. 28, pp. L2112-L2114, 1989.

[77] T. Paskova, "Development and prospects of nitride materials and devices with nonpolar surfaces," *Physica Status Solidi B-Basic Solid State Physics,* vol. 245, pp. 1011-1025, 2008.

[78] J. L. Weyher, "Characterization of wide-band-gap semiconductors (GaN, SiC) by defect-selective etching and complementary methods," *Superlattices and Microstructures,* vol. 40, pp. 279-288, 2006.

[79] B. A. Haskell, F. Wu, S. Matsuda, M. D. Craven, P. T. Fini, S. P. DenBaars, J. S. Speck, and S. Nakamura, "Structural and morphological characteristics of planar (11-20) a-plane gallium nitride grown by hydride vapor phase epitaxy," *Applied Physics Letters,* vol. 83, pp. 1554-1556, 2003.

[80] T. Paskova, P. P. Paskov, E. Valcheva, V. Darakchieva, J. Birch, A. Kasic, B. Arnaudov, S. Tungasmita, and B. Monemar, "Polar and nonpolar GaN grown by HVPE: Preferable substrates for nitride-based emitting devices," *Physica Status Solidi a-Applied Research,* vol. 201, pp. 2265-2270, 2004.

[81] H. C. Hsu, Y. K. Su, S. H. Cheng, S. J. Huang, J. M. Cao, and K. C. Chen, "Investigation of etch characteristics of non-polar GaN by wet chemical etching," *Applied Surface Science,* vol. 257, pp. 1080-1083, 2010.

[82] R. Kröger, "Defects and Interfacial Structure of a-plane GaN on r-plane Sapphire," in *Nitrides with Nonpolar Surfaces,* ed: Wiley-VCH Verlag GmbH & Co., pp. 287-318, 2008.

[83] J. M. Lee, C. Huh, D. J. Kim, and S. J. Park, "Dry-etch damage and its recovery in InGaN/GaN multi-quantum-well light-emitting diodes," *Semiconductor Science and Technology*, vol. 18, pp. 530-534, 2003.

[84] M. S. Abrahams and C. J. Buiocchi, "Etching of dislocations on low-index faces of GaAs," *Journal of Applied Physics*, vol. 36, p. 2855, 1965.

[85] Y. Jung, J. Ahn, K. H. Baik, D. Kim, S. J. Pearton, F. Ren, and J. Kim, "Chemical etch characteristics of N-Face and Ga-Face GaN by phosphoric acid and potassium hydroxide solutions," *Journal of the Electrochemical Society*, vol. 159, pp. H117-H120, 2012.

[86] H. Y. Kim, Y. Jung, S. H. Kim, J. Ahn, M. A. Mastro, J. K. Hite, C. R. Eddy, and J. Kim, "Wet etching of non-polar gallium nitride light-emitting diode structure for enhanced light extraction," *Journal of Crystal Growth*, vol. 326, pp. 65-68, 2011.

[87] T. Kozawa, T. Kachi, T. Ohwaki, Y. Taga, N. Koide, and M. Koike, "Dislocation etch pits in GaN epitaxial layers grown on sapphire substrates," *Journal of the Electrochemical Society*, vol. 143, pp. L17-L19, 1996.

[88] Y. Jung, K. H. Baik, F. Ren, S. J. Pearton, and J. Kim, "Effects of photoelectrochemical etching of N-polar and Ga-polar gallium nitride on sapphire substrates," *Journal of The Electrochemical Society*, vol. 157, pp. H676-H678, 2010.

[89] Y. Jung, J. Kim, S. Jang, K. H. Baik, Y. G. Seo, and S. M. Hwang, "Enhanced light extraction of nonpolar a-plane (11-20) GaN light emitting diodes on sapphire substrates by photo-enhanced chemical wet etching," *Optics Express*, vol. 18, pp. 9728-9732, 2010.

[90] S. R. Lunt, G. N. Ryba, P. G. Santangelo, and N. S. Lewis, "Chemical studies of the passivation of GaAs surface recombination using sulfides and thiols," *Journal of Applied Physics*, vol. 70, pp. 7449-7467, 1991.

[91] P. Frajtag, A. M. Hosalli, J. P. Samberg, P. C. Colter, T. Paskova, N. A. El-Masry, and S. M. Bedair, "Overgrowth of GaN on GaN nanowires produced by mask-less etching," *Journal of Crystal Growth*, vol. 352, pp. 203-208, 2012.

[92] I. Dziecielewski, J. L. Weyher, and W. Dzwolak, "On the hydrophobicity of modified Ga-polar GaN surfaces," *Applied Physics Letters*, vol. 102, 2013.

[93] S.-P. Chang, Y.-C. Chen, J.-K. Huang, Y.-J. Cheng, J.-R. Chang, K.-P. Sou, Y.-T. Kang, H.-C. Yang, T.-C. Hsu, H.-C. Kuo, and C.-Y. Chang, "Electrically driven nanopyramid green light emitting diode," *Applied Physics Letters,* vol. 100, p. 061106, 2012.

[94] J. Sim, K. Kim, S. Song, and J. Kim, "Suspended GaN nanowires as NO_2 sensor for high temperature applications," *Analyst,* vol. 138, pp. 2432-2437, 2013.

[95] V. Dobrokhotov, D. N. McIlroy, M. G. Norton, A. Abuzir, W. J. Yeh, I. Stevenson, R. Pouy, J. Bochenek, M. Cartwright, L. Wang, J. Dawson, M. Beaux, and C. Berven, "Principles and mechanisms of gas sensing by GaN nanowires functionalized with gold nanoparticles," *Journal of Applied Physics,* vol. 99, p. 104302, 2006.

[96] M. L. Huang, Y. C. Chang, C. H. Chang, Y. J. Lee, P. Chang, J. Kwo, T. B. Wu, and M. Hong, "Surface passivation of III-V compound semiconductors using atomic-layer-deposition-grown Al_2O_3," *Applied Physics Letters,* vol. 87, pp. 252104, 2005.

[97] F. Bechstedt, *Principles of Surface Physics*: Springer, 2003.

[98] P. J. Eng, T. P. Trainor, G. E. Brown Jr, G. A. Waychunas, M. Newville, S. R. Sutton, and M. L. Rivers, "Structure of the Hydrated α-Al_2O_3 (0001) Surface," *Science,* vol. 288, pp. 1029-1033, 2000.

[99] S. Tomoya, S. Hisao, H. Maosheng, N. Yoshiki, K. Satoshi, T. Satoru, Y. Kenji, N. Katsushi, T. R. Linda, and S. Shiro, "Direct evidence that dislocations are non-radiative recombination centers in GaN," *Japanese Journal of Applied Physics,* vol. 37, p. L398, 1998.

[100] J. S. Kim, M. Granström, R. H. Friend, N. Johansson, W. R. Salaneck, R. Daik, W. J. Feast, and F. Cacialli, "Indium–tin oxide treatments for single- and double-layer polymeric light-emitting diodes: The relation between the anode physical, chemical, and morphological properties and the device performance," *Journal of Applied Physics,* vol. 84, pp. 6859-6870, 1998.

[101] C. J. Sandroff, R. N. Nottenburg, J. C. Bischoff, and R. Bhat, "Dramatic enhancement in the gain of a GaAs/AlGaAs heterostructure bipolar transistor by surface chemical passivation," *Applied Physics Letters,* vol. 51, pp. 33-35, 1987.

[102] F. Steuber, J. Staudigel, M. Stössel, J. Simmerer, and A. Winnacker, "Reduced operating voltage of organic electroluminescent devices by plasma treatment of the indium tin oxide anode," *Applied Physics Letters,* vol. 74, pp. 3558-3560, 1999.

[103] P. J. Hotchkiss, M. Malicki, A. J. Giordano, N. R. Armstrong, and S. R. Marder, "Characterization of phosphonic acid binding to zinc oxide," *Journal of Materials Chemistry,* vol. 21, pp. 3107-3112, 2011.

[104] C. P. Cho, C. C. Chu, W. T. Chen, T. C. Huang, and Y. T. Tao, "Molecular modification on dye-sensitized solar cells by phosphonate self-assembled monolayers," *Journal of Materials Chemistry,* vol. 22, pp. 2915-2921, 2012.

[105] S. R. Lunt, P. G. Santangelo, and N. S. Lewis, "Passivation of GaAs surface recombination with organic thiols," *Journal of Vacuum Science & Technology B,* vol. 9, pp. 2333-2336, 1991.

[106] K. Adlkofer and M. Tanaka, "Stable surface coating of gallium arsenide with octadecylthiol monolayers," *Langmuir,* vol. 17, pp. 4267-4273, 2001.

[107] C. D. Bain, "A new class of self-assembled monolayers: Organic thiols on gallium arsenide," *Advanced Materials,* vol. 4, pp. 591-594, 1992.

[108] C. W. Sheen, J. X. Shi, J. Maartensson, A. N. Parikh, and D. L. Allara, "A new class of organized self-assembled monolayers: alkane thiols on gallium arsenide(100)," *Journal of the American Chemical Society,* vol. 114, pp. 1514-1515, 1992.

[109] V. M. Bermudez, "Adsorption of 1-octanethiol on the GaN(0001) surface," *Langmuir,* vol. 19, pp. 6813-6819, 2003.

[110] L. F. Prescott, G. R. Sutherland, J. Park, I. J. Smith, and A. T. Proudfoot, "Cysteamine, methionine, and penicillamine in the treatment of paracetamol poisoning," *The Lancet,* vol. 308, pp. 109-113, 1976.

[111] W. A. Gahl, G. F. Reed, J. G. Thoene, J. D. Schulman, W. B. Rizzo, A. J. Jonas, D. W. Denman, J. J. Schlesselman, B. J. Corden, and J. A. Schneider, "Cysteamine therapy for children with nephropathic cystinosis," *New England Journal of Medicine,* vol. 316, pp. 971-977, 1987.

[112] M. Losurdo, P. C. Wu, T.-H. Kim, G. Bruno, and A. S. Brown, "Cysteamine-based functionalization of InAs surfaces: Revealing the critical role of oxide interactions in biasing attachment," *Langmuir,* vol. 28, pp. 1235-1245, 2011.

[113] X. Ding, K. Moumanis, J. J. Dubowski, L. Tay, and N. L. Rowell, "Fourier-transform infrared and photoluminescence spectroscopies of self-assembled monolayers of long-chain thiols on (001) GaAs," *Journal of Applied Physics,* vol. 99, p. 054701, 2006.

[114] R. Stine and D. Y. Petrovykh, "Oriented self-assembled monolayers of bifunctional molecules on InAs," *Journal of Electron Spectroscopy and Related Phenomena,* vol. 172, pp. 42-46, 2009.

[115] I. Willner, E. Katz, and V. Yissar, "Biosensor and method comprising enzymes immobilized on semiconductors," ed: Google Patents, 2006.

[116] R. Munday, "Toxicity of thiols and disulphides: Involvement of free-radical species," *Free Radical Biology and Medicine,* vol. 7, pp. 659-673, 1989.

[117] J. Lovrić, H. Bazzi, Y. Cuie, G. A. Fortin, F. Winnik, and D. Maysinger, "Differences in subcellular distribution and toxicity of green and red emitting CdTe quantum dots," *Journal of Molecular Medicine,* vol. 83, pp. 377-385, 2005.

[118] Suryajaya, A. V. Nabok, A. K. Hassan, and A. Tsargorodskaya, "Characterization of CdS and ZnS nanoparticle semiconductors: For optoelectronics application," *Jurnal Fisika dan Aplikasinya,* vol. 7, pp. 110107-1-8, 2011.

[119] C. Qifan, Y. Dongzhi, and X. Shukun, "Conjugations between cysteamine-stabilized CdTe quantum dots and single stranded DNA," *Analytical Letters,* vol. 41, pp. 1964-1974, 2008.

[120] A. O. Choi, S. J. Cho, J. Desbarats, J. Lovrić, and D. Maysinger, "Quantum dot-induced cell death involves Fas upregulation and lipid peroxidation in human neuroblastoma cells," *Journal of Nanobiotechnology,* vol. 5, 2007.

[121] A. Hoshino, K. Fujioka, T. Oku, M. Suga, Y. F. Sasaki, T. Ohta, M. Yasuhara, K. Suzuki, and K. Yamamoto, "Physicochemical properties and cellular toxicity of nanocrystal quantum dots depend on their surface modification," *Nano Letters,* vol. 4, pp. 2163-2169, 2004.

[122] S. J. Cho, D. Maysinger, M. Jain, B. Röder, S. Hackbarth, and F. M. Winnik, "Long-term exposure to CdTe quantum dots causes functional impairments in live cells," *Langmuir,* vol. 23, pp. 1974-1980, 2007.

[123] M. Textor, L. Ruiz, R. Hofer, A. Rossi, K. Feldman, G. Hähner, and N. D. Spencer, "Structural chemistry of self-assembled monolayers of octadecylphosphoric acid on tantalum oxide surfaces," *Langmuir,* vol. 16, pp. 3257-3271, 2000.

[124] M. Dubey, T. Weidner, L. J. Gamble, and D. G. Castner, "Structure and order of phosphonic acid-based self-assembled monolayers on Si(100)," *Langmuir,* vol. 26, pp. 14747-14754, 2010.

[125] S. A. Paniagua, P. J. Hotchkiss, S. C. Jones, S. R. Marder, A. Mudalige, F. S. Marrikar, J. E. Pemberton, and N. R. Armstrong, "Phosphonic acid modification of indium-tin oxide electrodes: Combined XPS/UPS/contact angle studies," *Journal of Physical Chemistry C,* vol. 112, pp. 7809-7817, 2008.

[126] R. Maoz and J. Sagiv, "On the formation and structure of self-assembling monolayers. I. A comparative atr-wettability study of Langmuir—Blodgett and adsorbed films on flat substrates and glass microbeads," *Journal of Colloid and Interface Science,* vol. 100, pp. 465-496, 1984.

[127] R. Artzi, S. S. Daube, H. Cohen, and R. Naaman, "Adsorption of organic phosphate as a means to bind biological molecules to GaAs surfaces," *Langmuir,* vol. 19, pp. 7392-7398, 2003.

[128] W. C. Hughes, S. E. Koh, B. H. Augustine, and J. M. Polefrone, "Self-assembly of phosphonate monolayers on GaAs and GaN," *Proceedings of the Electrochemical Society,* vol. 2001, pp. 213-217, 2001.

[129] H. Kim, P. E. Colavita, P. Paoprasert, P. Gopalan, T. F. Kuech, and R. J. Hamers, "Grafting of molecular layers to oxidized gallium nitride surfaces via phosphonic acid linkages," *Surface Science,* vol. 602, pp. 2382-2388, 2008.

[130] T. Ito, S. M. Forman, C. Cao, F. Li, C. R. Eddy, M. A. Mastro, R. T. Holm, R. L. Henry, K. L. Hohn, and J. H. Edgar, "Self-assembled monolayers of alkylphosphonic acid on GaN substrates," *Langmuir,* vol. 24, pp. 6630-6635, 2008.

[131] B. S. Simpkins, S. Hong, R. Stine, A. J. Makinen, N. D. Theodore, M. A. Mastro, C. R. Eddy, and P. E. Pehrsson, "Assembly of phosphonic acids on GaN and AlGaN," *Journal of Physics D-Applied Physics,* vol. 43, 2010.

[132] F. Li, E. Shishkin, M. A. Mastro, J. K. Hite, C. R. Eddy, J. H. Edgar, and T. Ito, "Photopolymerization of self-assembled monolayers of diacetylenic alkylphosphonic acids on group-III nitride substrates," *Langmuir,* vol. 26, pp. 10725-10730, 2010.

[133] T. Ito, S. M. Forman, C. Cao, C. R. Eddy, M. A. Mastro, R. T. Holm, R. L. Henry, K. Hohn, and J. H. Edgar, "Monolayer formation on GaN surface via self-assembly," *State-of-the-Art Program on Compound Semiconductors 53,* vol. 11, pp. 97-101, 2007.

[134] L.-H. Peng, C.-H. Liao, Y.-C. Hsu, C.-S. Jong, C.-N. Huang, J.-K. Ho, C.-C. Chiu, and C.-Y. Chen, "Photoenhanced wet oxidation of gallium nitride," *Applied Physics Letters,* vol. 76, pp. 511-513, 2000.

[135] A. Zaouk, E. Salvetat, J. Sakaya, F. Maury, and G. Constant, "Various chemical mechanisms for the crystal growth of III–V semiconductors using coordination compounds as starting material in the MOCVD process," *Journal of Crystal Growth,* vol. 55, pp. 135-144, 1981.

[136] C. R. Company. *CRC Handbook of Chemistry and Physics (95 ed.),* 2014.

[137] C. M. Foster, R. Collazo, Z. Sitar, and A. Ivanisevic, "Aqueous stability of Ga- and N-polar gallium nitride," *Langmuir,* vol. 29, pp. 216-220, 2013.

[138] M. R. Lorenz, G. D. Pettit, and R. C. Taylor, "Band gap of gallium phosphide from 0 to 900˚K and light emission from diodes at high temperatures," *Physical Review,* vol. 171, pp. 876-881, 1968.

[139] N. Takeno, "Atlas of Eh-pH diagrams: Intercomparison of thermodynamic databases," R. C. f. D. G. Environments, Ed., ed. Japan: National Institute of Advanced Industrial Science and Technology, 2005.

[140] H. Hertz, "Ueber einen Einfluss des ultravioletten Lichtes auf die electrische Entladung," *Annalen der Physik,* vol. 267, pp. 983-1000, 1887.

[141] J. G. Jenkin, R. C. G. Leckey, and J. Liesegang, "The development of x-ray photoelectron spectroscopy: 1900–1960," *Journal of Electron Spectroscopy and Related Phenomena,* vol. 12, pp. 1-35, 1977.

[142] J. F. Watts and J. Wolstenholme, *An Introduction to Surface Analysis by XPS and AES*. West Sussex: John Wiley & Sons, 2003.

[143] A. Jablonski and C. J. Powell, "The electron attenuation length revisited," *Surface Science Reports,* vol. 47, pp. 33-91, 2002.

[144] N. Fairley, "Casa XPS," 2.3.16 PR ed: Casa Software Ltd, 2009.

[145] B. V. Crist, "A review of XPS data-banks," *XPS Reports,* vol. 1, pp. 1-52, 2007.

[146] J. Choi and E. G. Gillan, "Low-temperature solvothermal synthesis of nanocrystalline indium nitride and Ga-In-N composites from the decomposition of metal azides," *Journal of Materials Chemistry,* vol. 16, pp. 3774-3784, 2006.

[147] S. H. Lee, J. H. Boo, S. Y. Lee, S. H. Yoo, C. G. Kim, Y. K. Lee, and Y. Kim, "Growth of single crystalline GaN thin films on Si(111) substrates by high vacuum metalorganic chemical vapor deposition using a single molecular precursor," *Journal of Vacuum Science & Technology B,* vol. 22, pp. 2144-2148, 2004.

[148] G. D. Gilliland, "Photoluminescence spectroscopy of crystalline semiconductors," *Materials Science and Engineering: R: Reports,* vol. 18, pp. 99-399, 1997.

[149] K. K. Smith, "Photoluminescence of semiconductor materials," *Thin Solid Films,* vol. 84, pp. 171-182, 1981.

[150] M. A. Reshchikov and H. Morkoç, "Luminescence properties of defects in GaN," *Journal of Applied Physics,* vol. 97, p. 061301, 2005.

[151] S. Allen, X. Chen, J. Davies, M. C. Davies, A. C. Dawkes, J. C. Edwards, C. J. Roberts, J. Sefton, S. J. B. Tendler, and P. M. Williams, "Detection of antigen−antibody binding events with the atomic force microscope," *Biochemistry,* vol. 36, pp. 7457-7463, 1997.

[152] S. J. Wilkins, T. Paskova, and A. Ivanisevic, "Effect of etching with cysteamine assisted phosphoric acid on gallium nitride surface oxide formation," *Journal of Applied Physics,* vol. 114, p. 064907, 2013.

[153] D. N. Richards, D. Y. Zemlyanov, and A. Ivanisevic, "Kelvin probe force microscopy analysis of the covalent functionalization and DNA modification of gallium phosphide nanorods," *The Journal of Physical Chemistry C,* vol. 116, pp. 12613-12620, 2012.

[154] U. Hartmann, "Magnetic force microscopy," *Annual Review of Materials Science,* vol. 29, pp. 53-87, 1999.

[155] A. Noy, D. V. Vezenov, and C. M. Lieber, "Chemical force microscopy," *Annual Review of Materials Science,* vol. 27, pp. 381-421, 1997.

[156] F. J. Giessibl, "Advances in atomic force microscopy," *Reviews of Modern Physics,* vol. 75, pp. 949-983, 2003.

[157] G. Binnig, C. F. Quate, and C. Gerber, "Atomic Force Microscope," *Physical Review Letters,* vol. 56, pp. 930-933, 1986.

[158] S. Morita, R. Wiesendanger, and E. Meyer, *Noncontact Atomic Force MIcroscopy*. Berlin: Springer, 2002.

[159] M. Nonnenmacher, M. P. O'Boyle, and H. K. Wickramasinghe, "Kelvin probe force microscopy," *Applied Physics Letters,* vol. 58, pp. 2921-2923, 1991.

[160] O. A. Semenikhin, L. Jiang, T. Iyoda, K. Hashimoto, and A. Fujishima, "A Kelvin probe force microscopic study of the local dopant distribution in conducting polybithiophene," *Electrochimica Acta,* vol. 42, pp. 3321-3326, 1997.

[161] D. Fuertes Marrón, S. Sadewasser, A. Meeder, T. Glatzel, and M. C. Lux-Steiner, "Electrical activity at grain boundaries of Cu(In, Ga)Se_2 thin films," *Physical Review B,* vol. 71, p. 033306, 2005.

[162] P. Schmutz and G. S. Frankel, "Corrosion study of AA2024-T3 by scanning kelvin probe force microscopy and in situ atomic force microscopy scratching," *Journal of the Electrochemical Society,* vol. 145, pp. 2295-2306, 1998.

[163] R. S. Houk, V. A. Fassel, G. D. Flesch, H. J. Svec, A. L. Gray, and C. E. Taylor, "Inductively coupled argon plasma as an ion-source for mass-spectrometric determination of trace-elements," *Analytical Chemistry,* vol. 52, pp. 2283-2289, 1980.

[164] R. S. Houk and J. J. Thompson, "Inductively coupled plasma mass spectrometry," *Mass Spectrometry Reviews,* vol. 7, pp. 425-461, 1988.

[165] J. W. Olesik, "Elemental analysis using ICP-OES and ICP/MS," *Analytical Chemistry,* vol. 63, pp. 12A-21A, 1991.

[166] S. A. Smith, C. A. Wolden, M. D. Bremser, A. D. Hanser, R. F. Davis, and W. V. Lampert, "High rate and selective etching of GaN, AlGaN, and AlN using an inductively coupled plasma," *Applied Physics Letters,* vol. 71, pp. 3631-3633, 1997.

[167] D. Richards, P. Luce, D. Zemlyanov, and A. Ivanisevic, "Quantitative analysis of the functionalization of gallium phosphide with organic azides," *Scanning,* vol. 34, pp. 332-340, 2012.

[168] M. Miwa, A. Nakajima, A. Fujishima, K. Hashimoto, and T. Watanabe, "Effects of the surface roughness on sliding angles of water droplets on superhydrophobic surfaces," *Langmuir,* vol. 16, pp. 5754-5760, 2000.

[169] M. Rein, "Phenomena of liquid drop impact on solid and liquid surfaces," *Fluid Dynamics Research,* vol. 12, pp. 61-93, 1993.

[170] E. B. Dussan, "On the spreading of liquids on solid surfaces: Static and dynamic contact lines," *Annual Review of Fluid Mechanics,* vol. 11, pp. 371-400, 1979.

[171] A. P. Zhang, F. Ren, T. J. Anderson, C. R. Abernathy, R. K. Singh, P. H. Holloway, S. J. Pearton, and D. Palmer, "High-power GaN electronic devices," *Critical Reviews in Solid State and Materials Sciences,* vol. 27, pp. 1-71, 2002.

[172] C. Arisio, C. A. Cassou, and M. Lieberman, "Loss of siloxane monolayers from GaN surfaces in water," *Langmuir,* vol. 29, pp. 5145-5149, 2013.

[173] C. R. Chen, Y. C. Li, and T. H. Young, "Gallium nitride induces neuronal differentiation markers in neural stem/precursor cells derived from rat cerebral cortex," *Acta Biomaterialia,* vol. 5, pp. 2610-2617, 2009.

[174] L. Sugiura, "Dislocation motion in GaN light-emitting devices and its effect on device lifetime," *Journal of Applied Physics,* vol. 81, pp. 1633-1638, 1997.

[175] M. McLaurin, T. E. Mates, F. Wu, and J. S. Speck, "Growth of p-type and n-type m-plane GaN by molecular beam epitaxy," *Journal of Applied Physics,* vol. 100, p. 063707, 2006.

[176] E. T. Yu, X. Z. Dang, P. M. Asbeck, S. S. Lau, and G. J. Sullivan, "Spontaneous and piezoelectric polarization effects in III-V nitride heterostructures," *Journal of Vacuum Science & Technology B,* vol. 17, pp. 1742-1749, 1999.

[177] K. M. Song and H. Kim, "A comparative study on the optical and electrical properties of Si-doped polar and nonpolar GaN," *Japanese Journal of Applied Physics,* vol. 51, p. 051002, 2012.

[178] J. Neugebauer and C. G. Vandewalle, "Hydrogen in GaN - Novel aspects of a common impurity," *Physical Review Letters,* vol. 75, pp. 4452-4455, 1995.

[179] M. Hofstetter, J. Howgate, M. Schmid, S. Schoell, M. Sachsenhauser, D. Adiguzel, M. Stutzmann, I. D. Sharp, and S. Thalhammer, "In vitro bio-functionality of gallium nitride sensors for radiation biophysics," *Biochemical and Biophysical Research Communications,* vol. 424, pp. 348-353, 2012.

[180] E. Richter, C. Hennig, U. Zeimer, L. Wang, M. Weyers, and G. Trankle, "N-type doping of HVPE-grown GaN using dichlorosilane," *Physica Status Solidi a-Applications and Materials Science,* vol. 203, pp. 1658-1662, 2006.

[181] M. S. Makowski, D. Y. Zemlyanov, J. A. Lindsey, J. C. Bernhard, E. M. Hagen, B. K. Chan, A. A. Petersohn, M. R. Medow, L. E. Wendel, D. F. Chen, J. M. Canter, and A. Ivanisevic, "Covalent attachment of a peptide to the surface of gallium nitride," *Surface Science,* vol. 605, pp. 1466-1475, 2011.

[182] D. Q. Fang, A. L. Rosa, T. Frauenheim, and R. Q. Zhang, "Band gap engineering of GaN nanowires by surface functionalization," *Applied Physics Letters,* vol. 94, p. 073116, 2009.

[183] M. N. Ismail, T. L. Goodrich, Z. X. Ji, K. S. Ziemer, J. Warzywoda, and A. Sacco, "Assembly of titanosilicate ETS-10 crystals on organosilane-functionalized gallium nitride surfaces," *Microporous and Mesoporous Materials,* vol. 118, pp. 245-250, 2009.

[184] G. G. C. Arizaga, M. J. Oviedo, and O. E. C. Lopez, "Electrical properties of polycrystalline GaN films functionalized with cysteine and stabilization of GaN nanoparticles in aqueous media," *Colloids and Surfaces B-Biointerfaces,* vol. 98, pp. 63-71, 2012.

[185] Y. B. Pan, Z. J. Yang, Z. T. Chen, Y. Lu, T. J. Yu, X. D. Hu, K. Xu, and G. Y. Zhang, "Reduction of threading edge dislocation density in n-type GaN by Si delta-doping," *Journal of Crystal Growth,* vol. 286, pp. 255-258, 2006.

[186] C. Lee, J. K. Hite, M. A. Mastro, J. A. Freitas, C. R. Eddy, H. Y. Kim, and J. Kim, "Selective chemical etch of gallium nitride by phosphoric acid," *Journal of Vacuum Science & Technology A,* vol. 30, p. 040602, 2012.

[187] S. L. Qi, Z. Z. Chen, H. Fang, Y. J. Sun, L. W. Sang, X. L. Yang, L. B. Zhao, P. F. Tian, J. J. Deng, Y. B. Tao, T. J. Yu, Z. X. Qin, and G. Y. Zhang, "Study on the formation of dodecagonal pyramid on nitrogen polar GaN surface etched by hot H_3PO_4," *Applied Physics Letters,* vol. 95, p. 071114, 2009.

[188] T. Hino, S. Tomiya, T. Miyajima, K. Yanashima, S. Hashimoto, and M. Ikeda, "Characterization of threading dislocations in GaN epitaxial layers," *Applied Physics Letters,* vol. 76, pp. 3421-3423, 2000.

[189] D. S. Li, M. Sumiya, S. Fuke, D. R. Yang, D. L. Que, Y. Suzuki, and Y. Fukuda, "Selective etching of GaN polar surface in potassium hydroxide solution studied by x-ray photoelectron spectroscopy," *Journal of Applied Physics,* vol. 90, pp. 4219-4223, 2001.

[190] T. Paskova and K. R. Evans, "GaN substrates-progress, status, and prospects," *IEEE Journal of Selected Topics in Quantum Electronics,* vol. 15, pp. 1041-1052, 2009.

[191] B. R. Chakraborty, S. M. Shivaprasad, and D. N. Bose, "Study of oxygen plasma treated gan film using X-ray photoelectron spectroscopy (XPS) and secondary ion mass spectrometry (SIMS)," *Proceedings of the Eleventh International Workshop on the Physics of Semiconductor Devices, Vol 1 & 2*, vol. 4746, pp. 1010-1013, 2002.

[192] H. M. Ng, N. G. Weimann, and A. Chowdhury, "GaN nanotip pyramids formed by anisotropic etching," *Journal of Applied Physics*, vol. 94, pp. 650-653, 2003.

[193] Z. Chen, L. W. Su, J. Y. Shi, X. L. Wang, C. L. Tang, and P. Gao. (2012, June 2, 2013). *AFM Application in III-Nitride Materials and Devices* [Electronic].

[194] D. Y. Petrovykh, M. J. Yang, and L. J. Whitman, "Chemical and electronic properties of sulfur-passivated InAs surfaces," *Surface Science*, vol. 523, pp. 231-240, 2003.

[195] J. L. Weyher, S. Lazar, L. Macht, Z. Liliental-Weber, R. J. Molnar, S. Muller, V. G. M. Sivel, G. Nowak, and I. Grzegory, "Orthodox etching of HVPE-grown GaN," *Journal of Crystal Growth*, vol. 305, pp. 384-392, 2007.

[196] D. Richards, D. Zemlyanov, and A. Ivanisevic, "Assessment of the passivation capabilities of two different covalent chemical modifications on GaP(100)," *Langmuir*, vol. 26, pp. 8141-8146, 2010.

[197] J. W. J. Slavin, U. Jarori, D. Zemlyanov, and A. Ivanisevic, "Characterization of amino acid adlayers on InAs surfaces using X-ray photoelectron spectroscopy," *Journal of Electron Spectroscopy and Related Phenomena*, vol. 172, pp. 47-53, 2009.

[198] C. L. McGuiness, A. Shaporenko, C. K. Mars, S. Uppili, M. Zharnikov, and D. L. Allara, "Molecular self-assembly at bare semiconductor surfaces: Preparation and characterization of highly organized octadecanethiolate monolayers on GaAs(001)," *Journal of the American Chemical Society*, vol. 128, pp. 5231-5243, 2006.

[199] O. S. Nakagawa, S. Ashok, C. W. Sheen, J. Martensson, and D. L. Allara, "GaAs interfaces with octadecyl thiol self-assembled monolayer - structural and electrical-properties," *Japanese Journal of Applied Physics Part 1-Regular Papers Short Notes & Review Papers*, vol. 30, pp. 3759-3762, 1991.

[200] S. Evans, "Energy calibration secondary standards for X-ray photoelectron spectrometers," *Surface and Interface Analysis*, vol. 7, pp. 299-302, 1985.

[201] C. L. Hinkle, M. Milojevic, B. Brennan, A. M. Sonnet, F. S. Aguirre-Tostado, G. J. Hughes, E. M. Vogel, and R. M. Wallace, "Detection of Ga suboxides and their impact on III-V passivation and Fermi-level pinning," *Applied Physics Letters,* vol. 94, p. 162101, 2009.

[202] A. Sidorenko, H. Peisert, H. Neumann, and T. Chasse, "Substrate-dependent wetting layer formation during GaN growth: Impact on the morphology of the films," *Journal of Applied Physics,* vol. 102, p. 044907, 2007.

[203] H. P. Wampler, D. Y. Zemlyanov, K. Lee, D. B. Janes, and A. Ivanisevic, "Mixed adlayer of alkanethiol and peptide on GaAs(100): Quantitative characterization by X-ray photoelectron spectroscopy," *Langmuir,* vol. 24, pp. 3164-3170, 2008.

[204] P. A. Breeze, H. L. Hartnagel, and P. M. A. Sherwood, "An investigation of anodically grown films on GaAs using X-ray photoelectron spectroscopy," *Journal of the Electrochemical Society,* vol. 127, pp. 454-461, 1980.

[205] S. C. Ghosh, M. C. Biesinger, R. R. LaPierre, and P. Kruse, "The role of proximity caps during the annealing of UV-ozone oxidized GaAs," *Journal of Applied Physics,* vol. 101, p. 114321, 2007.

[206] N. J. Watkins, G. W. Wicks, and Y. L. Gao, "Oxidation study of GaN using x-ray photoemission spectroscopy," *Applied Physics Letters,* vol. 75, pp. 2602-2604, 1999.

[207] H. Iwasaki, Y. Mizokawa, R. Nishitani, and S. Nakamura, "X-ray photoemission study of the oxidation process at cleaved (110) surfaces of GaAs, GaP and InSb," *Japanese Journal of Applied Physics,* vol. 17, pp. 1925-1933, 1978.

[208] Y. C. Byun, C. Mahata, C. H. An, J. Oh, R. Choi, and H. Kim, "Interfacial and electrical properties of HfO_2 gate dielectrics grown on GaAs by atomic layer deposition using different oxidants," *Journal of Physics D-Applied Physics,* vol. 45, p. 435305, 2012.

[209] M. Wirde, U. Gelius, and L. Nyholm, "Self-assembled monolayers of cystamine and cysteamine on gold studied by XPS and voltammetry," *Langmuir,* vol. 15, pp. 6370-6378, 1999.

[210] M. W. Zhu, S. You, T. Detchprohm, T. Paskova, E. A. Preble, and C. Wetzel, "Various misfit dislocations in green and yellow GaInN/GaN light emitting diodes," *Physica Status Solidi a-Applications and Materials Science,* vol. 207, pp. 1305-1308, 2010.

[211] B. Monemar, P. P. Paskov, J. P. Bergman, A. A. Toropov, T. V. Shubina, T. Malinauskas, and A. Usui, "Recombination of free and bound excitons in GaN," *Physica Status Solidi B-Basic Solid State Physics,* vol. 245, pp. 1723-1740, 2008.

[212] T. Paskova, A. Hanser, E. Preble, K. Evans, R. Kroger, F. Tuomisto, R. Kersting, R. Alcorn, S. Ashley, C. Pagel, E. Valcheva, P. P. Paskov, and B. Monemar, "Defect and emission distributions in bulk GaN grown in polar and nonpolar directions: A comparative analysis," *Gallium Nitride Materials and Devices Iii,* vol. 6894, p. 68940D, 2008.

[213] A. H. Chin, T. S. Ahn, H. W. Li, S. Vaddiraju, C. J. Bardeen, C. Z. Ning, and M. K. Sunkara, "Photoluminescence of GaN nanowires of different crystallographic orientations," *Nano Letters,* vol. 7, pp. 626-631, 2007.

[214] D. B. Li, B. Ma, R. Miyagawa, W. G. Hu, M. Narukawa, H. Miyake, and K. Hiramatsu, "Photoluminescence study of Si-doped a-plane GaN grown by MOVPE," *Journal of Crystal Growth,* vol. 311, pp. 2906-2909, 2009.

[215] S. G. Jung, H. Jeon, G. S. Lee, S. M. Bae, K. H. Kim, S. N. Yi, M. Yang, H. S. Ahn, Y. M. Yu, S. W. Kim, S. H. Cheon, H. J. Ha, and N. Sawaki, "Characterization of GaN on GaN LED by HVPE method," *Journal of Ceramic Processing Research,* vol. 13, pp. S128-S131, 2012.

[216] C. Y. Jia, T. J. Yu, H. M. Lu, C. T. Zhong, Y. J. Sun, Y. Z. Tong, and G. Y. Zhang, "Performance improvement of GaN-based LEDs with step stage InGaN/GaN strain relief layers in GaN-based blue LEDs," *Optics Express,* vol. 21, pp. 8444-8449, 2013.

[217] M. A. Khan, M. Shatalov, H. P. Maruska, H. M. Wang, and E. Kuokstis, "III-nitride UV devices," *Japanese Journal of Applied Physics Part 1-Regular Papers Brief Communications & Review Papers,* vol. 44, pp. 7191-7206, 2005.

[218] D. F. Feezell, M. C. Schmidt, S. P. DenBaars, and S. Nakamura, "Development of nonpolar and semipolar InGaN/GaN visible light-emitting diodes," *MRS bulletin,* vol. 34, pp. 318-323, 2009.

[219] J. S. Speck and S. F. Chichibu, "Nonpolar and semipolar group III nitride-based materials," *MRS bulletin,* vol. 34, pp. 304-312, 2009.

[220] J. Rass, T. Wernicke, R. Kremzow, W. John, S. Einfeldt, P. Vogt, M. Weyers, and M. Kneissl, "Facet formation for laser diodes on nonpolar and semipolar GaN," *Physica Status Solidi a-Applications and Materials Science,* vol. 207, pp. 1361-1364, 2010.

[221] G. Y. Mak, E. Y. Lam, and H. W. Choi, "Precision laser micromachining of trenches in GaN on sapphire," *Journal of Vacuum Science & Technology B,* vol. 28, pp. 380-385, 2010.

[222] M. Y. Kim, Y. C. Park, S. S. Hong, B. K. Kim, D. W. Kim, and D. Y. Lee, "Focused ion beam nano patterning for fabrications of III-nitride light emitting diodes," *Emerging Lithographic Technologies XI, Pts 1 and 2,* vol. 6517, pp. M5171-M5171, 2007.

[223] C. K. Hsu, J. K. Sheu, J. K. Wang, M. L. Lee, K. H. Chang, S. J. Tu, and W. C. Lai, "Characteristics of slice InGaN/GaN light emitting diodes by focused ion beam milling," *Electrochemical and Solid State Letters,* vol. 14, pp. H343-H345, 2011.

[224] K. H. Baik, H. Y. Song, S. M. Hwang, Y. Jung, J. Ahn, and J. Kim, "Etched surface morphology of heteroepitaxial nonpolar (11-20) and semipolar (11-22) GaN films by photoenhanced chemical wet etching," *Journal of the Electrochemical Society,* vol. 158, pp. D196-D199, 2011.

[225] T. Paskova, R. Kroeger, S. Figge, D. Hommel, V. Darakchieva, B. Monemar, E. Preble, A. Hanser, N. M. Williams, and M. Tutor, "High-quality bulk a-plane GaN sliced from boules in comparison to heteroepitaxially grown thick films on r-plane sapphire," *Applied Physics Letters,* vol. 89, 2006.

[226] J. L. Weyher, G. Kamler, G. Nowak, J. Borysiuk, B. Lucznik, M. Krysko, I. Grzegory, and S. Porowski, "Defects in GaN single crystals and homoepitaxial structures," *Journal of Crystal Growth,* vol. 281, pp. 135-142, 2005.

[227] D. Zhuang and J. H. Edgar, "Wet etching of GaN, AIN, and SiC: A review," *Materials Science & Engineering R-Reports,* vol. 48, pp. 1-46, 2005.

[228] M. Seelmann-Eggebert, J. L. Weyher, H. Obloh, H. Zimmermann, A. Rar, and S. Porowski, "Polarity of (00.1) GaN epilayers grown on a (00.1) sapphire," *Applied Physics Letters,* vol. 71, pp. 2635-2637, 1997.

[229] T. Detchprohm, M. Zhu, Y. Li, Y. Xia, L. Liu, D. Hanser, and C. Wetzel, "Growth and characterization of green GaInN-based light emitting diodes on free-standing non-polar GaN templates," *Journal of Crystal Growth,* vol. 311, pp. 2937-2941, 2009.

[230] B. A. Haskell, F. Wu, M. D. Craven, S. Matsuda, P. T. Fini, T. Fujii, K. Fujito, S. P. DenBaars, J. S. Speck, and S. Nakamura, "Defect reduction in (11-20) a-plane gallium nitride via lateral epitaxial overgrowth by hydride vapor-phase epitaxy," *Applied Physics Letters,* vol. 83, pp. 644-646, 2003.

[231] A. A. Donskov, L. I. D'yakonov, A. V. Govorkov, Y. P. Kozlova, S. S. Malakhov, A. V. Markov, M. V. Mezhennyi, V. F. Pavlov, A. Y. Polyakov, N. B. Smirnov, T. G. Yugova, and S. J. Pearton, "Improved crystalline quality nonpolar a-GaN films grown by hydride vapor phase epitaxy," *Journal of Vacuum Science & Technology B,* vol. 26, pp. 1937-1941, 2008.

[232] F. Wu, M. D. Craven, S. H. Lim, and J. S. Speck, "Polarity determination of a-plane GaN on r-plane sapphire and its effects on lateral overgrowth and heteroepitaxy," *Journal of Applied Physics,* vol. 94, pp. 942-947, 2003.

[233] S. F. Chichibu, A. Uedono, T. Onuma, T. Sota, B. A. Haskell, S. P. DenBaars, J. S. Speck, and S. Nakamura, "Limiting factors of room-temperature nonradiative photoluminescence lifetime in polar and nonpolar GaN studied by time-resolved photoluminescence and slow positron annihilation techniques," *Applied Physics Letters,* vol. 86, 2005.

[234] C. P. Chen, A. Ganguly, C. H. Wang, C. W. Hsu, S. Chattopadhyay, Y. K. Hsu, Y. C. Chang, K. H. Chen, and L. C. Chen, "Label free dual sensing of DNA molecules Using GaN Nanowires," *Analytical Chemistry,* vol. 81, pp. 36-42, 2009.

[235] H. Kim, P. E. Colavita, K. M. Metz, B. M. Nichols, B. Sun, J. Uhlrich, X. Y. Wang, T. F. Kuech, and R. J. Hamers, "Photochemical functionalization of gallium nitride thin films with molecular and biomolecular layers," *Langmuir,* vol. 22, pp. 8121-8126, 2006.

[236] B. S. Kang, F. Ren, L. Wang, C. Lofton, W. H. W. Tan, S. J. Pearton, A. Dabiran, A. Osinsky, and P. P. Chow, "Electrical detection of immobilized proteins with ungated AlGaN/GaN high-electron-mobility transistors," *Applied Physics Letters,* vol. 87, 2005.

[237] C. M. De Silva, B. Pandey, F. Li, and T. Ito, "Adsorption of primary substituted hydrocarbons onto solid gallium substrates," *Langmuir,* vol. 29, pp. 4568-4573, 2013.

[238] R. G. Su, H. B. Liu, T. Kong, Q. Song, N. Li, G. Jin, and G. S. Cheng, "Tuning surface wettability of $In_xGa_{(1-x)}N$ nanotip arrays by phosphonic acid modification and photoillumination," *Langmuir,* vol. 27, pp. 13220-13225, 2011.

[239] A. M. B. do Rego, A. M. Ferraria, J. El Beghdadi, F. Debontridder, P. Brogueira, R. Naaman, and M. R. Vilar, "Adsorption of phenylphosphonic acid on GaAs (100) surfaces," *Langmuir*, vol. 21, pp. 8765-8773, 2005.

[240] G. Steinhoff, O. Purrucker, M. Tanaka, M. Stutzmann, and M. Eickhoff, "$Al_xGa_{1-x}N$ - A new material system for biosensors," *Advanced Functional Materials*, vol. 13, pp. 841-846, 2003.

[241] M. S. Makowski, S. Kim, M. Gaillard, D. Janes, M. J. Manfra, I. Bryan, Z. Sitar, C. Arellano, J. Xie, R. Collazo, and A. Ivanisevic, "Physisorption of functionalized gold nanoparticles on AlGaN/GaN high electron mobility transistors for sensing applications," *Applied Physics Letters*, vol. 102, 2013.

[242] C. E. Linsmeier, L. Wallman, L. Faxius, J. Schouenborg, L. M. Bjursten, and N. Danielsen, "Soft tissue reactions evoked by implanted gallium phosphide," *Biomaterials*, vol. 29, pp. 4598-4604, 2008.

[243] D. R. Webb, S. E. Wilson, and D. E. Carter, "Comparative pulmonary toxicity of gallium-arsenide, gallium(III) oxide, or arsenic(III) oxide intratracheally instilled into rats," *Toxicology and Applied Pharmacology*, vol. 82, pp. 405-416, 1986.

[244] M. J. C. Alcocer, P. P. Dillon, B. M. Manning, C. Doyen, H. A. Lee, S. J. Daly, R. O'Kennedy, and M. R. A. Morgan, "Use of phosphonic acid as a generic hapten in the production of broad specificity anti-organophosphate pesticide antibody," *Journal of Agricultural and Food Chemistry*, vol. 48, pp. 2228-2233, 2000.

[245] K. Mochizuki, T. Kikuchi, M. Sudoh, Y. Ishiguro, and T. Suzuki, "Comparison between Nafion and Polybenzimidazole (PBI) membranes for fuel cell type CO sensor," *Sensors, Actuators, and Microsystems (General) - 217th Ecs Meeting*, vol. 28, pp. 91-99, 2010.

[246] H. Morkoc, "Comprehensive characterization of hydride VPE grown GaN layers and templates," *Materials Science & Engineering R-Reports*, vol. 33, pp. 135-207, 2001.

[247] P. J. Hotchkiss, S. C. Jones, S. A. Paniagua, A. Sharma, B. Kippelen, N. R. Armstrong, and S. R. Marder, "The modification of indium tin oxide with phosphonic acids: Mechanism of binding, tuning of surface properties, and potential for use in organic electronic applications," *Accounts of Chemical Research*, vol. 45, pp. 337-346, 2012.

[248] S. D. Wolter, B. P. Luther, D. L. Waltemyer, C. Onneby, S. E. Mohney, and R. J. Molnar, "X-ray photoelectron spectroscopy and x-ray diffraction study of the thermal oxide on gallium nitride," *Applied Physics Letters,* vol. 70, pp. 2156-2158, 1997.

[249] R. Carin, J. P. Deville, and J. Werckmann, "An XPS study of GaN thin-films on GaAs," *Surface and Interface Analysis,* vol. 16, pp. 65-69, 1990.

[250] R. Schifano, E. V. Monakhov, B. G. Svensson, and S. Diplas, "Surface passivation and interface reactions induced by hydrogen peroxide treatment of n-type ZnO (000-1)," *Applied Physics Letters,* vol. 94, p. 132101, 2009.

[251] B. Monemar, P. P. Paskov, J. P. Bergman, A. A. Toropov, T. V. Shubina, and A. Usui, "Recombination dynamics of free and bound excitons in bulk GaN," *Superlattices and Microstructures,* vol. 43, pp. 610-614, 2008.

[252] P. P. Paskov, R. Schifano, B. Monemar, T. Paskova, S. Figge, and D. Hommel, "Emission properties of a-plane GaN grown by metal-organic chemical-vapor deposition," *Journal of Applied Physics,* vol. 98, p. 093519, 2005.

[253] S. Ghosh, P. Waltereit, O. Brandt, H. T. Grahn, and K. H. Ploog, "Electronic band structure of wurtzite GaN under biaxial strain in the M plane investigated with photoreflectance spectroscopy," *Physical Review B,* vol. 65, Feb 15 2002.

[254] M. S. Makowski, D. Y. Zemlyanov, and A. Ivanisevic, "Olefin metathesis reaction on GaN (0001) surfaces," *Applied Surface Science,* vol. 257, pp. 4625-4632, 2011.

[255] N. Chaniotakis and N. Sofikiti, "Novel semiconductor materials for the development of chemical sensors and biosensors: A review," *Analytica Chimica Acta,* vol. 615, pp. 1-9, 2008.

[256] P. B. Paramonov, S. A. Paniagua, P. J. Hotchkiss, S. C. Jones, N. R. Armstrong, S. R. Marder, and J. L. Bredas, "Theoretical characterization of the indium tin oxide surface and of its binding sites for adsorption of phosphonic acid monolayers," *Chemistry of Materials,* vol. 20, pp. 5131-5133, 2008.

[257] A. Sharma, B. Kippelen, P. J. Hotchkiss, and S. R. Marder, "Stabilization of the work function of indium tin oxide using organic surface modifiers in organic light-emitting diodes," *Applied Physics Letters,* vol. 93, p. 163308, 2008.

[258] S. Besbes, A. Ltaief, K. Reybier, L. Ponsonnet, N. Jaffrezic, J. Davenas, and H. Ben Ouada, "Injection modifications by ITO functionalization with a self-assembled monolayer in OLEDs," *Synthetic Metals,* vol. 138, pp. 197-200, 2003.

[259] S. H. Jee, S. H. Kim, J. H. Ko, and Y. S. Yoon, "Study on work function change of ITO modified by using a self-assembled monolayer for organic based devices," *Journal of the Korean Physical Society*, vol. 49, pp. 2034-2039, 2006.

[260] J. X. Chen, R. E. Ruther, Y. Z. Tan, L. M. Bishop, and R. J. Hamers, "Molecular adsorption on ZnO(10-10) single crystal surfaces: Morphology and charge transfer," *Langmuir*, vol. 28, pp. 10437-10445, 2012.

[261] B. B. Zhang, T. Kong, W. Z. Xu, R. G. Su, Y. H. Gao, and G. S. Cheng, "Surface functionalization of zinc oxide by carboxyalkylphosphonic acid self-assembled monolayers," *Langmuir*, vol. 26, pp. 4514-4522, 2010.

[262] W. S. Hwang, A. Verma, H. Peelaers, V. Protasenko, S. Rouvimov, H. Xing, A. Seabaugh, W. Haensch, C. V. de Walle, Z. Galazka, M. Albrecht, R. Fornari, and D. Jena, "High-voltage field effect transistors with wide-bandgap β-Ga_2O_3 nanomembranes," *Applied Physics Letters*, vol. 104, p. 203111, 2014.

[263] S. S. Kumar, E. J. Rubio, M. Noor-A-Alam, G. Martinez, S. Manandhar, V. Shutthanandan, S. Thevuthasan, and C. V. Ramana, "Structure, morphology, and optical properties of amorphous and nanocrystalline gallium oxide thin films," *Journal of Physical Chemistry C*, vol. 117, pp. 4194-4200, 2013.

[264] S. N. Lee, H. S. Paek, J. K. Son, T. Sakong, E. Yoon, O. H. Nam, and Y. Park, "Growth of InGaN multiple quantum wells and GaN eplilayer on GaN substrate," *Physica B-Condensed Matter*, vol. 376, pp. 532-535, 2006.

[265] S. J. Wilkins, M. Greenough, C. Arellano, T. Paskova, and A. Ivanisevic, "In situ chemical functionalization of gallium nitride with phosphonic acid derivatives during etching," *Langmuir*, vol. 30, pp. 2038-2046, 2014.

[266] C. L. Perkins, "Molecular anchors for self-assembled monolayers on ZnO: A direct comparison of the thiol and phosphonic acid moieties," *Journal of Physical Chemistry C*, vol. 113, pp. 18276-18286, 2009.

[267] S. C. Ghosh, M. C. Biesinger, R. R. LaPierre, and P. Kruse, "The role of proximity caps during the annealing of UV-ozone oxidized GaAs," *Journal of Applied Physics*, vol. 101, p. 114321, 2007.

[268] G. Schön, "Auger and direct electron spectra in X-ray photoelectron studies of zinc, zinc oxide, gallium, and gallium oxide," *Journal of Electron Spectroscopy and Related Phenomena*, vol. 2, pp. 75-86, 1973.

[269] C. Battocchio, I. Fratoddi, F. Bondino, M. Malvestuto, M. V. Russo, and G. Polzonetti, "Self assembling monolayers of dialkynyl bridged Pd(II) thiols obtained by thermally induced multilayer desorption: Thermal and chemical stability investigated by SR-XPS," *Chemical Physics Letters,* vol. 527, pp. 57-62, 2012.

[270] D. G. Castner, K. Hinds, and D. W. Grainger, "X-ray photoelectron spectroscopy sulfur 2p study of organic thiol and disulfide binding interactions with gold surfaces," *Langmuir,* vol. 12, pp. 5083-5086, 1996.

[271] Y. Suzuki, N. Sanada, A. Shimomura, and Y. Fukuda, "High-resolution XPS analysis of GaP(001), (111)A, and (111)B surfaces passivated by $(NH_4)2S_x$ solution," *Applied Surface Science,* vol. 235, pp. 260-266, 2004.

[272] V. M. Bermudez, "Study of oxygen chemisorption on the GaN(0001)-(1x1) surface," *Journal of Applied Physics,* vol. 80, pp. 1190-1200, 1996.

[273] O.-H. Nam, Michael D. Bremser, Brandon L. Ward, Robert J. Nemanich, and Robert F. Davis, "Growth of GaN and $Al_{0.2}Ga_{0.8}N$ on patterened substrates via organometallic vapor phase epitaxy," *Japanese Journal of Applied Physics,* vol. 36, p. L532, 1997.

[274] T. Paskova and K. R. Evans, "GaN substrates-progress, status, and prospects," *Selected Topics in Quantum Electronics, IEEE Journal of,* vol. 15, pp. 1041-1052, 2009.

[275] A. Usui, H. Sunakawa, A. Sakai, and A. A. Yamaguchi, "Thick GaN epitaxial growth with low dislocation density by hydride vapor phase epitaxy," *Japanese Journal of Applied Physics,* vol. 36, p. L899, 1997.

[276] J. K. Sheu, S. J. Chang, C. H. Kuo, Y. K. Su, L. W. Wu, Y. C. Lin, W. C. Lai, J. M. Tsai, G. C. Chi, and R. K. Wu, "White-light emission from near UV InGaN-GaN LED chip precoated with blue/green/red phosphors," *Photonics Technology Letters, IEEE,* vol. 15, pp. 18-20, 2003.

[277] S. T. Sheppard, K. Doverspike, W. L. Pribble, S. T. Allen, J. W. Palmour, L. T. Kehias, and T. J. Jenkins, "High-power microwave GaN/AlGaN HEMTs on semi-insulating silicon carbide substrates," *Electron Device Letters, IEEE,* vol. 20, pp. 161-163, 1999.

[278] D.-H. Kim, C.-O. Cho, Y.-G. Roh, H. Jeon, Y. S. Park, J. Cho, J. S. Im, C. Sone, Y. Park, W. J. Choi, and Q.-H. Park, "Enhanced light extraction from GaN-based light-emitting diodes with holographically generated two-dimensional photonic crystal patterns," *Applied Physics Letters*, vol. 87, p. 203508, 2005.

[279] C.-T. Huang, J. Song, W.-F. Lee, Y. Ding, Z. Gao, Y. Hao, L.-J. Chen, and Z. L. Wang, "GaN nanowire arrays for high-output nanogenerators," *Journal of the American Chemical Society*, vol. 132, pp. 4766-4771, 2010.

[280] H.-W. Lin, Y.-J. Lu, H.-Y. Chen, H.-M. Lee, and S. Gwo, "InGaN/GaN nanorod array white light-emitting diode," *Applied Physics Letters*, vol. 97, p. 073101, 2010.

[281] D. H. van Dorp, J. L. Weyher, M. R. Kooijman, and J. J. Kelly, "Photoetching mechanisms of GaN in alkaline $S_2O_8^{2-}$ Solution," *Journal of The Electrochemical Society*, vol. 156, pp. D371-D376, 2009.

[282] J. L. Weyher, F. D. Tichelaar, D. H. van Dorp, J. J. Kelly, and A. Khachapuridze, "The $K_2S_2O_8$–KOH photoetching system for GaN," *Journal of Crystal Growth*, vol. 312, pp. 2607-2610, 2010.

[283] T. Fujii, Y. Gao, R. Sharma, E. L. Hu, S. P. DenBaars, and S. Nakamura, "Increase in the extraction efficiency of GaN-based light-emitting diodes via surface roughening," *Applied Physics Letters*, vol. 84, pp. 855-857, 2004.

[284] Y. Jung, J. Ahn, K. H. Baik, D. Kim, S. J. Pearton, F. Ren, and J. Kim, "Chemical etch characteristics of N-face and Ga-face GaN by phosphoric acid and potassium hydroxide solutions," *Journal of The Electrochemical Society*, vol. 159, pp. H117-H120, 2011.

[285] J.-M. Lee, C. Huh, D.-J. Kim, and S.-J. Park, "Dry-etch damage and its recovery in InGaN/GaN multi-quantum-well light-emitting diodes," *Semiconductor Science and Technology*, vol. 18, p. 530, 2003.

[286] C. H. Chiu, T. C. Lu, H. W. Huang, C. F. Lai, C. C. Kao, J. T. Chu, C. C. Yu, H. C. Kuo, S. C. Wang, C. F. Lin, and T. H. Hsueh, "Fabrication of InGaN/GaN nanorod light-emitting diodes with self-assembled Ni metal islands," *Nanotechnology*, vol. 18, p. 445201, 2007.

[287] H.-M. Kim, D. S. Kim, D. Y. Kim, T. W. Kang, Y.-H. Cho, and K. S. Chung, "Growth and characterization of single-crystal GaN nanorods by hydride vapor phase epitaxy," *Applied Physics Letters*, vol. 81, pp. 2193-2195, 2002.

[288] J. Kuzmík, P. Javorka, M. Marso, and P. Kordos, "Annealing of Schottky contacts deposited on dry etched AlGaN/GaN," *Semiconductor Science and Technology*, vol. 17, p. L76, 2002.

[289] H.-Y. Kim, Y. Jung, S. H. Kim, J. Ahn, M. A. Mastro, J. K. Hite, C. R. Eddy Jr, and J. Kim, "Wet etching of non-polar gallium nitride light-emitting diode structure for enhanced light extraction," *Journal of Crystal Growth*, vol. 326, pp. 65-68, 2011.

[290] I. Dziecielewski, J. L. Weyher, and W. Dzwolak, "On the hydrophobicity of modified Ga-polar GaN surfaces," *Applied Physics Letters*, vol. 102, p. 043704, 2013.

[291] S. J. Wilkins, T. Paskova, and A. Ivanisevic, "Effect of etching with cysteamine assisted phosphoric acid on gallium nitride surface oxide formation," *Journal of Applied Physics*, vol. 114, p. 064907, 2013.

[292] T. Ito, S. Forman, C. Cao, C. Eddy, M. Mastro, R. Holm, R. Henry, K. Hohn, and J. Edgar, "Monolayer formation on GaN surface via self-assembly," *Meeting Abstracts*, vol. MA2007-02, p. 1264, 2007.

[293] C. F. Qiu, L. D. Wang, H. Y. Chen, M. Wong, and H. S. Kwok, "Room-temperature ultraviolet emission from an organic light-emitting diode," *Applied Physics Letters*, vol. 79, pp. 2276-2278, 2001.

[294] E. H. Williams, A. V. Davydov, V. P. Oleshko, K. L. Steffens, I. Levin, N. J. Lin, K. A. Bertness, A. K. Manocchi, J. A. Schreifels, and M. V. Rao, "Solution-based functionalization of gallium nitride nanowires for protein sensor development," *Surface Science*, vol. 627, pp. 23-28, 2014.

[295] T. Anderson, F. Ren, S. Pearton, B. S. Kang, H. T. Wang, C. Y. Chang, and J. S. Lin, "Advances in hydrogen, carbon dioxide, and hydrocarbon gas sensor technology using GaN and ZnO-based devices," *Sensors*, vol. 9, pp. 4669-4694, 2009.

[296] P. J. Hotchkiss, S. C. Jones, S. A. Paniagua, A. Sharma, B. Kippelen, N. R. Armstrong, and S. R. Marder, "The modification of indium tin oxide with phosphonic acids: Mechanism of binding, tuning of surface properties, and potential for use in organic electronic applications," *Accounts of Chemical Research*, vol. 45, pp. 337-346, 2011.

[297] J. L. Weyher, "Defect sensitive etching of nitrides: appraisal of methods," *Crystal Research and Technology*, vol. 47, pp. 333-340, 2012.

[298] P. Deb, H. Kim, V. Rawat, M. Oliver, S. Kim, M. Marshall, E. Stach, and T. Sands, "Faceted and vertically aligned GaN nanorod arrays fabricated without catalysts or lithography," *Nano Letters,* vol. 5, pp. 1847-1851, 2005.

[299] J. Weyher and J. Kelly, "Defect-selective etching of semiconductors," in *Springer Handbook of Crystal Growth*, G. Dhanaraj, K. Byrappa, V. Prasad, and M. Dudley, Eds., ed: Springer Berlin Heidelberg, pp. 1453-1476, 2010.

[300] P. B. Paramonov, S. A. Paniagua, P. J. Hotchkiss, S. C. Jones, N. R. Armstrong, S. R. Marder, and J.-L. Brédas, "Theoretical characterization of the indium tin oxide surface and of its binding sites for adsorption of phosphonic acid monolayers," *Chemistry of Materials,* vol. 20, pp. 5131-5133, 2008.

[301] S. A. Paniagua, P. J. Hotchkiss, S. C. Jones, S. R. Marder, A. Mudalige, F. S. Marrikar, J. E. Pemberton, and N. R. Armstrong, "Phosphonic acid modification of indium tin oxide electrodes: Combined XPS/UPS/Contact angle studies," *The Journal of Physical Chemistry C,* vol. 112, pp. 7809-7817, 2008.

[302] A. Ganguly, C.-P. Chen, Y.-T. Lai, C.-C. Kuo, C.-W. Hsu, K.-H. Chen, and L.-C. Chen, "Functionalized GaN nanowire-based electrode for direct label-free voltammetric detection of DNA hybridization," *Journal of Materials Chemistry,* vol. 19, pp. 928-933, 2009.

[303] B. Monemar, P. P. Paskov, J. P. Bergman, A. A. Toropov, T. V. Shubina, T. Malinauskas, and A. Usui, "Recombination of free and bound excitons in GaN," *physica status solidi (b),* vol. 245, pp. 1723-1740, 2008.

[304] S. F. Chichibu, A. Uedono, T. Onuma, T. Sota, B. A. Haskell, S. P. DenBaars, J. S. Speck, and S. Nakamura, "Limiting factors of room-temperature nonradiative photoluminescence lifetime in polar and nonpolar GaN studied by time-resolved photoluminescence and slow positron annihilation techniques," *Applied Physics Letters,* vol. 86, p. 021914, 2005.

[305] V. Jindal and F. Shahedipour-Sandvik, "Computational and experimental studies on the growth of nonpolar surfaces of gallium nitride," *Journal of Applied Physics,* vol. 107, p. 054907. 2010.

[306] S. C. Cruz, S. Keller, T. E. Mates, U. K. Mishra, and S. P. DenBaars, "Crystallographic orientation dependence of dopant and impurity incorporation in GaN films grown by metalorganic chemical vapor deposition," *Journal of Crystal Growth,* vol. 311, pp. 3817-3823, 2009.

[307] C. Queffelec, M. Petit, P. Janvier, D. A. Knight, and B. Bujoli, "Surface modification using phosphonic acids and esters," *Chemical Reviews*, vol. 112, pp. 3777-3807, 2012.

[308] G. J. Kuhlmann, C. Langley Research, and S. United, *A study to investigate the chemical stability of gallium phosphate oxide/gallium arsenide phosphide*. Washington, D.C.: [Springfield, Va.: National Aeronautics and Space Administration, Scientific and Technical Information Office], 1979.

[309] S. Paul, A. Helwig, G. Müller, F. Furtmayr, J. Teubert, and M. Eickhoff, "Opto-chemical sensor system for the detection of H_2 and hydrocarbons based on InGaN/GaN nanowires," *Sensors and Actuators B: Chemical*, vol. 173, pp. 120-126, 2012.

[310] B. Kaiser, D. Fertig, J. Ziegler, J. Klett, S. Hoch, and W. Jaegermann, "Solar hydrogen generation with wide band gap semiconductors: GaP(100) photoelectrodes and surface modification," *ChemPhysChem*, vol. 13, pp. 3053-3060, 2012.

[311] J. A. Goode, J. V. H. Rushworth, and P. A. Millner, "Biosensor regeneration: A review of common techniques and outcomes," *Langmuir*, 2014.

[312] A. N. Hattori, F. Kawamura, M. Yoshimura, Y. Kitaoka, Y. Mori, K. Hattori, H. Daimon, and K. Endo, "Chemical etchant dependence of surface structure and morphology on GaN(0001) substrates," *Surface Science*, vol. 604, pp. 1247-1253, 2010.

[313] R. L. Meek and S. Ne, "Anodic dissolution and selective etching of gallium phosphide," *Journal of the Electrochemical Society*, vol. 119, pp. 1148-1152, 1972.

[314] A. Shintani and S. Minagawa, "Etching of GaN using phosphoric acid," *Journal of the Electrochemical Society*, vol. 123, pp. 706-713, 1976.

[315] E. Kaminska, A. Piotrowska, A. Kaminska, and M. Klimkiewicz, "Etching procedures for GaP surfaces," *Surface Technology*, vol. 12, pp. 205-215, 1981.

[316] S. Avivi, Y. Mastai, G. Hodes, and A. Gedanken, "Sonochemical hydrolysis of Ga^{3+} ions: Synthesis of scroll-like cylindrical nanoparticles of gallium oxide hydroxide," *Journal of the American Chemical Society*, vol. 121, pp. 4196-4199, 1999.

[317] H. Yamanaka, T. Uragaki, S. Fujiwara, and M. Inoue, "Etching with hot phosphoric acid," ed: Google Patents, 1978.

[318] R. Flores-Perez, D. Y. Zernlyanov, and A. Ivanisevic, "Quantitative evaluation of covalently bound molecules on GaP (100) surfaces," *Journal of Physical Chemistry C*, vol. 112, pp. 2147-2155, 2008.

[319] W. Lueangchaichaweng, N. R. Brooks, S. Fiorilli, E. Gobechiya, K. F. Lin, L. Li, S. Parres-Esclapez, E. Javon, S. Bals, G. Van Tendeloo, J. A. Martens, C. E. A. Kirschhock, P. A. Jacobs, and P. P. Pescarmona, "Gallium oxide nanorods: Novel, template-free synthesis and high catalytic activity in epoxidation reactions," *Angewandte Chemie-International Edition*, vol. 53, pp. 1585-1589, 2014.

[320] S. J. Wilkins, T. Paskova, and A. Ivanisevic, "Modified surface chemistry, potential, and optical properties of polar gallium nitride via long chained phosphonic acids," *Applied Surface Science*, vol. 327, pp. 498-503, 2015.

[321] H. Y. Liu, B. Y. Chou, W. C. Hsu, C. S. Lee, and C. S. Ho, "Novel Oxide-Passivated AlGaN/GaN HEMT by Using Hydrogen Peroxide Treatment," *IEEE Transactions on Electron Devices*, vol. 58, pp. 4430-4433, 2011.

[322] H. Y. Liu, B. Y. Chou, W. C. Hsu, C. S. Lee, and C. S. Ho, "Temperature dependent investigation of AlGaN/GaN oxide-passivated HEMT by using hydrogen peroxide oxidation method," *ECS Journal of Solid State Science and Technology*, vol. 1, pp. Q86-Q90, 2012.

[323] J. Murata, A. Kubota, K. Yagi, Y. Sano, H. Hara, K. Arima, T. Okamoto, H. Mimura, and K. Yamauchi, "New chemical planarization of SiC and GaN using an Fe plate in H_2O_2 solution," *Silicon Carbide and Related Materials 2007, Pts 1 and 2*, vol. 600-603, pp. 815-818, 2009.

[324] N. Shiozaki, T. Sato, and T. Hashizume, "Formation of thin native oxide layer on n-GaN by electrochemical process in mixed solution with glycol and water," *Japanese Journal of Applied Physics Part 1-Regular Papers Brief Communications & Review Papers*, vol. 46, pp. 1471-1473, 2007.

[325] I. Németh, B. Kunert, W. Stolz, and K. Volz, "Heteroepitaxy of GaP on Si: Correlation of morphology, anti-phase-domain structure and MOVPE growth conditions," *Journal of Crystal Growth*, vol. 310, pp. 1595-1601, 2008.

[326] H. Morota and S. Adachi, "Properties of GaP(001) surfaces treated in aqueous HF solutions," *Journal of Applied Physics*, vol. 101, p. 113518, 2007.

[327] H. Y. Lee, B. K. Wu, and M. Y. Chern, "Study on the formation of zinc peroxide on zinc oxide with hydrogen peroxide treatment using X-ray photoelectron spectroscopy (XPS)," *Electronic Materials Letters,* vol. 10, pp. 51-55, 2014.

[328] L. C. Grabow, J. J. UhIrich, T. F. Kuech, and M. Mavrikakis, "Effectiveness of in situ NH_3 annealing treatments for the removal of oxygen from GaN surfaces," *Surface Science,* vol. 603, pp. 387-399, 2009.

[329] T. Bo, J. H. Lan, Y. L. Zhao, Y. J. Zhang, C. H. He, Z. F. Chai, and W. Q. Shi, "First-principles study of water adsorption and dissociation on the UO_2 (111), (110) and (100) surfaces," *Journal of Nuclear Materials,* vol. 454, pp. 446-454, 2014.

[330] X. Q. Zhang and S. Ptasinska, "Dissociative adsorption of water on an H_2O/GaAs(100) interface: In situ near ambient pressure XPS studies," *Journal of Physical Chemistry C,* vol. 118, pp. 4259-4266, 2014.

[331] D. L. Cui, J. Q. Pan, Z. C. Zhang, B. B. Huang, X. Y. Qin, M. H. Jiang, and S. M. Gao, "The stability and surface reactivity of gallium phosphide nanocrystals," *Progress in Crystal Growth and Characterization of Materials,* vol. 40, pp. 145-151, 2000.

[332] J. C. Philips, *Bonds and Bands in Semiconductors*. New York: Academic Press, 1973.

[333] A. Zaouk, E. Salvetat, J. Sakaya, F. Maury, and G. Constant, "Various chemical mechanisms for the crystal growth of III-V semiconductors using coordination compounds as starting material in the MOCVD process," *Journal of Crystal Growth,* vol. 55, pp. 135-144, 1981.

[334] J. Price, J. Barnett, S. Raghavan, M. Keswani, and R. Govindarajan, "A study of the interaction of gallium arsenide with wet chemical formulations using thermodynamic calculations and spectroscopic ellipsometry," *Microelectronic Engineering,* vol. 87, pp. 1661-1664, 2010.

[335] A. N. Hattori, F. Kawamura, M. Yoshimura, Y. Kitaoka, Y. Mori, K. Hattori, H. Daimon, and K. Endo, "Chemical etchant dependence of surface structure and morphology on GaN(0001) substrates," *Surface Science,* vol. 604, pp. 1247-1253, 2010.

[336] S. Tamang, G. Beaune, I. Texier, and P. Reiss, "Aqueous phase transfer of InP/ZnS nanocrystals conserving fluorescence and high colloidal stability," *ACS Nano,* vol. 5, pp. 9392-9402, 2011.

[337] S. Y. Alqaradawi, A. S. Aljaber, and M. M. Khader, "Activation and stabilization of gallium arsenide anode in an aqueous photoelectrochemical cell," *Thin Solid Films*, vol. 444, pp. 282-289, 2003.

[338] K. Krnel, G. Dražič, and T. Kosmač, "Degradation of AlN Powder in Aqueous Environments," *Journal of Materials Research*, vol. 19, pp. 1157-1163, 2004.

[339] A. Tanaka, "Toxicity of indium arsenide, gallium arsenide, and aluminum gallium arsenide," *Toxicology and Applied Pharmacology*, vol. 198, pp. 405-411, 2004.

[340] W. Shotyk, M. Krachler, and B. Chen, "Contamination of canadian and european bottled waters with antimony from PET containers," *Journal of Environmental Monitoring*, vol. 8, pp. 288-292, 2006.

[341] A. Tanaka, M. Hirata, Y. Kiyohara, M. Nakano, K. Omae, M. Shiratani, and K. Koga, "Review of pulmonary toxicity of indium compounds to animals and humans," *Thin Solid Films*, vol. 518, pp. 2934-2936, 2010.

[342] N. K. C. Twarakavi and J. J. Kaluarachchi, "Arsenic in the shallow ground waters of conterminous United States: Assessment, health risks, and costs for MCL compliance," *Journal of the American Water Resources Association*, vol. 42, pp. 275-294, 2006.

[343] W. H. Organization, "Antimony in drinking-water," G. f. d.-w. quality, Ed., ed. Germany: World Health Organization, 2003.

[344] J. J. R. Frausto da Silva and R. J. P. Williams, *The biological chemistry of the elements: the inorganic chemistry of life*, 2nd ed. Oxford: Oxford University Press, 2001.

[345] L. Mueller, H. Traub, N. Jakubowski, D. Drescher, V. Baranov, and J. Kneipp, "Trends in single-cell analysis by use of ICP-MS," *Analytical and Bioanalytical Chemistry*, vol. 406, pp. 6963-6977, 2014.

[346] G. Pearson and G. Greenway, "A highly efficient sample introduction system for interfacing microfluidic chips with ICP-MS," *Journal of Analytical Atomic Spectrometry*, vol. 22, pp. 657-662, 2007.

[347] B. G. Yacobi and D. B. Holt, *Cathodoluminescence microscopy of inorganic solids*: Springer Science & Business Media, 1990.

[348] G. Guzmán and M. Herrera, "Cathodoluminescence of GaN nanorods and nanowires grown by thermal evaporation," *Semiconductor Science and Technology,* vol. 29, p. 025001, 2014.

[349] M. W. Knight, T. Coenen, Y. Yang, B. J. M. Brenny, M. Losurdo, A. S. Brown, H. O. Everitt, and A. Polman, "Gallium Plasmonics: Deep Subwavelength Spectroscopic Imaging of Single and Interacting Gallium Nanoparticles," *ACS Nano,* 2015.

[350] E. W. Williams, A. M. White, A. Ashford, C. Hilsum, P. Porteous, and D. R. Wright, "(In,Ga)P alloys: photoluminescence excitation and cathodoluminescence of zinc doped indirect gap alloys," *Journal of Physics C: Solid State Physics,* vol. 3, p. L55, 1970.

[351] D. R. Glenn, H. Zhang, N. Kasthuri, R. Schalek, P. K. Lo, A. S. Trifonov, H. Park, J. W. Lichtman, and R. L. Walsworth, "Correlative light and electron microscopy using cathodoluminescence from nanoparticles with distinguishable colours," *Sci. Rep.,* vol. 2, 2012.

[352] V. I. Petrov, "Cathodoluminescence microscopy," *Physics-Uspekhi,* vol. 39, p. 807, 1996.

[353] H. Spanggaard and F. C. Krebs, "A brief history of the development of organic and polymeric photovoltaics," *Solar Energy Materials and Solar Cells,* vol. 83, pp. 125-146, 2004.

[354] R. Haitz and J. Y. Tsao, "Solid-state lighting: 'The case' 10 years after and future prospects," *physica status solidi (a),* vol. 208, pp. 17-29, 2011.

[355] P. H. Mutin, V. Lafond, A. F. Popa, M. Granier, L. Markey, and A. Dereux, "Selective surface modification of SiO_2-TiO_2 supports with phosphonic acids," *Chemistry of Materials,* vol. 16, pp. 5670-5675, 2004.

[356] I. Cimalla, F. Will, K. Tonisch, M. Niebelschütz, V. Cimalla, V. Lebedev, G. Kittler, M. Himmerlich, S. Krischok, J. A. Schaefer, M. Gebinoga, A. Schober, T. Friedrich, and O. Ambacher, "AlGaN/GaN biosensor—effect of device processing steps on the surface properties and biocompatibility," *Sensors and Actuators B: Chemical,* vol. 123, pp. 740-748, 2007.

[357] K. H. Tran Ba, M. A. Mastro, J. K. Hite, C. R. Eddy, and T. Ito, "Nitrogen-polar gallium nitride substrates as solid-state pH-selective potentiometric sensors," *Applied Physics Letters,* vol. 95, p. 142501, 2009.